Polymeric Microneedle Device for Transcutaneous Delivery of Antigen and Chemotherapeutics

THESIS

Submitted in partial fulfilment

of the requirements for the degree of

DOCTOR OF PHILOSOPHY

by

SHUBHMITA BHATNAGAR
ID No. 2014PHXF0003H

Under the supervision of

Prof. Venkata Vamsi Krishna Venuganti

BITS Pilani

Pilani | Dubai | Goa | Hyderabad

BIRLA INSTITUTE OF TECHNOLOGY AND SCIENCE, PILANI
2018

BIRLA INSTITUTE OF TECHNOLOGY AND SCIENCE, PILANI

<u>CERTIFICATE</u>

This is to certify that the thesis entitled "**Polymeric Microneedle Device for Transcutaneous Delivery of Antigen and Chemotherapeutics**" and submitted by **SHUBHMITA BHATNAGAR** ID No. **2014PHXF0003H** for award of Ph.D. of the Institute embodies original work done by her under my supervision.

Signature of the Supervisor:

Name in capital letters: **VENKATA VAMSI KRISHNA VENUGANTI**

Designation   : **Associate Professor**

Date:

Acknowledgements

"There is freedom waiting for you,

On the breezes of the sky,

And you ask "What if I fall?"

Oh but my darling,

What if you fly?"

— Erin Hanson

This thesis work would not have been possible without the guidance, support and help of several individuals. I thank everyone directly or indirectly involved in the completion of this work.

I owe utmost gratitude to my research supervisor, Dr. Venkata Vamsi Krishna Venuganti, Associate Professor, Department of Pharmacy, BITS Pilani, Hyderabad Campus for the opportunity to be involved in a novel, clinically relevant research project. His positive outlook, scientific acuity and confidence in my research inspired me to push boundaries throughout my time as his student.

Next, I wish to thank my Doctoral Advisory Committee (DAC) members, Prof. P. Yogeeswari and Prof. Swati Biswas, for reviewing my thesis work and providing constructive criticism to my work. I thank Prof. Souvik Bhattacharyya, Vice Chancellor, Prof. G. Sundar, Director, BITS Pilani, Hyderabad Campus, Prof. S. C. Sivasubramanian, Acting Registrar, Prof. Sanjay Kumar Verma, Dean, Academic Research, Prof. Niranjan Swain, Dean, General Administration, Prof. A. Bhattacharya, Associate Dean, Sponsored Research and Consultancy Division, and Associate Dean, Academic Research Division, BITS-Pilani, Hyderabad, for providing excellent work facilities and an absorbing research environment.

Abstract

Microneedles have been used to deliver a wide variety of different low molecular weight drugs, biotherapeutics and vaccines, including reports of clinical trials with a number of small molecules, biomacromolecules and vaccines. Microneedles have also been employed for delivery of actives into the eye and into cells. The aim of the current thesis work was to understand the deliverability of different drug molecules from polymeric microneedles. Corn protein zein, and synthetic polymers polyvinyl alchohol and polyvinyl pyrrolidone were used to fabricate microneedles in two different designs and geometries.

Zein microneedles were investigated for their potential for transcutaneous immunization. Conical microneedles with a height of 974.6 ± 13.8 μm and a base diameter of 362.7 ± 13.8 μm with a smooth surface were formed using the micromolding technique. The insertion of zein microneedles and the delivery of the model antigen, ovalbumin into the skin was confirmed by histological examination and confocal microscopy. Using fluorescence labelled *S. epidermidis*, a significantly lower permeation of bacteria was seen with microneedle treatment against hypodermal syringe application. Stability of ovalbumin coated on zein microneedles was investigated using SDS-PAGE and circular dichroism. Stability evaluation of ovalbumin coated zein microneedles suggested 2–month stability of the preparation under ambient and cold conditions. Transcutaneous immunization studies in Balb/c mice showed significantly ($p < 0.001$) greater antibody titers (total anti-OVA IgG, IgG1, and IgG2a) after the application of ovalbumin coated zein microneedles and intradermal injection of ovalbumin compared with the control group. Splenocyte proliferation further suggested that ovalbumin coated

zein microneedles have the ability to enhance the antigen presentation to the T-cells and to induce a long-lasting immune response

Zein microneedles were further studied for delivery of two chemotherapeutic agents with contrasting physicochemical characteristics, tamoxifen and gemcitabine. Entrapment or coating of chemotherapeutic agents in zein microneedles was optimized to achieve greater loading efficiency. The greatest loading achieved was 607 ± 21 and 1459 ± 74 µg for tamoxifen and gemcitabine using the entrapment approach, respectively. Tamoxifen was not seen to permeate across skin using the any of the treatment approaches. Tamoxifen coated microneedles delivered drug into the viable epidermis with no permeation across skin. The poke-and-patch approach provided greater skin permeation for gemcitabine compared to drug entrapment or coating.

To improve the drug loading and permeation of anticancer agents, dissolvable microneedles were prepared using polyvinyl alcohol/polyvinyl pyrrolidone. Pyramidal microneedles were prepared using high molecular grade polyvinyl pyrrolidone while a flexible pedestal was prepared with blend of polyvinyl alcohol and polyvinyl pyrrolidone. Microneedles with a height of 597.16 ± 31.48 µm and base width of 245.83 ± 16.13 µm were formed. Two chemotherapeutic agents used in breast cancer, doxorubicin and docetaxel were loaded into the prepared microneedles individually as well as in combination. Mechanical strength of microneedles for skin insertion was confirmed using a texture analyzer. Efficient insertion and delivery of doxorubicin into skin was further confirmed using confocal laser scanning microscopy. Permeation of DOX from DOX+DTX loaded microneedles across murine skin was observed to be $73.14 \pm 7.19\%$ at the end of 48h. DTX permeation was seen to both lesser and slower compared to DOX.

About 67.20±15.24% of DTX was recovered from the viable epidermis after 48h of permeation. Tumor efficacy studies in 4T1 tumor bearing mice revealed significantly higher reduction in rate of tumor volume increase with DOX+DTX MN group against control. This was comparable with the DOX+DTX intratumoral injection treatment group. Further, lesser toxicity and higher survival rates were observed with MN treatment groups especially with doxorubicin.

Table of contents

List of figures

List of tables

List of abbreviations

MN	Microneedle
PTH	Parathyroid hormone
CMC	Carboxymethyl cellulose
PVA	Polyvinyl alcohol
PVP	Polyvinyl pyrrolidone
HPMC	Hydroxypropyl methyl cellulose
HA	Hyaluronic acid/sodium hyaluronate
SA	Sodium alginate
PLA	Poly (lactic acid)
PLGA	Poly(d,l-lactide-co-glycolide)
OVA	ovalbumin
ZMN	Zein microneedles
TMX	Tamoxifen
GCB	Gemcitabine
DOX	Doxorubicin
DTX	Docetaxel
FT-IR	Fourier-transform infrared spectroscopy
MTT	3-[4,5-Dimethylthiazol-2-yl]- 2,5-diphenyltetrazolium bromide
DMSO	Dimethyl sulfoxide
MW	Molecular weight
MWCO	Molecular weight cut-off
PBS	Phosphate buffer saline
PEG	Polyethylene glycol
HPLC	High performance liquid chromatography
XRD	X-ray diffraction
DSC	Differential scanning calorimetry
TEER	Tranepidermal electrical resistance
TEWL	Transepidermal water loss
DMN	Dissolving microneedle
FITC	Fluorescein isothiocyanate
CD	Circular dichroism

OCT	Optimum cutting temperature
rpm	Rotations per minute
RT	Room temperarute
SD	Standard deviation
UV	Ultraviolet
λmax	Wavelength maxima for UV-absorbance
µg	Microgram
µM	Micro molar
ºC	Degree Celsius
mg	Milligram
min	Minutes
ml	Millilitre
mm	Millimetre
nm	Nanometre

Chapter 1
Problem Statement

The most common drug delivery systems include oral and injectable formulations. Oral delivery systems suffer from disadvantages including extensive first pass metabolism, gastric degradation, enzymatic degradation, poor bioavailability and food based interactions. The injectable systems provide immediate action and higher bioavailability but are painful and invasive. Also, injectable formulations, almost inevitably need an expert personnel for administration. Accidental needle sticks causing disease transmission with used syringes is a threat with injectable formulations. The amount of waste generated in terms of syringes, needles, ampoules or vials and plastic packaging is another side of the coin that cannot be ignored. Moreover, sterility and stability of injectable formulations is imperative, making their manufacture, transport and storage conditions critical.

Transdermal drug delivery provides a promising alternative for delivery of drugs against injectable formulations. Application of drug loaded transdermal patches have a number of advantages over oral and parenteral systems. Transdermal delivery systems are generally painless, non invasive or minimally invasive, bypass first pass metabolism, avoid dose dumping, and can release drug in a sustained release manner. However, passive diffusion of drugs through the skin is only limited to molecules with certain physicochemical properties (the Lipinski's rule of five) (Prausnitz & Langer, 2008). This is largely attributed to the barrier property of skin endowed by the stratum corneum, the topmost layer of the epidermis. The stratum corneum is the principal protective layer and comprises of 8–16 layers of flattened, stratified and fully keratinised dead cells. Due to its composition of rigid keratinocytes embedded in a lipid matrix, the stratum corneum greatly limits the number of drug compounds that can be

passively delivered through the skin. Favourable candidates for percutaneous delivery are traditionally small in size (molecular weight<500Da), have low melting points and have low therapeutic doses (Naik, Kalia, & Guy, 2000).

A variety of techniques are used to decrease the barrier property of the skin including physical methods like iontophoresis, sonophoresis, electroporation and microneedles or chemical techniques like use of permeation enhancers. Microneedles are micron sized needles which combine the advantages of a hypodermic syringe and a transdermal patch. The microneedles pierce the skin and create microchannels which allow for transport of molecules into and across the skin. Since these microneedles do not reach the lower dermis where nerve endings and blood vessels reside, there is no pain or bleeding associated.

The choice of material for fabrication of microneedles is generally based on mechanical strength of the material, biocompatibility and biodegradability. The fabrication process depends on the needle material and the geometry. Microneedles have been prepared using various materials and different manufacturing techniques. Previously, most of the microneedles for transdermal drug delivery were solid or hollow microneedles fabricated from silicon, metal or glass using micromachining, lithography or etching. The fabrication costs in these cases are very high due to the precision tools used, limiting its use for mass-production. The micromolding technique which involves the use of a master mold and a corresponding needle free negative secondary mold can be used to prepare polymeric microneedles. Polymeric microneedles prepared by micromolding offer a cost-effective solution for mass production since the same master and production mold can be re-used to make hundreds of polymeric microneedle arrays (Bediz et al., 2014). Only in the past few years, fabrication of microneedles

using polymers has gained significant attention. Biocompatible and/or biodegradable polymers have also been used to fabricate microneedles in the recent years. However, the range of polymers used for fabricating microneedles has been limited. There is a need for use of better biocompatible and biodegradable polymers for preparation of microneedles.

Use of biocompatible polymers have been stressed in the preparation of microneedles previously. The major motivation behind use of biocompatible and biodegradable polymers for microneedle fabrication is its safety aspect if the needle breaks and is left in the skin. Zein, the protein from corn provides an excellent substrate for microneedle fabrication. Zein has previously been used to prepare coatings, chewing gums, adhesives etc., (Lawton, 2002). Zein, being a protein is also expected to interact better with protein based drugs, increasing their loading in case of coated microneedles and also improving the stability of protein drug compared to that in a solution or suspension.

From a practical perspective, the physiochemical properties of the molecule, specifically its hydrophilicity do not allow it to pass through the skin barrier and achieve therapeutic concentrations. Such molecules are excellent candidates for transdermal drug delivery. It might seem that transport of a molecule across skin as influenced by its physicochemical would not play a role when delivered using microneedles. However, the microneedle substrate properties, the drug loading or coating technique and use of polymers to achieve higher coating efficiencies can affect the way drug is loaded and released. There is a need to understand this behaviour if the best material and process combinations are to be found.

Microneedles can also be used to deliver chemotherapeutics to cancers which are superficial or can be reached through the skin like head and neck cancers, breast cancer and melanoma. The drug would form a depot which diffuses over time providing sustained release. Delivering chemotherapeutics using microneedles could reduce the side effectives that accompany non targeted oral or injectable therapies. Also, drugs with difficult physicochemical properties for injectable or oral formulations could be formulated using the microneedle approach.

Chapter 2

Objectives and specific aims

Microneedle system has been developed to deliver chemical and biological agents through the stratum corneum, which is the main barrier to drug delivery. Polymer microneedles have been fabricated from various kinds of polymers, including biocompatible, biodegradable, and water-soluble polymers. Polymer microneedles offer the benefits of ease of fabrication, cost-effectiveness, and mass production, as well as provide controlled drug release using the water solubility and degradation properties of polymer. Micromolding technique for preparation of polymeric microneedles further offers an inexpensive and scalable way for preparation of these microneedles. Both small molecules and macromolecules can be delivered using microneedles. Drugs can be coated onto/loaded into microneedles based on the substrate properties and desired therapeutic concentrations. Co-delivery of multiple therapeutic agents can also be achieved with microneedle based transdermal delivery.

To this end, the overall objective of this study is to investigate the feasibility of using polymeric microneedles as a carrier for delivery of small and macromolecule therapeutics. In the present thesis, breast cancer and transcutaneous immunization were taken as models to prove our hypothesis. Zein, polyvinyl alcohol and polyvinyl pyrrolidone were used for preparation of microneedles. Zein is a prolamin and is the alcohol-soluble protein of corn which has been used in the manufacture of biodegradable plastic, coatings, cosmetics, chewing gum, etc. PVA and PVP are FDA-approved, highly water soluble polymers which are used in a variety of dosage forms. Anticancer drugs, tamoxifen, gemcitabine, doxorubicin and docetaxel were small molecules studied for microneedle assisted transdermal drug delivery. Doxorubicin and docetaxel are given alone or in combination for metastatic breast cancer and locally advanced

breast cancer respectively. Tamoxifen is administered both as prophylactic and therapeutic treatment for early and locally advanced breast cancer. Gemcitabine is administered for metastatic breast cancers. Ovalbumin was used as model antigen for transcutaneous immunization. Ovalbumin is the most widely used antigen used as a model for immunization studies *in vitro* and *in vivo*.

The major objectives and specific aims for this work are listed below.

Objective I. Ovalbumin loaded zein microneedles for transcutaneous vaccination

Specific aims:

(i) To prepare and characterize ovalbumin loaded zein microneedles

(ii) To study the release and skin permeation of ovalbumin from loaded zein microneedles.

(iii) To study the transfer of microbial load with use of zein microneedles

(iv) To study the environmental stability of ovalbumin loaded zein microneedles.

(v) To study the efficacy of ovalbumin loaded zein microneedles for transcutaneous immunization *in vivo*.

Objective II. Zein microneedles for delivery of breast cancer agents, tamoxifen and gemcitabine

Specific aims:

(i)   To design, fabricate and characterize zein microneedles.

(ii) To study the drug loading and *in vitro* release behavior of gemcitabine and tamoxifen from zein microneedles.

(iii) To study the skin permeation of tamoxifen and gemcitabine after application of drug loaded zein microneedles to skin.

Objective III. Co-delivery of doxorubicin and docetaxel using dissolvable polymer microneedles for treatment of local breast cancer

Specific aims:

(i) To design, prepare and characterize dissolvable microneedles for transdermal drug delivery.

(ii) To study the drug loading, *in vitro* drug release and *ex vivo* skin permeation of anticancer drugs from dissolvable polymeric microneedles.

(iii) To study the efficacy of drug loaded polymer microneedles for treatment of breast cancer.

Chapter 3

Background and literature review

3.1 The skin

The skin is the largest organ of the human body and covers over $1.8m^2$ of body surface in an adult. Although approximately 3 mm thick, the skin is an uneven, elastic and excellent barrier membrane to the internal anatomical parts of the body. The skin is made of two distinct layers as discussed by Barry et al. – a stratified avascular cellular epidermis and dermis layer beneath made of connective tissue (Barry, 1987). A basement membrane serves as an anchor and also structurally and functionally separates the epidermis and dermis. A graphical representation of the skin structure is shown in figure 3.1.

The thickness of the epidermis varies between 50–150 μm at different parts of the body. The epidermis has no innervation of blood vessels; the transport of nutrients to epidermis generally occurs via diffusion through intercellular matrix after selective permeation across the basement membrane. The epidermis is further divided into four sublayers: stratum corneum, stratum granulosum, stratum spinosum and stratum basale. The primary cells called the corneocytes or keratinocytes originate in the stratum basale and travel upwards. As the cells move outward, they secrete keratins and become thin, hard and dry forming the stratum corneum.

This horny dead layer is composed of 8-16 layers of flat non nucleated completely keratinized dead cells. The journey from the basale towards stratum corneum takes about 12-14 days. At the stratum corneum, each cell is about 34 to 44 μm long, 25 to 36 μm wide and 0.15 to 0.20 μm thick and is replaced every 2-3 weeks (Neena Washington, 2001).
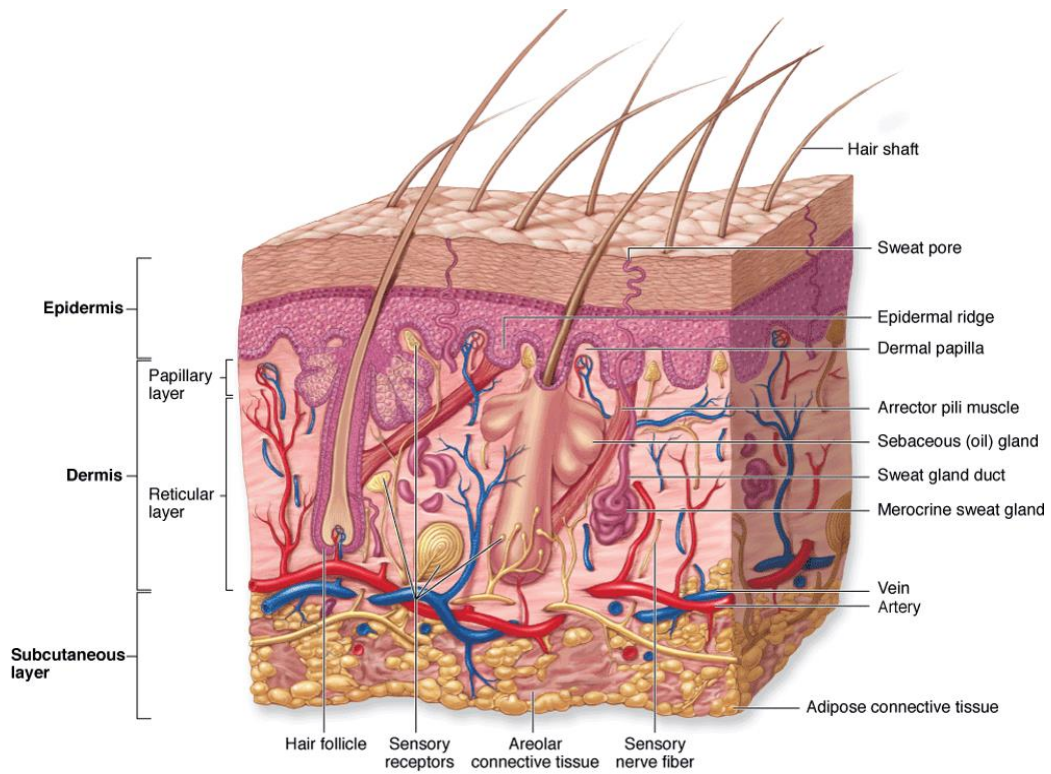
Figure 3.1 Structure of the skin. Image adapted (Mescher, 2013)
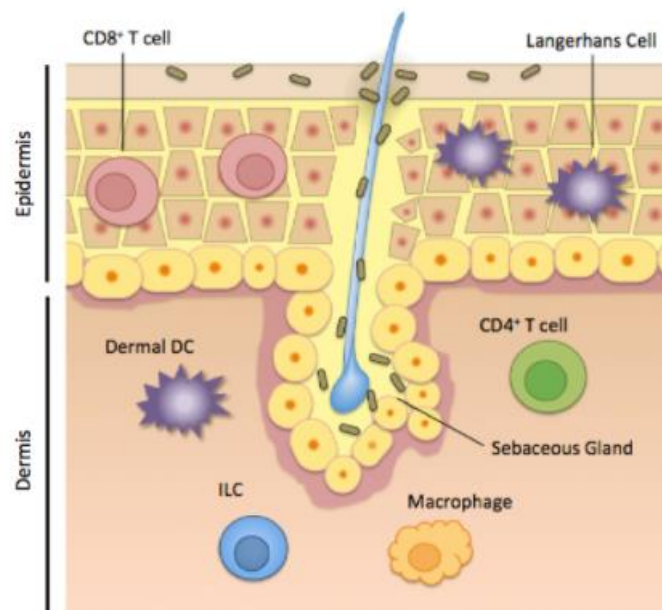
Figure 3.2 Cellular components of the skin immune system. Modified image adapted form (Pasparakis, Haase, & Nestle, 2014). ILC: Innate lymphoid cells

The structure of stratum corneum has been closely studied owing to its principal barrier nature limiting skin permeation. The 'brick and mortar' model is most often used to describe its structure. The model describes the stratum corneum with corneocytes as bricks cemented into a sea of intercellular lipid 'mortar'. Due to the continuous hydrophobic path formed by the intercellular lipids, permeation of drug molecules is a challenge. Various techniques are used to disrupt this structure and form a hydrophilic path to allow drug permeation.

3.1.1 Immune system of the skin

Streilein first proposed a branch of the immune system specialized to provide cutaneous immunity. He introduced the concept of skin associated lymphoid tissue (SALT) in 1978. SALT is analogous to the gut, bronchial, or conjunctival associated lymphoid tissues (Streilein, 1983). Immunity can be classified broadly as innate immunity and adaptive immunity. The physical barrier, stratum corneum in the skin forms the innate (physical) part of the immunity. The adaptive immune system reacts when there is a breach to the stratum corneum. The cellular and molecular components along with the stratum corneum form the skin immune system. Langerhans cells, keratinocytes, T lymphocytes, mast cells, dermal dendritic cells and melanocytes form the cellular components of the skin (Figure 3.2)

The Langerhans cells form the first line of defense for the cellular component of the skin immune system. In 1868, Paul Langerhans, a medical student observed intraepidermal dendritic cells in skin impregnated with gold chloride. These cells make up 2–4% of the epidermal cells forming a "immunological net" parallel to the skin surface (Wolff & Stingl, 1983) (Salmon, Armstrong, & Ansel, 1994).

Langerhans cells present antigen in the context of class II MHC molecules to naive T cells in the induction of cell-mediated immunity and to memory and effector T cells in the expression of cutaneous immune responses (Streilein, Grammer, Yoshikawa, Demidem, & Vermeer, 1990).

Apart from LCs, T cells are also part of the skin immune system. T cells can be categorized based on expression of CD4 (T helper cells) or CD8 (cytotoxic T lymphocytes). Helper T cells (Th), cells are CD4 positive. Between the types of T helper cells, Th 1 promotes inflammation, secretes IL-3, interferon, and tumor necrotic factor while Th 2 cells stimulate B cells to produce antibodies, and secrete IL-4, IL-6 and IL-10. Cytotoxic T cells (Tc) which are CD 8 positive are capable of destroying allergenic and virally infected cells. Similar to the Langerhans cells in the epidermis, another subpopulation of the dendritic cells is found in the dermis. DDCs are primarily located in the vicinity of the superficial vascular plexus. Mature DDCs express high levels of MHC-class I and class II molecules in addition to adhesion and co-stimulatory molecules such as CD54, CD58, CD80, CD86 and CD40 which are required for interaction with T cells (Lotze & Thomson, 2001). Further, melanocytes produce a number of cytokines that may mediate inflammation in the epidermis and dermis.

3.2 Transdermal drug delivery system

Delivery through skin is considered as an attractive alternative to oral and parenteral drug delivery. Transdermal delivery systems have been used to delivery drugs locally as well as systemically. These delivery systems can be for cosmetic purposes (eg. anti-ageing serums, dermarollers etc. for fine lines and wrinkles), occlusive purposes (e.g. sunscreens for protection from UV exposure), topical drug delivery (e.g. local anaesthetics) or systemic drug delivery (e.g. scopolamine

for motion sickness). However, the barrier properties of skin limit the transport of molecules. There are three ways in which a molecule can pass through the skin, (i) through sweat pores, (ii) through skin appendages or (iii) through the stratum corneum. Alternatively, the delivery routes can be classified as intercellular (between the corneocytes, through the intercellular matrix) and transcellular (through the protein filled cells and across lipid-rich regions in tandem) based on the hydrophilicity of the molecules and transport route as shown in Figure 3.3. For each penetrant, the relative importance of these dual routes depends among other things upon its solubility (or chemical potential), its partition coefficients for the various phases and its diffusivities within these phases, be they proteinaceous or lipid.(Barry, 1987) Only molecules with optimal physicochemical properties can passively diffuse through the skin membrane. Relatively hydrophilic molecules follow the transcellular pathway and as the hydrophobicity of molecule increases, it would be transported through the lipid filled intercellular path.
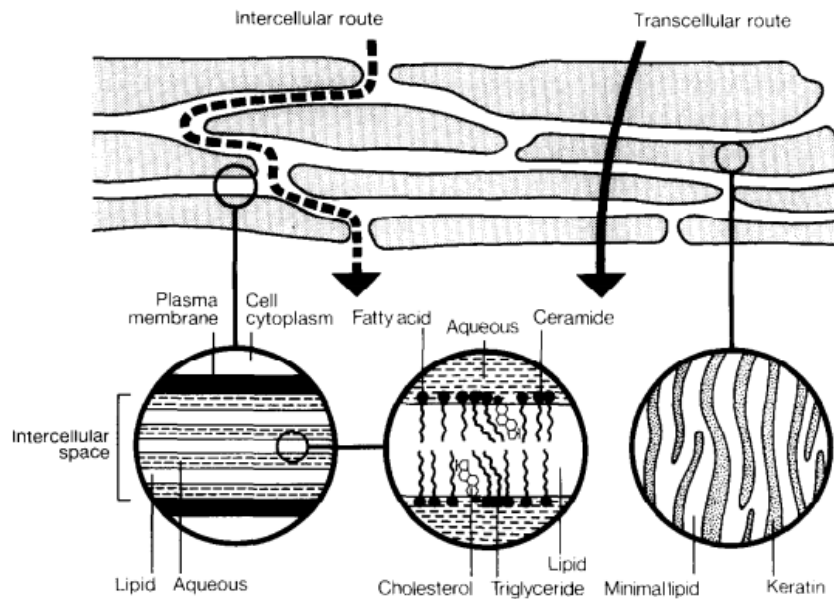
Figure 3.3 Suggested routes of drug penetration through human stratum corneum; macroscopic and molecular domains. Image reprinted from (Barry, 1987).

Over the years, many different chemical and physical permeation enhancement techniques have been developed. Prausnitz et al have categorized these techniques based on generations (Prausnitz & Langer, 2008). First generation techniques include topical creams, topical gels, topical ointments, topical sprays and almost all of the transdermal patches. The second generation techniques aim to disrupt the stratum corneum barrier (reversibly) and include a driving force to increase transdermal penetration while not harming the normal deeper lying cells. Second generation techniques majorly include most of the chemical permeation enhancers, iontophoresis and noncavitational ultrasound. The third generation of transdermal delivery systems have a major impact on the stratum corneum ensuring its stronger and longer disruption while being highly localized so as to not disturb the surrounding or deeper tissues. Third generation delivery systems include combination of chemical enhancers, bioenhancers,

electroporation, cavitational ultrasound, microdermabrasion, thermal ablation and microneedles.

The first transdermal patch which was approved for systemic delivery was in 1979 for sustained release of scopolamine for three days to treat motion sickness (Wiedersberg & Guy, 2014). A transdermal patch essentially contains a drug reservoir and layer to control the release of drug through the patch. The most widely used system for transdermal drug delivery is the membrane-permeation controlled system, in which diffusion across a polymer membrane controls the delivery rate (Neena Washington, 2001). Approximately 19 patches including those with nicotine, menthol, and estradiol are commercially available to date (H. Lee et al., 2017). Transdermal patches are largely limited to drugs with certain physicochemical properties and disease conditions.

Chemical enhancers facilitate skin penetration of the drug by interacting with skin proteins and increasing drug solubility. Most of the known chemical permeation enhancers belong to the following groups: alcohols, fatty acids, esters, azone, amides, hydrocarbons, surfactants, terpenes, sulfoxides and phospholipids (Münch, Wohlrab, & Neubert, 2017). Suitably designed combinations of permeation enhancers can work where conventionally used permeation enhancers fail since certain enhancer combinations are particularly potent when present at specific and narrow compositions.

Ions of soluble salts can be introduced into the skin using iontophoresis. Electrically charged drugs can be made to penetrate deeper into the skin by applying an electric field across the skin. Uncharged or weakly charged compounds could also move by electroosmotic flow of water generated by the

favoured movement of mobile cations (e.g., Na+) instead of fixed anions (e.g., keratin) (Pikal, 2001).

Ultrasound has been used to increase the permeation of various drugs. The concept of ultrasound for transdermal delivery was first reported by Fellinger and Schmidt in 1950 for the successful treatment of polyarthritis using hydrocortisone ointment combined with ultrasound. The effects of noncavitational ultrasound are limited to increasing the permeability of small lipophilic molecules since more aggressive ultrasound is associated with tissue heating and damage to deeper tissues (Prausnitz & Langer, 2008). When using cavitational ultrasound for transdermal delivery, the ultrasound is concentrated in the region of bubbles; since bubbles are more difficult to grow and oscillate within densely-packed tissue, cavitation preferentially occurs within the coupling medium (e.g., a hydrogel) between the ultrasound transducer and skin. Cavitation bubbles oscillate and implode at the skin surface, generating localized shock waves that impact the skin creating imperfections in stratum corneum structure. These imperfections increase permeability of hydrophilic small molecules and macro molecules through skin (Ogura, Paliwal, & Mitragotri, 2008). Short timed high voltage electrical pulses (electroporation) have been shown to increase transdermal transport for small (fentanyl, timolol, orcalcein etc.), large molecules (LHRH, calcitonin, heparin, FITC-dextran etc.) as well as DNA (Alkilani, McCrudden, & Donnelly, 2015) (Hooper, Golden, Ferro, & King, 2007).

Recently, small peptides (1000–1500 Da) have been recognized as safer replacements in improving the skin delivery of small and large molecules into and across the skin (Y. Chen et al., 2006) (Hsu & Mitragotri, 2011). Another application, thermal ablation utilizes μs–ms long heat pulses generated by

electrical filaments, radiofrequency electrodes or lasers, which create microscopic holes in the skin allowing even larger molecules to pass through with greater flux. Preclinical studies have demonstrated enhanced penetration of human growth hormone and interferon α-2b using thermal ablation. A cosmetic approach to remove stratum corneum known as dermabrasion has been employed to increase the permeation of drugs across skin. The technique involves sand blasting at a microscopic scale. Microdermabrasion is known to increase the permeation of drugs such as lidocaine and 5-fluorouracil (Herndon, Gonzalez, Gowrishankar, Anderson, & Weaver, 2004) while vaccination using this approach has also been reported (Harvinder S. Gill et al., 2009) (Glenn et al., 2007).

3.3 Microneedles

Among the most recent and promising techniques to improve drug permeation into and across the skin is the application of microneedles (MN). MN could be single or an array of micron-sized needles that can penetrate the epidermis and upper dermal layer of the skin. Each MN typically has a diameter of a few hundred microns which recedes towards a sharp tip, with a total length of up to 1000 μm (Donnelly, Raj Singh, & Woolfson, 2010). MN bypass the stratum corneum to deliver actives directly to the epidermis or dermis. The length of the MN and insertion forces determine the depth of tissue insertion. Since MN generally do not penetrate beyond the reticular dermis, they do not cause bleeding or pain as the epidermis does not contain blood vessels and nerve innervations. Moreover, the MN can tailored to act in a variety of ways based on its material of construction, drug loading approach and treatment approaches.

3.3.1 History of microneedles

The term 'microneedle' has been reported in research literature in as early as 1921 when Robert Chambers used MN for micro-dissection of echinoderm egg by injecting the needle into the nucleus of the egg (Chambers, 1921). A previous study reported in 1914 by the same author used a similar approach where male germ cells of Disosteira Carolina, a grasshopper, and of Periplaneta Americana, a cockroach, were dissected using a 'needle'(Chambers, 1914).

The concept of MN for drug delivery was first reported in a US patent filed on May 17, 1971 (patent granted June 22, 1976) for an invention by Martin S Gerstel and Virgil A Place. Here, MN were described as a drug delivery device comprising a number of projections, where the projections extend from the drug reservoir, intended to penetrate into the skin for localized or systemic delivery of the drug. The patent described both solid and hollow MN (Gerstel & Place, 1976). Although, the concept of MN was introduced by Gerstel and Place, the term 'microneedle' was introduced in 1998 by Henry et al. which was also the first report of MN being used for skin delivery (Henry, McAllister, Allen, & Prausnitz, 1998). MN were prepared using reactive ion etching micro- fabrication technology and increases the permeation of calcein in skin four times than passive topical application. Over the next year, different types of needles were reported. The first drug coated MN based device was reported by Pistor Michel Louis Paul in another patent describing MN as a device comprising micro- puncturing structure in combination with drug applied on the surface of the MN or on the skin pretreated with MN (Paul, 1975).

In 2001, Alza Corporation reported development of solid metallic MN for the transdermal delivery of antisense oligonucleotides (Bevers, 2001). The first report on use of MN for skin immunization was published in 2002 where Mikszta et al. reported the efficacy of silicon microprojections for immunization with naked plasmid DNA in a mouse model (Mikszta et al., 2002). The study also evaluated the safety of the microprojections in human subjects based on erythema and edema scores. The first study reporting feasibility of MN assisted transdermal delivery of macro- molecules and nanoparticles was published in 2003 by McAllister et al. Solid and hollow MN were used for delivering insulin, albumin and 100 nm sized latex beads through human cadaver skin (McAllister et al., 2003).

Dissolvable MN were reported for the first time in 2005 by Miyano et al. where an array of maltose MN containing ascorbate-2-glycoside as a model drug were prepared and studied in healthy human volunteers (Miyano et al., 2005). The MN were well tolerated and they spontaneously dissolved in the skin releasing ascorbate into the epidermis and dermis. In 2005, the first report on use of hollow glass-MN for extracting dermal interstitial fluid for monitoring of glucose was published (Wang, Cornwell, & Prausnitz, 2005). The first report on cosmetic application of MN (collagen induction therapy) was published in 2005 by Fernandes et al. Skin tightening and wrinkle reduction after application of MN-roller over target skin in the patients was observed (Fernandes, 2005). Over the past decade, MN have not only been developed for cosmetic and drug delivery applications, but also have been explored for biological fluid sampling, allergy testing, vaccination, and photodynamic therapy, among other applications

(Bhatnagar, Dave, & Venuganti, 2017). Figure 3.4 shows a chronological timeline of the events in MN development.

3.3.2 Microneedle designs

MN can be classified based on different parameters including material of construction, applications, manufacturing technique, and the design. Figure 3.5 shows a general classification of MN.

There are different mechanisms of MN application in the skin using different kinds of MN. The development and advancement of MN designs has been based on various limitations of the previously available designs. The first MN for therapeutic applications were fabricated out of silicon. Since then, MN have been fabricated out of different materials, including glass, metals, polymer, and ceramic, and in a variety of shapes and sizes, as needed for different therapeutic applications. Few of these have been tested in the clinical setup and patented. For example, the BD Soluvia™ and MicronJet 600™ which have been approved for marketing.MN assisted therapeutic delivery started off with the "poke and patch" approach using solid metal or silicon MN. The "poke and patch" approached utilizes solid MN, generally made of metal or silicon, to pretreat the skin. This pretreatment creates micropores in the skin. The pretreatment is followed by application of drug formulation, generally a transdermal patch. This technique has been shown to increase the penetration of a number of drugs. However, it suffers from various disadvantages including lesser permeation due to absence of a driving force for passage into skin and faster resealing of skin pores. Alternatively, drug was coated onto these solid MN and allowed to be inserted into the skin.
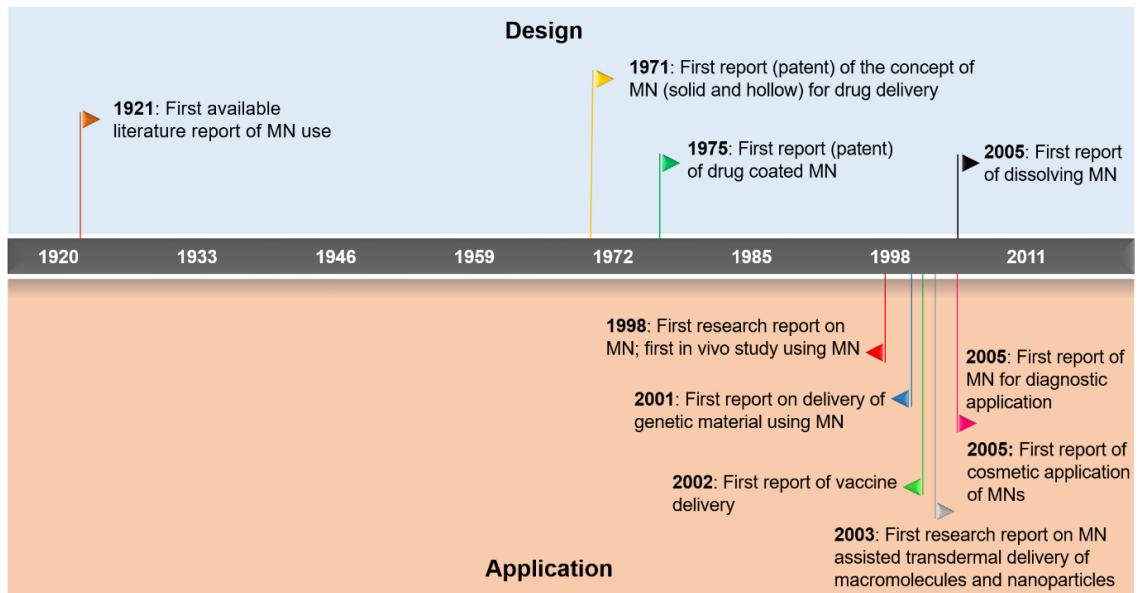
Figure 3.4 Chronological timeline of microneedle development with important design and application milestones. Image reprinted from (Bhatnagar et al., 2017).
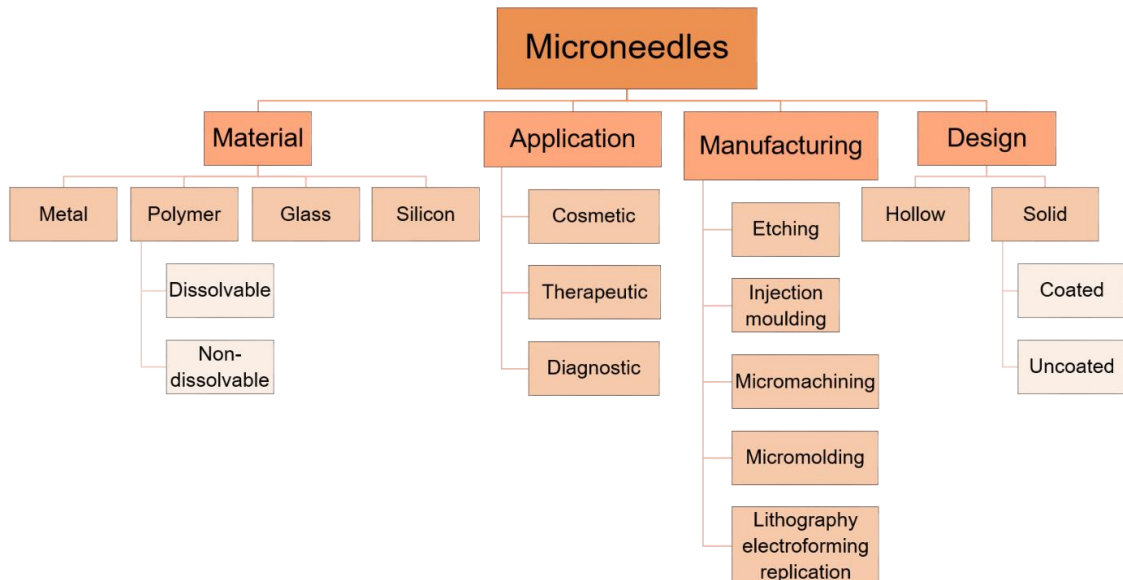
Figure 3.5 General classification of microneedles. Image reprinted from (Bhatnagar et al., 2017).

This technique called the "coat and poke" approach worked better but could only be used for drugs with very low doses generally vaccines. To overcome these problems, hollow MN were invented. The hollow MN could be inserted into the skin and would allow for passage of the drug solution into the skin driven by pressure. The use of hollow MN for drug delivery is called the "poke and flow" approach. The fact that hollow MN were susceptible to clogging, could not be used outside clinical setups and were made of glass or metal which could break off and be left in the skin causing injuries, paved way to the development of polymeric MN.
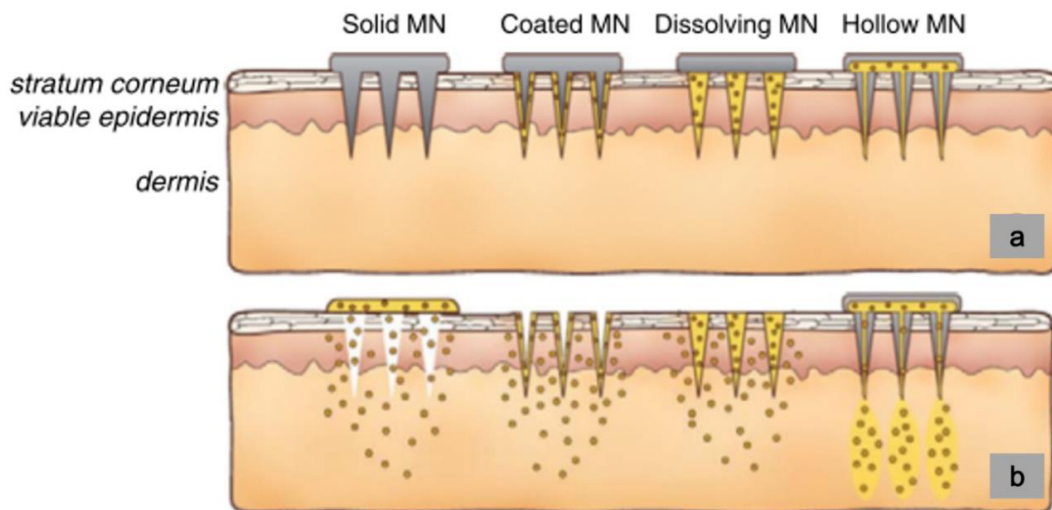
Figure 3.6 Different mechanisms of microneedles applications in the skin (a) and respective drug release strategy (b). Image reprinted from (Y.-C. Kim, J.-H. Park, & M. R. Prausnitz, 2012).

Polymeric MN could be made from biocompatible and biodegradable materials containing the drug of choice either encapsulated within the polymer matrix or coated over prepared polymeric needles. The physicochemical properties of drug play a major role in preparation of drug coated MN. Polymeric MN, which dissolve upon insertion into skin and releasing the encapsulated cargo

have also bee developed to further enhance the drug delivery and reducing the time of action. Schematic representation of the different techniques of drug delivery through MN are shown in Figure 3.6. We discuss the various MN designs under the broader subsections of "hollow" and "solid" MN below.

3.3.2.1 Hollow MN

Hollow MN provide a defined channel for drug delivery into the skin. Hollow MN enable pressure-driven flow of a liquid formulation. Injection of drug solutions through the hollow MN can provide control over the time and amount of drug delivered, and can achieve a wide variety of delivery profiles (Wang, Cornwell, Hill, & Prausnitz, 2006). When designing a hollow MN, care should be taken with the tip design. The tip design of hollow MN is crucial since it directly affects the mechanical strength of needle and the skin insertion behaviour. The needle tip should allow for continuous flow of fluid without the opening getting clogged. Larger tip radii need greater force of insertion, whereas smaller tip openings are susceptible to blockage. Interestingly, needles with opening on the side instead of centre of the needle tip offer better flow and lesser clogs (Bal, Caussin, Pavel, & Bouwstra, 2008).

Hollow MN are generally made of metals or silicon. These can be fabricated as in-plane or out-of-plane needles (Figure 3.7). In-plane MN are formed parallel to the fabrication surface where a range of MN lengths and designs can be machined. Sophisticated machinery is required for fabrication of in-plane MN. This design also offers easier integration with lab-on-chip techniques. Out-of-plane MN can be defined as a back plate seamlessly combined with MN vertically protruding from the surface. These are formed perpendicular to the fabrication surface and are relatively easy to machine to obtain a large

density of needles per array (Gardeniers et al., 2003) Out-of-plane MN can be hollow or solid in structure.

In-plane microneedles   Out-of-plane microneedles
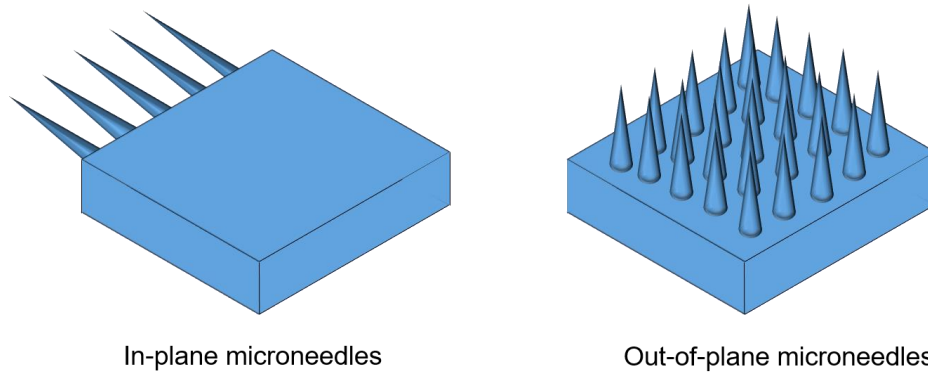
Figure 3.7 In-plane and out-of-plane microneedles.

Originally, hollow MN were prepared by pulling borosilicate glass with a micropipette puller. Post preparation, these needles were bevelled to 20–30° angles. The needle tips were sharp with tip radii between 15–40 μm. These needles were used to deliver insulin to adults (Wang et al., 2006). Over time, considerably smaller hollow MN have been fabricated using stainless steel and silicon. These needles have been fabricated in different needle shapes including cylindrical, conical, rectangular and pyramidal (Baron, Passave, Guichardaz, & Cabodevila, 2008; Diehl & Jensen, 2007; Meyer, Markowicz, Rendon, Smithson, & Simmers, 2014). MN developed for diagnostic purposes also largely involve the use of hollow MN for extraction of micro-quantities of interstitial fluid (Romanyuk et al., 2014; Strambini et al., 2015). The only MN products for therapeutic use approved by the FDA for marketing are based on hollow MN. BD Soluvia™, the first MN device approved for transdermal application is a prefilled liquid injection device including include hollow MN tip for delivery of therapeutics (Quinn, Kearney, Courtenay, McCrudden, & Donnelly, 2014). It is essentially a 1.5mm long 30G hollow stainless steel needle connected to a glass

prefilled syringe shielding system that jackets the needle (Figure 3.8a). The injection can deliver between 100 and 200 µl of fluid. Another approved hollow MN system is the MicronJet 600™ (NanoPass Technologies, Israel). It is produced using the Micro-Electro-Mechanical System (MEMS) fabrication technology. It consists of a single 3D crystal silicon chip which is etched to yield three pyramid shaped needles, each 600 µm long with sharp tips to penetrate the epidermis. The tip is followed by a conduit for fluid delivery (Figure 3.8c and d). The chip is mounted on a plastic base support which can fix to any typical syringe forming a direct passage for fluid delivery.
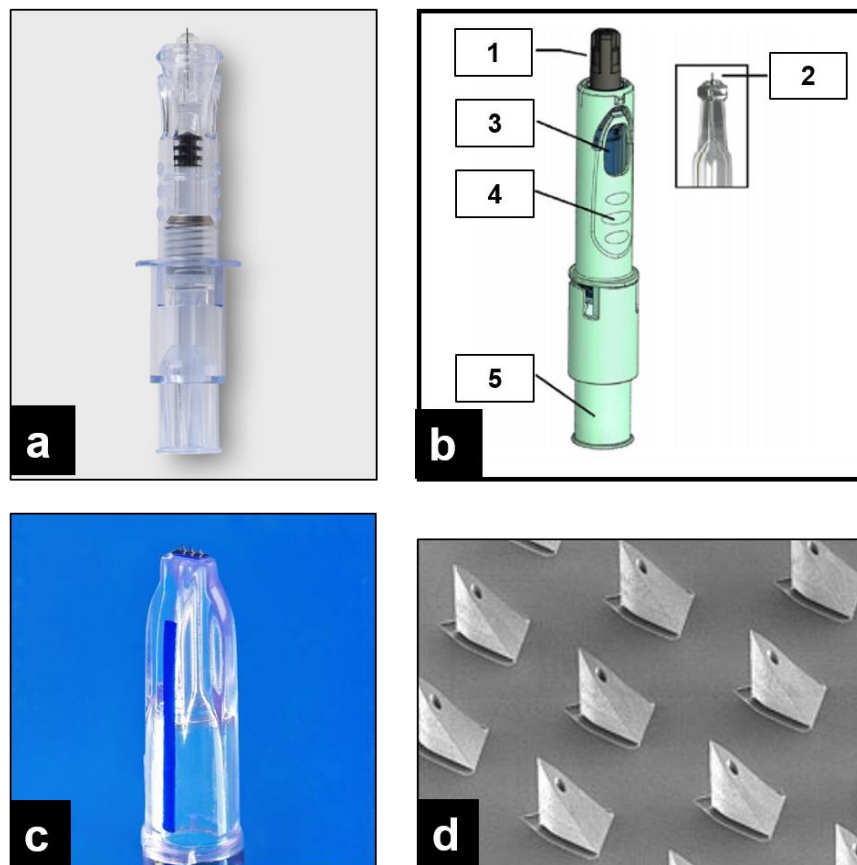
Figure 3.8 Hollow microneedle designs approved for market. (a) BD Soluvia™; (b) Different parts of BD™ Micro Injection System: MN shield (1), MN attached to the syringe tip (2), space to view vaccine solution (3), pads for finger grip (4) and plunger rod (5); (c) The MicronJet 600™ MN assembly; (d) SEM image of MicronJet™ MN. Image adapted from (Bhatnagar et al., 2017).

3.3.2.2 Solid MN

The first solid MN were prepared from silicon using micromachining technique (Mikszta et al., 2002). Over the last two decades, studies have reported multiple solid MN designs with silicon. Technological advances in the micromachining in the 1990's paved way to easier fabrication of solid MN made from metal or silicon. Metals such as stainless steel, titanium and nickel are most

commonly used to fabricate solid MN. Commonly, wet or dry etching, 3D laser ablation, laser cutting and metal electroplating methods are used for fabricating solid MN. Laser cutting followed by electro-polishing offers a versatile solution for fabrication of solid MN with varied shapes and geometries (H. S. Gill & Prausnitz, 2007). Both metal and silicon based solid MN were initially used for skin pre-treatment for the 'poke and patch' approach but their major use now involves them to be coated with the therapeutics of interest for drug delivery. Surface modifications of these MN have been made in many cases for better attachment to drugs, mainly proteins and peptides (van der Maaden et al., 2014). Even though the manufacture of silicon and metal MN using micromachining techniques bids likelihood for high throughput manufacturing, it suffers a setback due to involvement of intricate multi-step processes and the need for highly specialized and expensive machining tools.
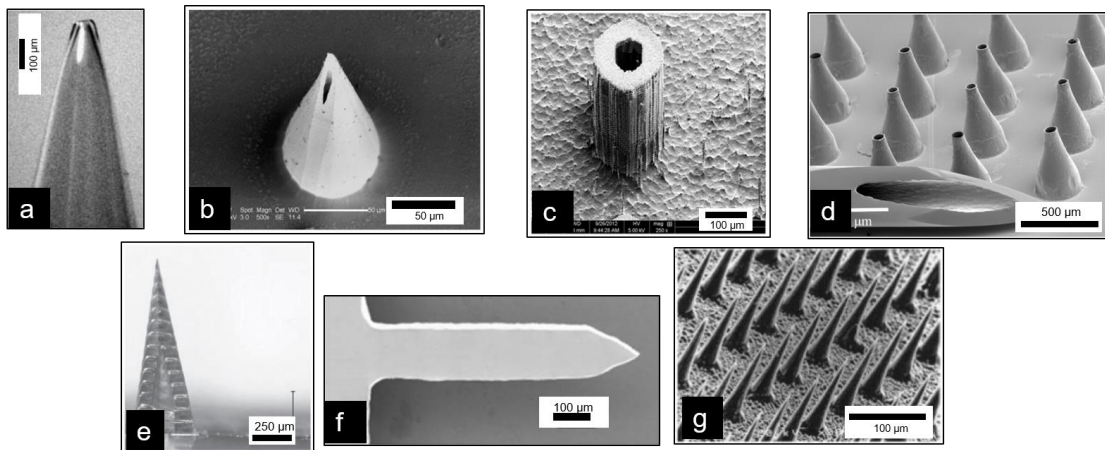
Figure 3.9 Different hollow and solid microneedle designs. (a) Hollow bevel tip borosilicate glass MN; (b) Hollow MN fabricated using SU-8 photoresist polymer; (c) Hollow MN fabricated using silicon; (d) Nickel MN against a conventional 27G hypodermic needle tip; (e) Silicon MN for potentiometric K^+ determination in interstitial fluid; (f) Single solid stainless steel needle; (g) Sharp tapered silicon solid MN (Bhatnagar et al., 2017).

3.3.3 Polymer MN

Polymeric MN have been prepared using a number of techniques including hot air blowing, micromolding, and injection molding. The droplet-born air blowing technique involves polymeric solution placed as fixed volume drops on a glass or metal substrate. Another plate is slowly added above the drops to touch them. The plates are then pulled away slowly while hot air is passed between the plates drying the polymer. Finally, the thin fragile polymeric thread connection between the two plates is cut resulting in sharp polymeric needles on two plates.

In the microinjection method, a molten plastic substance is injected between two micro-machined molds that contain microhole and micropillar arrays. Once the desired shape of the MN array has been formed, the mold and the plastic material are cooled down. Next, the molds are separated and the plastic MN array is detached from the mold structures.

Polymer MN prepared using micromolding technique offer the advantage of easier and cost effective manufacturing processes. This technique involves fabrication of a master mold which is basically a replica of the desired final design. This master mold is used to prepare a negative needle free secondary mold, generally prepared using polydimethyl siloxane. The use of polydimethylsiloxane (PDMS) in micromolding process has been widely used to replicate microstructures due to its low cost, durability, and transparency. The secondary mold is in turn used to cast polymer MN by pouring/injecting the polymer solution into the mould followed by drying/curing. The primary mold can be formed using metals or silicon using the micromachining techniques or could be made from one of the photopolymers using a high precision 3D printer.

Physicochemical nature of the molecule to be loaded, required therapeutic dose and intended site of action, physical and chemical properties of the polymer used for MN preparation, the technique used for preparation and the length, geometry and number of needles are few major factors to be considered for MN preparation using polymers. A number of polymers, natural, synthetic or semisynthetic have been used to fabricate needles. Most commonly used polymers include poly-lactide-co-glycolide acid (PLGA), poly-L-lactic acid (PLA), poly-glycolic acid (PGA), hyaluronic acid (HA), poly(vinyl pyrrolidone) (PVP), polyvinyl alcohol (PVA), sodium alginate, chitosan, zein, carboxymethyl cellulose (CMC), and hydroxypropyl cellulose (HPC) (Bhatnagar et al., 2017; Y. C. Kim, J. H. Park, & M. R. Prausnitz, 2012). Of these, CMC, PVA, PVP, and hyaluronic acid can be used to form dissolvable MN that can be left inside the skin to dissolve rapidly. Polymers like polycaprolactone can be melted and casted into the molds to develop MN which can be peeled off quickly as the polymer solidifies. The hot air blowing technique can be used to prepare needles with polymeric preparations that dry quickly under higher temperatures but with actives which are not thermosensitive/thermolabile. Materials such as PVP can be used to make dissolvable MN. The vinyl pyrrolidone monomer has a ring structure chemical backbone that gives mechanical strength by increasing intramolecular rigidity which is important for insertion of MN into skin. PVP dissolves rapidly in water to concentrations up to 50% enabling quick release of encapsulated drug molecules after insertion into skin.

MN have also been formulated out of materials like silk, chondroitin sulfate, ceramics, and sugars such as maltose, galactose, and dextrin. Various polymeric MN designs are shown in Figure 3.10. In another step further, MN have

been designed to include micro- and nanoparticles within (for polymeric MN) or on the needle tips (for solid metal MN) (Ma, Boese, Luo, Nitin, & Gill, 2015; J. H. Park, Allen, & Prausnitz, 2006). Interesting MN designs where polymer MN were formed on a bubble at the base, or over metal pedestals or shafts. These designs have shown better skin insertion.

3.3.4 Therapeutic applications of MN

MN were first theorised for drug delivery decades ago, but became the subject of significant research in the mid 1990's when microfabrication technology supported their manufacture. MN have since been used to deliver a broad range of different drugs, biotherapeutics, protein drugs and vaccines. Influenza vaccination using a hollow MN has even been used for clinical use. Moreover, apart from applications in the skin, MN have also been adapted for delivery of therapeutics into the eye and into cells.

3.3.4.1 MN mediated delivery of small molecules

Looking at the published literature, MN have been used to deliver a variety of small molecules including plant extracts (S. Y. Park et al., 2014; Puri, Nguyen, & Banga, 2016), dyes (Caffarel-Salvador et al., 2015), local anaesthetics (Jyoti Gupta, Denson, Felner, & Prausnitz, 2012), antibacterial and antifungal agents (Bhatnagar et al., 2018; Boehm, Miller, Schell, Perfect, & Narayan, 2013), chemotherapeutics (Hao, Li, Zhou, Yang, & Qian, 2017) and anti-hypertensive agents (Kaur, Ita, Popova, Parikh, & Bair, 2014). MN have been shown to treat superficial cancers including oral cancers, breast cancer and ovarian cancer. A large number of studies have shown the proof of concept in animal models for cancer. Doxorubicin entrapped nanoparticles have been coated over metal MN

inserted into buccal tissues and tongue (Ma et al., 2015). A more efficient penetration of doxorubicin was observed in porcine buccal tissue than free drug injection.
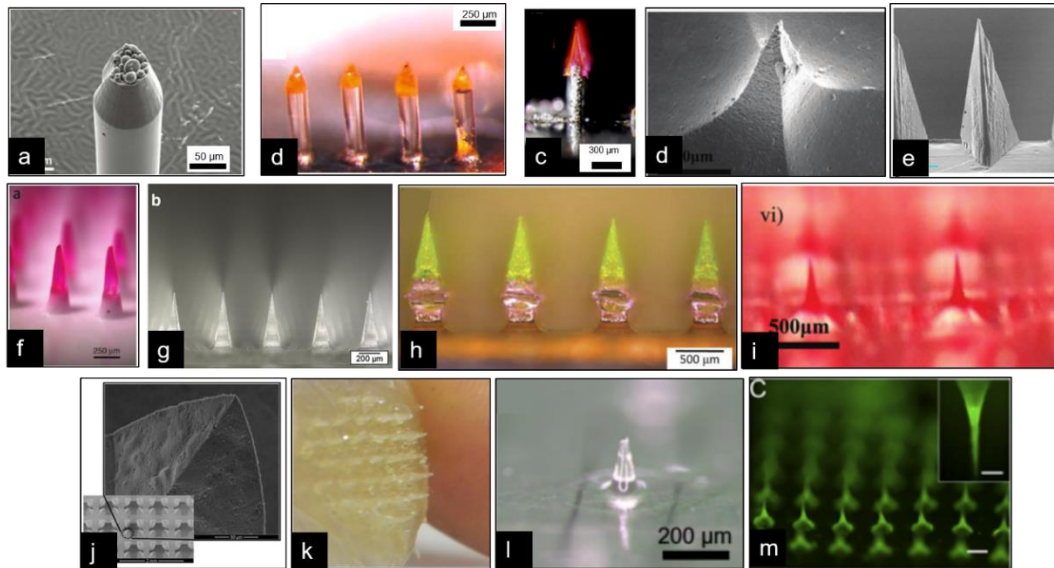
Figure 3.10 Polymer microneedles for transdermal drug delivery. (h) SEM image showing loaded PLA microspheres at the tip of PLGA; (i) Bevel calcein loaded PLGA MN; (j) Dissolvable PVA/PVP MN encapsulating sulforhodamine as separable arrowhead MN over a metal shaft, (k) SEM image of MN prepared using silk; (l) MN prepared using maltose; (f) dissolvable PVP MN for vaccination against influenza; (g) Hyaluronic acid dissolvable MN incorporating exenatide; (h) Chitosan MN for Transdermal Delivery of Luteinizing Hormone-releasing Hormone; (i) MN prepared with silk fibroin; (j) microporous ceramic needles loaded with ovalbumin for transcutaneous immunization; (k) MN prepared from fishscale nanocellulose blends; (l) Bright-field microscopy image of single dissolving MN of epidermal growth factor loaded dissolving MN by by droplet-born air blowing; (m) Crosslinked HA based MN (MN)-array patches integrated with hypoxia-sensitive hyaluronic acid vesicles containing insulin and

GO$_x$. Images reprinted from (Bhatnagar et al., 2017; Boks et al., 2015; M.-Y. CHEN et al., 2017; Huh et al., 2018; Olatunji & Olsson, 2015; Sullivan et al., 2010; Tsioris et al., 2012; J. Yu et al., 2015; Zhu et al., 2014).

Potential of coated MN for improved dermal delivery of 5-aminolevulinic acid for phodynamic theray (PDT) of skin tumors has also been studied (Jain, Lee, & Gill, 2016). With the "poke and patch" approach, a higher penetration of 5-FU and significant tumor reduction was seen in the B16F10 melanoma model in mice (Naguib, Kumar, & Cui, 2014). Polymeric MN, specifically dissolvable ones have been loaded with chemotherapeutics to deliver drug to accessible solid tumors. A light-activable MN system repeatedly and simultaneously provided photothermal therapy and chemotherapy to superficial tumors exerting synergistic anticancer effect has been developed. Embeddable polycaprolactone MN were prepared containing a photosensitive nanomaterial (lanthanum hexaboride) and doxorubicin. The MN base plate was prepared using poly(vinyl alcohol)/polyvinylpyrrolidone. When exposed to near-infrared light, the embedded MN array uniformly heated the target tissue to induce a large thermal ablation area and then melts at 50°C to release loaded doxorubicin in a broad area, thus destroying tumors. This formulation was tested in 4T1 xenograft model in Balb/c mice. MN-mediated synergistic therapy (doxorubicin+ NIR) completely eradicated 4T1 tumors within 1 week after a single application of the MN and three cycles of laser treatment (M.-C. Chen, Lin, & Ling, 2015). In another study, MN assisted DNA vaccination against cervical cancer was shown to be more effective inn terms of TC1 tumor progression in C57BL/6 mice than the intramuscular injection (Ali et al., 2017). Near-Infrared Responsive PEGylated gold nanorod coated Poly(L-lactide) MN have been formulated an shown to

enhance the antitumor efficiency of Docetaxel loaded mPEG-PDLLA micelles for treating A431 tumor in immunecompromised mice (Hao, Dong, et al., 2017).

A limited number of clinical studies using MN with small molecules have been reported. Recently, Zosano Pharma's ZP-Zolmitriptan patch completed a Phase I trial with 10 volunteers (Kellerman, Lickliter, Mardell, & von Stein, 2016). A low dose zolmitriptan patch resulted in higher C_{max} than a higher dose oral zolmitriptan administration. Delivery of lidocaine using hollow glass MN was compared against intravenous injection was compared in a clinical trial involving 15 healthy volunteers (Jyoti Gupta et al., 2012). The results revealed insignificant differences depth of anaesthesia induced between treatments. Additionally, lesser VAS pain scores with MN use than hypodermic needle usage, however the taken for same volume injection with MN took a significant longer 20–40s against 3–5s with hypodermic syringe. Lesser pain was observed with IV catheter insertion after MN application compared with hypodermic injection.

Systemically acting drugs with larger doses cannot be encapsulated into or coated onto needles. In such cases, drug delivery into skin after pre-treatment may work well. Such a molecules, naltrexone, which undergoes significant first pass metabolism when administered orally, has been evaluated in the clinical setup. An array of 50 stainless steel needles, 0.65 mm each, were used to pretreat the skin in 9 healthy volunteers followed by application of naltrexone transdermal patch. Control group's skin was not pre-treated. The blood plasma concentrations after control treatment yielded negligible amounts of naltrexone against steady state concentrations within 2 h after MN pretreatment. In a similar clinical setup, dyclonine delivery has been evaluated in 25 healthy individuals (Li et al., 2010).

Over the last 3 years, exceptional amount of work has been conducted studying the deliverability of small molecules using polymeric MN. Delivery of lidocaine and coumarin was attempted using three layered MN. Drug and NIR absorbers were loaded within PCL which formed the tip of the MN while a supporting array made of PLA was attached using a PVA/PVP layer between them. Drug release was initiated with laser irradiation. Lidocaine delivered by the implanted MN was rapidly absorbed into the blood circulation within 10 min and has a bioavailability of at least 95% relative to the subcutaneous injection (M.-C. Chen, Chan, Ling, & Su, 2017). In another study, acyclovir was loaded into dissolvable MN prepared using Gantrez S-97® to deliver acyclovir for treatment of cold sores (herpes labialis) caused by the herpes simplex virus type 1 (HSV-1). The needles completely dissolved within 2h and successfully provided intradermal delivery of acyclovir over a 48 h period. Acyclovir levels in the skin delivered using MN arrays were superior to those generated by the control cream formulation (Pamornpathomkul et al., 2018). PVP and methacrylate MN have been used to deliver tranexamic acid as a new treatment for melasma. The needles did not show any acute dermal toxicity and were shown to effectively release drug in the skin until complete needle dissolution at 7 hours (A. Machekposhti, Soltani, Najafizadeh, Ebrahimi, & Chen, 2017). Meloxicam, for the treatment of arthritis has also been loaded into dissolvable MN prepared with either PVP/PCL or PVA/PVP. PVP/PCL MN offered several advantages, including rapid release of the encapsulated drug (91.72% within 30 min), efficient drug delivery to skin (79.18%), no obvious skin irritation, a decent relative bioavailability (122.3%) (in SD rats), and strong anti-inflammatory and analgesic effects (in Balb/c mice) (J. Chen et al., 2018). The PVA/PVP MN completely dissolved in 60 minutes. The ex

vivo permeation across rat skin was also found to improve by 2.58 folds along with significantly high skin deposition as compared to plain drug solution (Amodwala, Kumar, & Thakkar, 2017).

Vitamins like Vitamin K and ascorbic acid have also been shown to be delivered using dissolving MN made with Gantrez S-97 or CMC/HA respectively (Huh et al., 2018; Hutton et al., 2018).

3.3.4.2 MN mediated delivery of macromolecules

The stability of proteins during formulation preparation and storage has been an issue. It has been demonstrated that the proteins in the solid state had increased stability during thermal processing than the proteins in the aqueous solution (J. H. Park et al., 2006; Yang et al., 2016). The delivery of macromolecules using MN technology has been attempted for various macromolecules. Proteins with enzymatic or regulatory activity including insulin, desmopressin, erythropoietin, lysozyme, glucagon, glucagon-like peptide-1 (GLP-1), parathyroid hormone (PTH), growth hormone and etanercept have been attempted to be delivered using MN (W. Chen et al., 2017; Y. C. Kim et al., 2012; Jeong Woo Lee, Choi, Felner, & Prausnitz, 2011).

Currently, insulin is administered subcutaneously using a syringe, insulin pen, jet injector or insulin pump which are painful and have lesser patient compliance (J. Gupta, Felner, & Prausnitz, 2011). Insulin delivery using MN is economical, painless and is expected to increase patient compliance. A large number of clinical studies have reported that the pharmacokinetic and pharmacodynamic profiles are comparable for subcutaneous injection and MN are comparable (J. Gupta et al., 2011; Lahiji, Dangol, & Jung, 2015; Ling & Chen,

2013). The safety and efficacy of insulin administered using MN was first evaluated in 10 healthy male adult volunteers (Pettis et al., 2011). Stainless steel MN of various lengths (1.25, 1.5 or 1.75 mm) were used to inject used insulin lispro (10 IU) under euglycemic clamp conditions. The control was same dose subcutaneous injection. A rapid insulin action with shorted T_{max} was observed with MN mediated delivery. Moreover, a higher extent of absorption for shorter MN lengths (1.25 and 1.5 mm) and statistically higher peak insulin concentrations were observed in comparison to the subcutaneous delivery group. Transient localized redness and edema was reported at injection sites. The hollow glass MN discussed in previous sections have also been largely studied in the clinic for insulin delivery. The glass hollow MN has also been evaluated in both paediatric and adolescent populations (Jyoti Gupta, Felner, & Prausnitz, 2009; Norman, Brown, Raviele, Prausnitz, & Felner, 2013). Table 3.1 presents the complete list of studies reported for macromolecule delivery using MN-based devices. Amongst the ongoing clinical trials for diabetes management using MN, a recently completed Phase II clinical trial with MN for type 1 diabetes mellitus management includes the use of glucagon MN patch (NCT02459938).

A good amount of published papers report the delivery of insulin using polymeric MN. Rapidly dissolved MN from 3-aminophenylboronic acid-modified alginate (Alg-APBA) and hyaluronate (HA) were prepared by Yu et al. Alginate was chemically modified by 3-aminophenylboronic acid to prepare Alg-APBA which can form linkages with glucose and realize self-regulated release of insulin. The encapsulated insulin maintained high pharmacological activity, revealing a sustained hypoglycemic effect in diabetic mice with the relative pharmacologic availability (RPA) and relative bioavailability (RBA) at 90.5 ± 6.8 % and 92.9 ±

7.0 %, respectively.(W. Yu, Jiang, Zhang, et al., 2017) Sharp needles with high aspect ratios were prepared by glutaraldehyde crosslinked gelatin/calcium sulphate. Post administration to diabetic rats, the released insulin from biodegradable composite MN exhibited effective hypoglycemic effect for longer time compared with that of subcutaneous injection route (W. Yu, Jiang, Liu, Li, Chen, et al., 2017). Similar pharmacological activity of insulin has been demonstrated when loaded into bioceramic composite MN made from gelatin and hydroxyapatite (W. Yu, Jiang, Liu, Li, Tong, et al., 2017). Stimuli responsive delivery of insulin using polymer MN has been attempted using polymeric MN. In a recently published novel design, glucose- and H_2O_2- responsive polymeric vesicles (PVs) were incorporated with transcutaneous MN for delivery of insulin. The PVs were self-assembled from a triblock copolymer involving with polyethylene glycol (PEG), poly(phenylboronic acid) (PPBA, glucose-sensitive block) and poly(phenylboronic acid pinacol ester) (PPBEM, H_2O_2-sensitive block). After loading with insulin and glucose oxidase (GOx), the drug- loaded PVs displayed a basal insulin release as well as an elevated insulin release in response to hyperglycemic states. The transdermal delivery of insulin to the diabetic rats ((insulin+GOx)-loaded MN) presented an effective hypoglycemic effect compared with that of subcutaneous injection or only insulin-loaded MN (Tong et al., 2018). MN prepared using two PVP grades with a PVP/CMC backing have been prepared with encapsulated insulin. Insulin-loaded PVP MN patches were administered to diabetic mice to evaluate glycemic control. The relative pharmacologic availability revealed that the MN patch has an immediate and effective effect on hypoglycemic administration (I. C. Lee, Wu, Tsai, Chen, &

Wu, 2017). The same research group have also revealed similar results with insulin loaded into gelatin/CMC MN patches.

The stability of insulin has always been a concern when formulating into novel delivery systems. Denaturation of insulin may occur during formulation processes. CMC-based MN have successfully incorporated a variety of protein compounds, including BSA and lysozyme, and were found to be stable after two months of storage (Jeong W. Lee, Park, & Prausnitz, 2008). Recombinant human growth hormone (rhGH) and insulin were stably embedded in MN patches and stored at room temperature for 15 months and one month, respectively(Ito, Hagiwara, Saeki, Sugioka, & Takada, 2006; Jeong Woo Lee et al., 2011). PTH was coated onto MN and retained most of its bioactivity after up to 18 months at room temperature and 60% humidity (Ameri, Wang, & Maa, 2010).

Researchers have investigated the applicability of MN-mediated transdermal technique to deliver monoclonal antibodies. Studies have shown that more than 80% of monoclonal immunoglobulin G (IgG) was recovered with stable tertiary conformation after the dissolution of hyaluronanic acid (HA) dissolvable MN (Mönkäre et al., 2015). Moreover, no formations of IgG aggregation or HA/IgG complexes were detected during the MN preparation process.

Other macromolecules like the Parathyroid hormone (PTH) have been administered using MN in the clinical setup. Zosano Pharma introduced the ZP-PTH patch which consists of 1300 densely arranged titanium MN within an area of 2 sq. cm (Figure 3.11) (Daddona, Matriano, Mandema, & Maa, 2011). The MN array is attached to an adhesive patch and secured within a disposable retainer for

easy application. Phase I clinical trial with Zosano Pharma's PTH loaded patch (ZP-PTH) was conducted in healthy post-menopausal women to evaluate the effects of administration site, patch wear duration, and the PTH dosing (NCT02478879). The Phase I trial revealed a rapid PTH plasma profile with three fold higher T_{max}, and two fold shorter $T_{1/2}$ in comparison to the marketed PTH subcutaneous injection. Further, Phase II clinical trial was conducted with 165 postmenopausal women with osteoporosis (Daddona et al., 2011). The Phase II trial results established the safety, efficacy and tolerability of the ZP-PTH patch. With ZP-PTH, a consistent dose dependent effect for AUC and C_{max} (Figure 3.11b) along with increase in bone mineral density, even at the hip site, was noted.
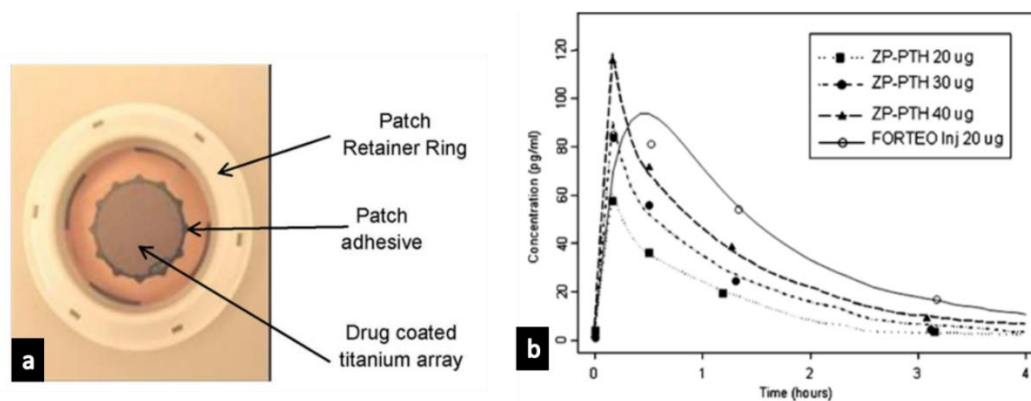
Figure 3.11 (a) Zosano Pharma's (ZP) patch; (b) Phase 2 clinical evaluation of parathyroid hormone (PTH) pharmacokinetics from different doses in ZP-PTH and marketed FORTEO® injection.

In a preclinical setup, chitosan MN were tested for deliverability of goserelin (luteinizing hormone-releasing hormone analogue) as androgen-deprivation therapy (ADT) for prostate cancer. Completely embeddable MN were prepared with chitosan and a dissolvable polyvinyl alcohol/polyvinyl pyrrolidone supporting array. Goserelin could be loaded to 73.3±2.8 μg per MN patch. After applying goserelin-containing MN to ICR mice, serum LH levels increased

initially and then declined below baseline at day 7. In contrast, serum testosterone levels increased to reach a peak at day 14 and then declined to a castration level at day 21 followed by maintenance for 2 weeks (M.-Y. CHEN et al., 2017).

Apart from insulin and hormones, high molecular weight molecules like cyclosporin A and epidermal growth factor (EGF) have also been loaded onto polymeric MN have shown to be effective both in vitro and in vivo (Huh et al., 2018; Jeong, Kim, Kim, & Park, 2018).

Table 3.1 Published clinical studies for delivery of macromolecules using MN. Tabulated data from (Bhatnagar et al., 2017).

Aim of the study	Study population	Therapeutic agent(s)	Delivery technique	Number of subjects	Outcome of the study
1. Determination of minimum insertion depth required for effective bolus delivery of insulin through an MN device in subjects under fasted condition. 2. Assessment of insulin delivery with a bolus infusion immediately prior to a 75 g carbohydrate meal	Subjects with T1DM for 2 years (38 and 43 years)	**Test and Control**: IL	**Test**: Hollow glass MN **Control**: 9mm catheter infusion set	**Test**: 1 **Control**: 1	Faster insulin absorption and reduction in glucose levels when MN were inserted at a depth of 1mm in the skin
Comparison of the pharmacokinetics, postprandial glycemic response and the pain associated with ID insulin delivery using an MN against a conventional catheter	Subjects with T1DM (11–43 years)	**Test and Control**: IL	**Test**: Hollow glass MN **Control**: 9-mm-long subcutaneous catheter	**Test**: 5* **Control**: 5*	Faster insulin pharmacokinetic and better glucose control in test group
Assessment of pharmacokinetics and pharmacodynamic postprandial glycemia in T1DM adults with insulin administered by MN versus SC delivery followed by a standardized liquid meal	Men (18–55 years) with T1DM for 1–15 years	**Test and Control**: IL; RHI	**Test**: 34Gx1.5-mm steel MN **Control**: SC injection	**Test**: 29* **Control**: 29*	Similar PPG between ID RHI and SC IL, both at -2 min; Significantly faster uptake, shorter t_{max}, higher C_{max}, and shorter half-life for ID IL and ID RHI PK data in comparison to SC administration
Assessment of pain and onset and offset of insulin PK in children and adolescents with T1DM upon insulin ID delivery using hollow MN versus SC insulin pump.	10–18 year children and adolescents with T1DM for ≥2 years	**Test and Control**: IL	**Test**: < 1mm hollow MN Control: syringe pump (SC)	**Test**: 16* **Control**: 16*	Significantly lower MN insertion pain Vs. subcutaneous catheter; 22 and 34 min faster insulin onset time and offset time respectively against SC delivery
Comparison of PK and PD effects of IL administration by MN based ID or SC route followed by two daily	Adults (18–55 years) with T1DM	**Test and Control**: IL	**Test**: 34G x 1.5 mm needle	**Test**: 22*	Rapid ID availability against SC route for different doses and meal; Significantly lesser

Aim of the study	Study population	Therapeutic agent(s)	Delivery technique	Number of subjects	Outcome of the study
standardized meals			**Control**: standard SC injection	**Control**: 22*	intrasubject and intersubject variability for Tmax after ID administration.
Evaluation of the clinical PK /PD of PTH(1-34) delivered using a drug coated MN patch for the treatment of osteoporosis	Phase I: Healthy (40–85 years) Phase II: Osteoporotic women (50–81 years)	**Test**: ZP-PTH (Phase I and Phase II) **Control:** FORTEO® (rhPTH 1-34)	**Test:** ZP-PTH patch **Control:** SC injection; Blank ZP patch	Phase I **Test**: 25* **Control**: 23* Phase II **Test:** 99 **Control:** 66	Comparative C_{max} and shorter T_{max} compared to FORTEO® control; significant improvement in spine bone mineral density in the test group

ID: intradermal, SC: subcutaneous; IM: intramuscular; T1DM: Type 1 diabetes mellitus; ID: intradermal, SC: subcutaneous; IM: intramuscular; IL: Lispro Insulin, RHI: regular human insulin;

3.3.4.3 MN for vaccine delivery

Traditionally, majority of the vaccines are administered intramuscularly or subcutaneously. These routes bypass the skin's immune system delivering vaccines to regions with no considerable concentration of antigen presenting cells (Prausnitz, Mikszta, Cormier, & Andrianov, 2009). MN target the rich network of antigen presenting cells in the epidermis and the dermis and have been established as an alternative route of delivery for vaccines. A number of reports studying MN-based vaccination have demonstrated comparable or higher immunogenicity to conventional routes of administration, dose sparing benefits, and overall higher level of antigen stability (Suh, Shin, & Kim, 2014). MN based vaccine delivery has been widely studied for influenza immunization (Van Damme et al., 2009). The clinically approved and marketed MN systems, Soluvia™ microinjection (BD Bioscience) and MicronJet™ (Nanopass technologies) are used for intradermal delivery of influenza vaccine. In the preclinical setup, MN have been used for vaccination against influenza, anthrax, and DNA vaccination against cervical cancer (Ali et al., 2017; Mikszta et al., 2006; Stinson et al., 2017).

A number of human trials for assessing the safety, tolerability and immune response generation using BD Soluvia™ microinjection have been conducted. The same have been listed in Table 3.2. Intradermal vaccination using the same system was also seen to be equally effective in older population (Holland et al., 2008). This is primarily relevant as almost 90% of the influenza associated deaths in the US occur in the elderly population (Thompson et al., 2010). In a phase II study with 1107 elderly individuals (60–85 years), intradermal vaccination (15 or 21 µg haemagglutinin/ strain) using the BD microinjection system resulted in superior immune responses than 15 µg vaccine administered intramuscularly (Holland et al., 2008). Moreover, the

Phase III clinical trial for the same intradermal injection in 3707 adults aged 60–85 years also demonstrated statistically higher geometric mean haemagglutinin inhibition antibody titres and seroprotection rates compared to conventional intramuscular dose (Arnou et al., 2009). The BD Soluvia™ microinjection has also been seen to be effective and safe in immune compromised patients (kidney transplant patients were detected as non-responders to Vaxigrip® (Sanofi Pasteur, France) although studies have also reported contradictory results (with lung transplant patients) (Manuel et al., 2011; Morelon et al., 2010). The MicronJet™ has also been reported reported to be safe and effective in various clinical trials conducted with different target populations (Table 3.2) Delivery of influenza vaccine using the MicronJet has shown to be dose sparing and superior against the regular Mantoux technique (Levin, Kochba, & Kenney, 2014).

Apart from influenza, MN based delivery of vaccine has also been demonstrated for other conditions, however, only a handful of clinical trials have been registered using MN vaccination other than influenza. While the BD Soluvia™ has been extensively researched for vaccination against influenza, the MicronJet™ has shown promising results in a Phase III study for delivery of inactivated polio vaccine (IPV) in 6–14 week-old infants sponsored by the U.S. Center for Disease Control and Prevention (CDC) and the International Center for Diarrheal Disease Research, Bangladesh (NCT01813604) (Levin, Kochba, Hung, & Kenney, 2015). Also, recently, a Phase II clinical trial compared intradermal polio vaccine administered using the MicronJet™ against the conventional intramuscular injection (Troy et al., 2015). The study established dose sparing with the MicronJet™.

Most MN in the market or clinical trials for vaccination do not fit the true definition of "MN" since the needle length goes up to 1.5mm. Although, the length of

MN has been shown to have little or no effect on the antibody responses (Widera et al., 2006), selecting suitable needle length is important in terms of bleeding, pain and microbial contamination. Since hollow MN were the first ones to be fabricated, and allow for larger volumes to be administered with a variety of delivery profiles, they have been most widely used in clinical setup for vaccination.

Much recently a number of research publications have reported the use of polymer MN for delivery of vaccines. Albumin has been used as a model antigen for vaccination in a number of studies. BSA was loaded into embeddable chitosan MN which were left into the skin. SD rats immunized with MN had significantly high antibody levels for 18 weeks against intramuscular injection. Moreover, a 2.5-fold dose sparing was observed (M.-C. Chen, Lai, Ling, & Lin, 2018). Dissolvable MN system has been used effectively for DNA vaccination. HPV subtypes (16, 18) are associated with the development of cervical cancer, with oncoproteins E6 and E7 responsible for pathogenesis. PVP based MN were used for DNA vaccination against cervical cancer. McCarthy and coworkers used a peptide RALA which condenses DNA into cationic nanoparticles and a polymeric polyvinylpyrrolidone (PVP) MN (MN) patch for cutaneous delivery of the loaded NPs (Ali et al., 2017). Mice vaccinated with MN/RALA-E6/E7 were richer in E6/E7-specific IgGs, presented greater T-cell-mediated TC-1 cytotoxicity and contained more IFN-γ than sera from mice that intramuscular NP injection. Moreover, MN/RALA-E6/E7 delayed TC-1 tumor initiation in a prophylactic model and slowed tumor growth in a therapeutic model of vaccination.

Table 3.2 Published clinical studies for vaccination against influenza using MN. Tabulated data from (Bhatnagar et al., 2017).

Aim of the study	Study population	Therapeutic agent(s)	Delivery technique	Number of subjects	Outcome of the study
Evaluation of safety and immunogenicity of different doses and administration routes of virosomal influenza vaccine in older population	Healthy (≥65 years)	**Test**: investigational virosomal vaccine (different doses) **Control**: Intanza™; Inflexal V™, MF59 adjuvanted Fluad™	**Test**: MicronJet 600™ (ID); 25G needle (IM) **Control**: Soluvia™; 25G needle (IM)	**Test**: 184 **Control**: 186	Higher immunogenicity with ID across most of the parameters and strain
Evaluation of safety and immunogenicity of low-dose influenza vaccines delivered via the ID route	Healthy (18–40 years)	**Test**: standard flu shot (different doses of α-RIX®) **Control**: standard flu shot (α-RIX®)	**Test**: MicronJet™ (ID) **Control**: standard IM injection	**Test**: 120 **Control**: 60	Similar immunogenic responses between full-dose IM vaccine and low dose ID
Evaluation of safety and immunogenicity after IM and ID delivery of influenza vaccine	Healthy (18–40 years)	**Test**: TIV (Fluvirin®) **Control**: TIV (Fluvirin®)	**Test**: 27 G x 1/2 in. BD PrecisionGlide™ **Control**: standard IM injection	**Test**: 50 **Control**: 50	No significant differences between seroprotection and seroconversion between two groups
To evaluate the safety and immunogenicity of intradermal influenza vaccination in patients with renal transplant and non-responders to the conventional influenza vaccine	Renal transplant patients (18–60 years) which were non-responders to conventional influenza administration	**Test**: prepared from Vaxigrip® **Control**: Vaxigrip®	**Test**: Soluvia™ (ID) **Control**: standard IM injection	**Test**: 31 **Control**: 31	Higher antibody response with ID vaccination

Aim of the study	Study population	Therapeutic agent(s)	Delivery technique	Number of subjects	Outcome of the study
To demonstrate (1) noninferiority and (2) superiority of one (or more) of the two ID administered vaccines over the IM control vaccine	Healthy (>65 years)	**Test**: from monovalent lots used to prepare Vaxigrip® [different doses] **Control**: from monovalent batches used to prepare Vaxigrip®	**Test**: BD Microinjection System **Control**: standard IM injection	**Test**: 738 **Control**: 358	Superior GMTs, seroprotection rates, seroconversion rates, and mean titer with ID vaccine
Evaluation of safety and immunogenicity of conventional IM dose and low dose ID immunizations (monovalent 2009 H1N1 vaccine) in chronically ill patients	Chronically ill adults	**Test**: Low dose (20%) Panenza® **Control**: Full dose Panenza®	**Test**: MicronJet 600™ (ID) **Control**: standard IM injection	**Test**: 18 **Control**: 17	Insignificant difference between seroconversion and seroprotection rates for the groups on day 21
Evaluation of safety and immunogenicity of conventional full dose IM and reduced dose ID immunization administered using two different devices in chronically ill patients	Chronically ill adults	**Test**: reduced doses Intanza® (ID) **Control**: Fluzone® (IM)	**Test**: MicronJet 600™ **Control**: BD Soluvia™, standard IM injection	**Test**: 131 **Control**: 131	Superior seroprotection rate, seroconversion rate, and the GMT of the H1N1 strains in the test group
To compare two methods of intradermal delivery: the Mantoux technique using a conventional needle and the novel MicronJet™	Healthy adults	**Test and control**: 2007/2008-season virosomal adjuvanted influenza vaccine	**Test**: MicronJet™ (ID) **Control**: Matoux technique, standard IM injection	**Test**: 56 **Control**: 224	Statistically higher geometric mean fold rise with ID vaccination
To compare low-dose non-adjuvanted ID, full-dose non-adjuvanted IM and full-dose MF59-adjuvanted IM immunizations in the elderly	Healthy (≥65 years)	**Test**: non adjuvanted low-dose TIV **Control**: MF59	**Test**: MicronJet™ **Control**: standard IM injection	**Test**: 93 **Control**: 177	Superior immune response with full-dose MF59-adjuvanted IM immunization against the low-dose non-adjuvanted ID

Aim of the study	Study population	Therapeutic agent(s)	Delivery technique	Number of subjects	Outcome of the study
population		adjuvanted Fluad®/ Agriflu®			immunization
A comparison of trivalent split-virion ID influenza immunization (9 µg of haemagglutinin /strain in 0.1 mL dose) to the conventional IM immunization with full dose inactivated influenza vaccine.	Healthy (18–57 years)	**Test**: TIV **Control**: Vaxigrip®	**Test**: BD™ Microinjection System (30G 1.5 mm) **Control**: standard IM injection	**Test**: 588 **Control**: 390	Non-inferior humoral immune responses in test group
To evaluate whether the immunogenicity of an ID inactivated TIV (15µg haemagglutinin /strain/0.1ml dose) is higher to that of a conventional full dose IM vaccine	Healthy (≥60 years)	**Test**: same monovalent batches used to prepare Vaxigrip® **Control**: Vaxigrip®	**Test**: Soluvia™ (ID) **Control**: standard IM injection	**Test**: Year I (2618); Year II (502+2456); Year III (463+223+2226) **Control**: Year I (1089); Year II (512); Year III (226)	ID group demonstrated higher seroprotection rates post second and third vaccinations

ID: intradermal, SC: subcutaneous; IM: intramuscular; TIV: trivalent influenza vaccine

3.3.5 Status of ongoing clinical trials

MN-based devices can be used to surmount the skin barrier and enhance the delivery of therapeutic agents through skin. MN can be utilized for localized and systemic drug delivery applications. Several MN-based products have been developed as a result of extensive pre- clinical testing. Table 3.3 provides a list of active clinical trials (ongoing, recruiting or completed) evaluating the safety and efficacy of MN based therapeutic delivery as on 24th January 2017. Majority of these clinical trials were performed for influenza vaccination and insulin delivery in diabetes subjects. Two of these trials involve MN pretreatment followed by drug application (NCT02596750, NCT02594644). Recently, clinical trials for glucose measurement using MN (NCT02682056) and safety assessment of an allergy patch test using MN (NCT02995057) have been initiated. Additionally, dissolvable MN are being studied for delivering doxorubicin as experimental treatment for T- cell lymphoma. A Phase I clinical study for the same is expected to initiate in near future with 54 volunteers (NCT02192021).

A parathyroid hormone-related protein (PTHrP) analog called Abaloparatide, is in clinical development for treatment of osteoporosis for which a Phase II clinical trial with coated MN patch has recently been completed. The trial involves 250 post-menopausal women with osteoporosis. The trial results are yet to be reported.

Table 3.3. Currently active clinical trials (recruiting, ongoing, and completed) with MN for therapeutic applications.

Investigated indication	Therapeutic agent/Diagnostic test	Type of MN	CT Phase	NCT Identifier*
Influenza	Inactivated influenza vaccine	MN patch	I	NCT02438423
Influenza	S-OIV H1N1 vaccination	MicronJet 600^{TM}	Not provided	NCT01049490
Influenza	Flu vaccine (Fluarix®)	MicronJet Device	Not provided	NCT00558649
Influenza	TIV 2010/2011 influenza vaccine	MicronJet^{TM}	Not provided	NCT01304563
Influenza	Intanza®	MN injection	I/II	NCT01707602
Influenza	Agriflu®, Fluad®, Intanza®, Vaxigrip®	BD MN injection	IV	NCT01368796
Influenza	Influenza vaccine	BD microinjection	II/III	NCT00258934, NCT00383526
Influenza	Influenza vaccine	BD microinjection	Not provided	NCT00296829
Influenza (in renal transplant patients)	Influenza vaccine	BD Soluvia ^{TM}	II	NCT00606359
Influenza	Fluarix®	MicronJet^{TM}	Not provided	NCT00558649
Influenza	Quadravalent influenza vaccine	Fluzone® intadermal	Not provided	NCT01737710
Influenza	Inactivated influenza vaccine	MN patch	I	NCT02438423
Poliomyelitis	Inactivated and Live Polio Vaccines	MicronJet 600^{TM}	III	NCT01813604
Polio	inactivated polio vaccine booster dose	MicronJet 600^{TM}	II	NCT01686503
Varicella Zoster Infection	Anti-varicella zoster antibody	MN syringes	Not provided	NCT02329457

Investigated indication	Therapeutic agent/Diagnostic test	Type of MN	CT Phase	NCT Identifier*
Diabetes Mellitus Type1	Insulin	Hollow glass MN	II/III	NCT00837512
	Insulin	MicronJet™	0	NCT00602914
	Insulin and glucagon	MicronJet™	II	NCT01684956
	Insulin	BD Research Catheter (34G x 1.5 mm needle)	I/II	NCT01557907
	Glucagon	MN type not provided	Not provided	NCT02459938
	Insulin	BD Research Catheter (34G x 1.5 mm needle)	I/II	NCT01120444, NCT00553488
Diabetes Mellitus Type ½	Insulin	BD Research Catheter Set (34G x 1.5 mm needle)	I/II	NCT01061216
Postmenopausal Osteoporosis	Parathyroid hormone	ZP-PTH MN patch (titanium MN)	I	NCT02478879
Postmenopausal Osteoporosis	Abaloparatide	Coated 3M Microstructured Transdermal System (MTS)	II	NCT01674621
None	Saline	FLUGEN 101.2 MN based delivery device	Not provided	NCT01767324, NCT01767337
None	Lidocaine and saline	MicronJet™	Not provided	NCT00539084
Cutaneous T Cell Lymphoma	Doxorubicin	Dissolvable MN array	Not provided	NCT02192021
Uveitis	Triamcinolone acetonide	MN injection	I/II	NCT01789320

Investigated indication	Therapeutic agent/Diagnostic test	Type of MN	CT Phase	NCT Identifier*
Migraine	Zolmitriptan	MN patch	II/III	NCT02745392
Psoriasis	Daivobet®	MN hyaluronic acid patch (Therapass®, RMD-6.5A)	Not provided	NCT02955576
None	Glucose (measurement)	'hydrogel MN patch'	Not provided	NCT02682056
Allergy	Allergic patch test	Gold/silver coated or uncoated hollow MN	NA (safety demonstration)	NCT02995057
Pain	Lidocaine	MN roller (MR2 roller, Clinical Resolution Laboratories, Inc.)	Not provided	NCT02596750
Actinic keratosis	Aminolevulinic Acid	MN roller (MR200, Clinical Resolutions Laboratory, Inc.)	Not provided	NCT02594644

* searched and reported from www.clinicaltrials.gov website; DM: Diabetes Mellitus; TIV: trivalent inactivated influenza vaccine.

3.3.6 Regulatory status of MN devices

Skin treatments have become as common as facials and body spas. Terminologies such as microneedling, dermaroller, and laser resurfacing are common knowledge among the general population. Most private clinics, salons and spas, and beauty centres offer these services with promises for a blemish free, glowing, healthy, young skin. A wide range of dermarollers are available over the counter at pharmacies or online for home use. The question to be asked is: Are these devices safe?

FDA's Center for Devices and Radiological Health (CDRH) is responsible for regulating firms who manufacture, repackage, relabel, and/or import medical devices sold in the United States. Currently, FDA classifies approximately 1,700 different generic types of devices, which are grouped into 16 medical specialties referred to as panels. Each of these generic types of devices is assigned to one of three regulatory classes based on the level of control necessary to assure the safety and effectiveness of the device. This class sets the pre-market path – exempt (Class I), 510(k) (Class II) or pre-market approval (PMA) (Class III). (Information from: https://fdaatty.com/fda-microneedling-regulations-status-update/)

Devices claiming to be Class I must have a needle length less than 0.3 mm such as to only puncture the outer dead layers of the skin. Also, these devices cannot claim any therapeutic benefits and the label, design, functions and marketing has to strictly follow the guidelines for Class I. Class II device as those for which general controls alone are insufficient to provide reasonable assurance of the safety and effectiveness of the device. These special controls are usually device-specific and are given on FDA's website. These devices require Premarket Notification 510(k) submission and commercial distribution is not possible until a letter of substantial equivalence is

received from the FDA. Class III devices require pre-market approval as they are considered high risk devices that pose a significant risk of illness or injury. The PMA process is more rigorous and clinical data needs to be provided for supporting claims (Pawar, 2017).

Most of the MN-device companies register and list their MN devices under regulation 21 CFR 878.4820, which is a Class I 510(k) exempt classification with an intended use for general dermabrasion and has been indicated for acne/minor injury-related scar revision, tattoo removal, blemish removal etc. Such devices does not alter the form and function of the body or skin in this matter in any way. However, some of the products that are available in market, although claim to be Class I, are not actually abiding by the Class I guidelines. Some even mention as "FDA cleared" or "FDA approved", while only being FDA listed/registered. Registration/listing has nothing to do with the clearance of the device for sale.

Till September 2017, the FDA had no clear guidelines on microneedling devices. However, in September 2017, the FDA has issued a draft guidance detailing when it considers "microneedling" products to be medical devices and subject to regulation. Specific claims that would meet the definition of a medical device include (1) treatment of scars (e.g., acne scars, atrophic scars, hypertrophic scars, burn scars), wrinkles and deep facial lines, cellulite and stretch marks, dermatoses, acne, alopecia (2) stimulating collagen production or angiogenesis, (3) promoting wound healing. The guideline, moreover, advises that the appropriate regulatory pathway for microneedling devices is likely to be a *de novo* classification process. FDA would expect the *de novo* application to have details such as (but not limited to) needle material, geometry, length, sharpness, biocompatibility information and adjustability with schematic drawings and illustrations. The application should address risks such as infection, blood

vessel and nerve damage, skin inflammation, allergic reactions, and other potential adverse events. Reusable microneedling devices will also need to submit usability testing data, sterilization information and cleaning/disinfection details.

3.4 Summary

The MN landscape has radically grown over the last 20 years. Microfabrication technology has allowed for a variety of different MN designs for drug delivery to the skin and other targets. MN have been prepared in different designs, out of a variety of materials to deliver a range of cosmeceuticals and therapeutics. MN have been in use, clinically or at home for management of skin scars, wrinkles, acne, alopecia, etc. Preclinical and clinical studies have demonstrated MN based delivery of low molecular weight drugs including naltrexone and lidocaine and agents for photodynamic therapy; macromolecules including albumin, parathyroid hormone and insulin; vaccines including influenza, polio, rabies, BCG, West Nile virus, HPV and others; and delivery of DNA. MN have also been used to target the diseases of the eye, targeting delivery to cornea, sclera and suprachoroidal space. Ocular delivery has been targeted to the cornea, sclera and suprachoroidal space using solid and hollow MN. Additionally, MN have been used to extract fluids from the body for diagnostic applications. With the large amount of clinical and preclinical data being generated with MN, a number of MN devices in the market and many in developmental pipeline, MN are poised to influence the drug delivery scenario in the immediate future.

Chapter 4

Zein microneedles for transcutaneous vaccine delivery: fabrication, characterization and *in vivo* evaluation using ovalbumin as model antigen

4.1 Introduction

Majority of the vaccines are administered using hypodermic needles. Syringe-based injections have been associated with multiple disadvantages including needle-phobia, needle-injuries, usage of contaminated needles, and requirement of a healthcare professional among others (Babiuk et al. 2000; Nir et al. 2003; Sirnonsen et al. 1999). Recent dramatic improvements in precision engineering allowed for design and fabrication of micron-scale devices that can be used to deliver vaccines (Luttge 2016). There has been a tremendous interest in development of microneedle devices for transcutaneous therapeutic and vaccine delivery, and for cosmetic applications (Kim, Park, and Prausnitz 2012; McCrudden et al. 2015). This lead to publication of many research reports and commercial approval of few microneedle-based devices (Marshall, Sahm, and Moore 2016). The approved devices include BD Soluvia® to deliver influenza vaccine and Dermaroller® for cosmetic skin application. Furthermore, multiple microneedle-based transcutaneous delivery systems are under various phases of clinical studies (Pettis and Harvey 2012).

The major advantage associated with microneedle-based devices over hypodermic syringes include minimal invasion inside the skin membrane, thereby reducing needle stick injuries, and improving user compliance (Kim and Prausnitz 2011). Microneedles have shown to be effective for transcutaneous immunization. More recently, it was understood that multiple factors influence the utilization of microneedles for transcutaneous immunization. In addition to the needle size, shape, aspect ratio, distance of separation between needles; the material of construction has been found to be an important contributor to antigen loading,

skin insertion, antigen release, and stability of the antigen (Bediz et al. 2014). Hence, the initial microneedles made of stainless steel, silica, and ceramic paved way for development of microneedles made of biocompatible polymeric materials (Demir, Akan, and Kerimoglu 2013). These biocompatible polymeric microneedles have been made of polymers like poly-lactide-co-glycolide, hyaluronic acid, carboxymethyl cellulose, sodium alginate, chitosan, polyvinyl pyrrolidone and polyvinyl alcohol (Park, Allen, and Prausnitz 2005). Most of these microneedle patches have been prepared using a simple micromolding technique (Banga 2011; Sullivan et al. 2010). However, clinical development of polymer-based microneedles has been limited by the mechanical strength of needles, antigen stability and release characteristics.

To that end, here we report fabrication of microneedle array made of zein protein. Gorham in 1821 first described zein after isolating the protein from maize (Gorham 1821). Since then, numerous research reports have been published and many patents granted for better techniques of extraction of zein from maize. Zein is classified as a prolamin and is the alcohol-soluble protein of corn (Osborne 1916). Essentially, zein is a mixture of four proteins of different molecular sizes and solubility: α, β, γ, and δ (Coleman and Larkins 1999). α-Zein accounts for 70% of the total content followed by 20% of γ-zein. Zein is insoluble in water alone and is soluble in binary solvents such as hydroalcoholic preparations (Lawton 2002).

Zein has been used in the manufacture of biodegradable plastics, fibers, adhesives, coatings, inks, cosmetics, textiles and chewing gum (Shukla and Cheryan 2001). Currently, film coating has been the most successful application of zein in the food and pharmaceutical industry. Zein being a protein itself is

expected to form molecular interactions with protein-based active molecules and enhance their loading and delivery. Surprisingly, to the best of our knowledge, zein has never been used to prepare drug delivery devices including microneedles. We report microneedles made of zein for transcutaneous delivery of model antigen, ovalbumin (OVA).

Zein microneedles (ZMN) were prepared by micromolding technique. The disadvantages associated with traditional microfabrication based etching techniques including high cost and difficult scale-up, can be overcome by micromolding technique. Micromolding technique requires a master mold which can be prepared using metal, silicon or polymers like acrylobutadiene styrene (ABS) and a secondary mold prepared with polydimethyl siloxane (PDMS). This PDMS mold can be re-used to make hundreds of polymeric microneedle arrays. 3D printing technique was used to prepare an ABS master mold. The ZMN were evaluated for their feasibility to deliver ovalbumin as a model antigen into the skin for transcutaneous immunization.

4.2 Materials and Methods

4.2.1 Materials

Zein, fluorescein isothiocynate (FITC) and Bradford reagent were purchased from Sigma Aldrich Chemical Company (Bengaluru, India). OVA from chicken egg white (catalog number A5503, with ≥98% assay) was purchased from Sigma Aldrich Chemical Company and was utilized without any further purification. Sylgard® 184 was purchased from Dow Corning (Midland, MI, USA). Stock cultures of *Staphylococcus epidermidis* were obtained from Microbial Type Culture Collection and Gene Bank (MTCC), Chandigarh, India.

Nutrient agar, nutrient media, Roswell Park Memorial Institute (RPMI) 1640 culture medium, fetal bovine serum and 100× penicillin were purchased from Himedia Labs, India. HRP-conjugated anti-mouse IgG, IgG1, IgG2a were purchased from Santa Cruz Biotechnology Inc., USA. Milli-Q (Millipore, USA) water was used for all the experiments.

4.2.2 Fabrication of the ZMN

Pro/ENGINEER (PTC Creo 2.0) was used to design the microneedle arrays and generate stereolithography (STL) files for 3D printing. The microneedles in the primary mold were designed with a length of 1500 μm length, base diameter of 400 μm and a 25 μm tip radius. The array was designed to contain 36 microprojections in 1 cm^2 area in a 6 x 6 pattern. This design was utilized to print acrylonitrile butadiene styrene (ABS) master mold using poly-jet 3D printer (Objet30 Scholar, Stratasys Inc., USA). This master mold was subsequently used for fabrication of a production mold made of polydimethylsiloxane (PDMS). Sylgard$^{®}$ 184 silicone elastomer and curing agent were mixed in 10:1 w/w ratio and allowed to stand for 30 min for removal of air bubbles. This mixture was poured over the ABS mold till it was completely filled. Entrapped air bubbles were removed by vacuum application for 10 min. The PDMS was then allowed to bake at 100°C for 4 h in a hot air oven. Completely cured samples were then kept in a freezer to shrink before careful removal of PDMS molds using a scalpel blade.

Zein (60% w/w) was prepared using 90% ethanol. Glycerol (10% w/w) and polyethylene glycol 400 (PEG 400, 10% w/w) were used as plasticizers. This

mixture was added to PDMS molds under vacuum and allowed to air dry for 48 h. Then, the ZMN were carefully removed and used for characterization.

4.2.3 Characterization of the ZMN

The prepared ZMN were examined for uniformity, length of needle and base diameter using optical microscope (Olympus IX53, Olympus, Japan). The mechanical strength of ZMN and required skin insertion force were studied using a texture analyzer (Stable Microsystems, UK). For determining mechanical strength, microneedle array was placed on a heavy duty platform with needles facing upwards. A 10 mm cylindrical Delrin probe (part code P/10) connected to a 50 kg load cell was set at equal distance from the platform for all test measurements. Texture analyzer was set in compression mode with the probe compressing the microneedle array at a speed of 0.5 mm/sec to a maximum distance of 0.8 mm. The probe was held in place for 5 sec. ZMN prepared without adding plasticizers were also characterized with the same experimental parameters. Force Vs. displacement curve was plotted to calculate bending force. Excised mouse skin was used to determine required skin insertion force for penetration of microneedles. A double-sided adhesive tape was used to adhere ZMN to a moveable 10 mm cylindrical probe. The skin sample was secured on a polystyrene block with epidermis facing the probe. The probe was lowered onto the skin at a speed of 0.5 mm/s and a force of 0.4 N/needle or 1 N/needle was applied. Later, the skin sample was stained with methylene blue for 20 min for visualization of pores. Photographs of the ZMN were collected before and after insertion using a digital camera (Canon EOS 1200D with Canon EF 100mm f/2.8 Macro USM lens).

4.2.4 Preparation of the OVA entrapped or coated ZMN

Two strategies were followed to load ovalbumin in microneedles. For preparation of OVA entrapped ZMN, OVA was added to the zein mixture in the water phase and then this mixture was used for ZMN casting. The amount of OVA entrapped in a single needle was calculated using the below equation.

$$Amount\ of\ OVA\ in\ a\ single\ needle =$$

$$\frac{Amount\ OVA\ added\ to\ one\ ZMN}{Average\ weight\ of\ OVA\ loaded\ ZMN}$$

$$\times\ average\ weight\ of\ a\ single\ needle$$

OVA coated ZMN were prepared by dip coating method. ZMN were dipped in OVA (40 mg/ml, HEPES buffer, pH 7.0) for 30 min. The coated ZMN were allowed to air dry for 24 h.

4.2.5 *In vitro* release of OVA from the ZMN

In vitro release studies were performed by placing the microneedle array in phosphate buffer (pH 7.4) in a 12-well plate such that only needles were in contact with the buffer medium. The system was incubated in a shaker at 37 °C and 40 rpm. Samples were withdrawn from the media after 1 h. The OVA concentration in the release samples was determined using Bradford's assay. For that, 250 µl of Bradford's reagent was added to 5 µl of sample in a 96 well-plate and incubated for 10 min. The absorbance was recorded at 595 nm wavelength. The concentration was determined after comparison with a standard calibration curve (0.1 – 1.4 mg/ml of OVA, R^2=0.999).

The amount of OVA released in phosphate buffer after insertion of ZMN in excised skin was evaluated. OVA coated ZMN were inserted into mouse skin for 30 min. Then the amount of OVA released from ZMN in 1 h was determined using Bradford's assay.

4.2.6 Stability of OVA coated ZMN

The stability of OVA released from OVA coated ZMN was determined by sodium dodecyl sulfate polyacrylamide gel electrophoresis (SDS-PAGE; 5% stacking gel; 12% resolving gel, 0.75 mm thickness). OVA released from OVA coated ZMN before and after insertion in excised mouse skin was collected and mixed with 5× sample loading buffer (β-mercaptoethanol (5%), bromophenol blue (0.02%), glycerol (30%), SDS (10%), Tris-Cl (250 mM, pH 6.8)). Electrophoresis was performed in vertical gel electrophoresis unit (Hoefer Inc., USA) at 100 V for 2 h. Protein bands were visualized (Gel Doc XR$^+$ Imaging system, BioRad, USA) after staining with Coomassie brilliant blue.

The physical stability of OVA coated ZMN and OVA was studied after storage at different environmental conditions. Blank and OVA coated ZMN were stored at cold condition (2-8°C), room temperature (RT) and at accelerated storage condition (40°C ± 2°C and 75% ± 5% RH) (Table 4.1). Different OVA coated ZMN samples were collected after 15, 30, 60 and 90 days for analysis.

Table 4.1 Storage conditions for stability study of blank and OVA coated ZMN

Stability condition	Temperature	Humidity	Packaging
Cold condition	2-8 °C	Not monitored	ZMN placed in 12 well plates and wrapped with aluminum foil
Room temperature	25 °C	Not monitored	ZMN placed in 12 well plates and wrapped with aluminum foil
Accelerated condition	40 °C	75% ± 5% RH	ZMN individually wrapped loosely in aluminum foil and placed in plastic container

The amount of OVA released from coated ZMN in 1 h in phosphate buffer (pH 7.2) was determined using Bradford's assay. The integrity of released OVA was studied by SDS-PAGE as described above. The secondary structure of OVA released from ZMN was evaluated using circular dichroism spectroscopy (JASCO J-1500 CD spectrometer). For that, the samples were dialyzed against degassed buffer (10 mM KH_2PO_4, 50 mM Na_2SO_4, pH 7.4) overnight and filtered using 0.22 μm membrane filter before analysis. Far-UV spectra were recorded between 250 and 200 nm wavelength using a cuvette of 0.1 cm path length at 25°C. Process parameters including scan speed (50 nm/min), data pitch (1 nm), data integration time (1 sec) and number of accumulations (3) were kept constant. Data was represented as mean residue ellipticity (deg cm^2 /dmol) after buffer subtraction.

4.2.7 Confocal laser scanning microscopy (CLSM)

For CLSM studies, OVA was labeled with fluorescein isothiocyanate (FITC). FITC (3 mg/ml FITC in anhydrous DMSO) was added drop wise to 4 ml of OVA solution (25 mg/ml in carbonate buffer pH 9) under continuous stirring.

The reaction was incubated overnight at 4°C. Free FITC was removed from the conjugate by dialyzing against PBS (pH 7.4) using a regenerated cellulose membrane (Molecular wt. cut-off 12 kDa, Spectrum Labs, USA).

Thin layer chromatography with mobile phase containing chloroform: methanol: ammonium hydroxide (5:4:1) was performed to confirm the complete removal of free FITC. The number of moles of FITC conjugated to OVA was determined by UV-visible spectroscopy (SpectraMax M4, Molecular Devices Inc., USA). The conjugate was also characterized using Fourier transform Infrared Spectroscopy (FT/IR-4200, Jasco Inc., USA). Samples (2 mg) were mixed with potassium bromide at 1: 100 ratio before analysis. Spectra were recorded in the range of 4000 – 400 cm^{-1} wavenumber at a spectral resolution of 2 cm^{-1} in a dynamic reflectance sample holder.

FITC-OVA was coated on ZMN as described in above sections. Then, FITC-OVA coated ZMN were inserted into excised BALB/c mouse skin. Fluorescence microscope (Olympus IX53, Olympus Corporation, Japan) was used to capture fluorescence micrograph of ZMN before and after insertion into the skin.

To evaluate the depth of penetration of ZMN and release of OVA within skin, CLSM studies were performed. Previously shaved excised mouse skin was used for insertion of FITC-OVA ZMN. The ZMN were inserted into skin and held in place for 30 minutes using occlusive tape. After removal of ZMN, the skin sample was placed on a glass slide and covered with cellophane tape. Argon laser (488 nm wavelength) was used to excite FITC and emission intensity was detected at 520 nm wavelength. Images were captured in the XYZ plane (plane parallel to

the mouse skin) using 10× objective lens. The skin surface (z=0 µm) was considered as the imaging plane with brightest fluorescence. Optical sections were obtained at a 1 µm step size from skin surface through the z-axis. Other parameters including scan size (512 x 512), scan speed (400 Hz), pinhole (53 µm), pinhole airy (1 AU) laser (0.7998 % of 0.0390 W) and gain (100) were kept constant. The 3D confocal reconstruction images were also obtained to visualize the penetration of microneedles in the skin.

4.2.8 Histological examination

Skin was collected from the abdomen of previously shaved Balb/c mice. The excised Balb/c mouse abdominal skin was mounted on a polystyrene block and OVA coated ZMN were inserted into the skin for 30 minutes. Then the skin sample was embedded in optimum cutting temperature (OCT) compound at -80 °C. The skin sample was sectioned at a thickness of 6 µm using cryostat (CM1520, Leica Biosystems, Germany). Later, skin sections were dried overnight, and stained with hematoxylin and eosin (Sigma Aldrich). Microscopic images were acquired using an optical microscope.

4.2.9 Skin penetration of bacteria after the ZMN application

To study the influence of ZMN application on skin penetration of microorganisms, FITC labeled *Staphylococcus epidermidis* was used. Freeze dried *Staphylococcus epidermidis* (MTCC 435) cultures were reconstituted using nutrient medium and subcultured. Bacterial cells were harvested by centrifugation at 10,000 × g at 4 °C for 5 min and suspended in 1 ml of 0.1 M sodium bicarbonate buffer. The optical density was measured at 600 nm and adjusted at 0.1 to obtain a concentration of 10^7 cfu/ml. This was further validated by total

viable counting upon plating onto agar plates and counting after incubating at 37 °C for 24-48 h. FITC stock solution (250 µl of 10 mg/ml in dimethyl sulfoxide) was added for every 5 ml of bacterial suspension. The culture was incubated while shaking for 30 minutes in the dark. Then the bacterial cells were washed 3-times with sterile phosphate buffer to remove unbound FITC. The cells were resuspended in nutrient medium and optical density was determined. A sample of 1 µl volume was smeared onto a glass slide, fixed with heat and observed under brightfield and fluorescence microscope. The bacterial suspension was stored at 2-8°C for not more than 1 week for further experimentation.

The permeation of *S. epidermidis* across mouse skin was studied using a Franz diffusion cell apparatus (PermeGear Inc. USA). Skin sample was sandwiched between the donor and receptor compartment (5 ml of sterilized and degassed PBS). The complete setup was maintained at 37°C by recirculating water from a temperature controlled water bath. The donor compartment was charged with 1 ml aliquot of FITC labelled *S. epidermidis* (10^7 cfu) and incubated for 24 h under sterile conditions. The donor compartment was covered with Parafilm®. After 24 h, the culture from donor compartment was withdrawn and the skin sample was treated in three different methods: puncturing with hypodermic needle, inserting ZMN and disrupting the skin using a biopsy punch. A 24G hypodermic needle was inserted completely into the skin and removed within 30 sec. The ZMN were inserted in skin sample for 30 min. ZMN were previously exposed to UV light for 15 min for reducing bioburden. A sterile biopsy punch of diameter 8 mm was used to disrupt the skin surface by punching. The used hypodermic syringe, ZMN and biopsy punch were placed in 5 ml sterile PBS, ultrasonicated for 15 min to dislodge all bacteria. This PBS sample was plated on

agar and incubated at 37°C for 24 h to count colony forming units. Similarly, for control measurements, the bacteria attached to skin surface were dislodged and plated onto agar for total viable colony counting. Furthermore, samples (100 µl) were withdrawn from the receptor compartment after 0.25, 0.5, 1, 2, 4, 5, 6, 12 and 24 h of skin treatment. Total viable count of bacteria was determined after 24 h incubation at 37°C in nutrient agar. For CLSM studies, the skin sample was placed on a glass slide and held with cellophane tape. Images were acquired using CLSM as described above.

4.2.10 Transcutaneous immunization studies

Female Balb/c mice (4-6 weeks) were procured from National Institute of Nutrition, Hyderabad, India. All the experiments were performed after approval from the institutional animal ethics committee (IAEC) of BITS Pilani. The mice were fed with standard laboratory diet and were provided with clean drinking water *ad libitum*. The animals were divided into six groups with 5 mice in each group. The groups include 1) control (no ZMN insertion); 2) blank ZMN; 3) OVA entrapped ZMN; 4) OVA coated ZMN; 5) blank ZMN insertion followed by OVA solution application; 6) OVA intradermal injection. OVA intradermal injections were given by dissolving ovalbumin in PBS (pH 7.4). For topical immunization, the mice were anesthetized with isoflurane (E-Z systems, USA) and the dorsal skin was shaved using a hair clipper. ZMN was inserted into the skin and held in place using an occlusive tape. The ZMN was inserted for 30 min or 4 h for OVA coated ZMN and OVA entrapped ZMN, respectively. For OVA application after ZMN pretreatment, OVA solution was topically applied after 1 min insertion of blank ZMN. The amount of OVA administered through intradermal injection was 5 µg. The amount of OVA topically applied after ZMN pre-treatment was 100 µg.

On the other hand, the amount of OVA delivered using ZMN that was released within skin after insertion is not quantified. However, OVA release studies (1 h sampling) were performed to determine, approximately the amount of OVA released inside skin. The amount of OVA available within skin after OVA entrapped ZMN insertion was ~80 μg. In the case of OVA coated ZMN, the total OVA released was ~600 μg. For all treatment groups, mice were immunized on day 1, 22 and 43. Blood samples were collected from the retro-orbital plexus on day 21, 42 and 63. Serum was separated from the blood by centrifugation at 4000 rpm for 20 min at 4°C and stored at -80°C for further analysis.

Enzyme linked immunosorbent assay (ELISA) technique was used to determine the OVA specific antibodies (IgG, IgG1 and IgG2a) in serum samples. A 96 well high binding flat bottom micro-titer plates (Himedia Labs, India) were coated with ovalbumin (1 μg/well in bicarbonate buffer, pH 9.6). The plates were incubated at 4°C overnight. Then, unbound antigen was removed by washing 3-times with wash buffer (PBS 7.4 + 0.05% Tween 20). Free sites were blocked with 200 μl blocking buffer (PBS 7.4 + 1% BSA + 0.05% Tween 20) for 30 min followed by 3-time wash step. Serum samples (100 μl, diluted 1: 200 for total IgG, 1: 160 for IgG1 and 1: 40 for IgG2a in sample diluent, PBS 7.4 + 1% BSA) were added to the wells and incubated for 1 h. Later, HRP-conjugated anti-mouse IgG/ IgG1/ IgG2a (100 μl; 1: 6000 in sample diluent) was incubated for 1 h followed by 5-time wash step. Finally, 100 μl of 3, 3', 5, 5'-tetramethylbenzidine (TMB) substrate solution was added to each well and incubated in the dark for 15 min. The reaction was stopped by adding 100 μl of 2 N H_2SO_4. Absorbance intensity was determined at 450 nm wavelength using a micro-plate reader (Spectramax M4, Molecular Devices Inc., USA)

4.2.11 Splenocyte proliferation assay

In vitro splenocyte proliferation assay was performed to investigate the ability of memory T cells to recognize the antigen upon re-stimulation. Mice were sacrificed on day 64 after immunization and spleen was harvested under sterile conditions. The spleen was placed in ice cold PBS (pH 7.4) and gently mashed using the back of syringe plunger. The loose spleen mass was then passed through a cell strainer (40 μm pore size, Himedia Labs, India) into 15 ml centrifuge tubes. The tubes were centrifuged at 2500 rpm for 5 min. The cells were washed 2-times with ice cold PBS and single cell suspension of splenocytes was prepared in RPMI 1640 medium supplemented with 1% fetal bovine serum (FBS). The suspension was centrifuged at 2500 rpm at 25°C for 5 min and the supernatant was discarded. RBC lysis buffer (150 mM NH_4Cl, 10 mM $KHCO_3$, 1 mM EDTA-2Na, pH 7.2) was added to lyse the erythrocytes. The cells were again centrifuged after addition of RPMI 1640 medium. The pellet was redispersed in RPMI 1640 media and the cells were counted using Neubauer chamber. Splenocytes were seeded in a 96 well plate at 50,000 cells/well and treated with blank RPMI medium, OVA (50 μg/ml) or positive control concanavalin A mitogen (Con A) (1 μg/ml) for 72 h. At the end of treatment, the medium was removed and the cells were incubated with 50 μl of MTT solution (0.5 mg/ml) for 4 h. Then, DMSO (150 μl) was added to dissolve formazan crystals. Absorbance was measured at 540 nm in a UV-visible spectrophotometer. Stimulation index (SI) was calculated using below equation.

$$Stimulation\ Index\ (SI) = \frac{A_{540nm}\ of\ Con\ A\ or\ OVA\ treated\ cells}{A_{540nm}\ of\ RPMI\ 1640\ treated\ cells}$$

4.3 Results

4.3.1 Characterization of ZMN

ZMN were fabricated using micro-molding technique where a poly-jet 3D printer was used to print master mold. Figure 4.1 shows the scheme of fabrication of ZMN. Figure 4.1d and 1e show a solvent casted ZMN array and a microscopic image of two microneedles, respectively. The needles are seen arranged in a 6 x 6 array within an area of 1 cm^2. The needles were conical shape with the average height and base width of 974.6 ± 13.8 μm and 362.7 ± 13.8 μm (n=10), respectively. The surface of microneedles was smooth with no observable stress on the microneedle structures (Figure 4.1e).
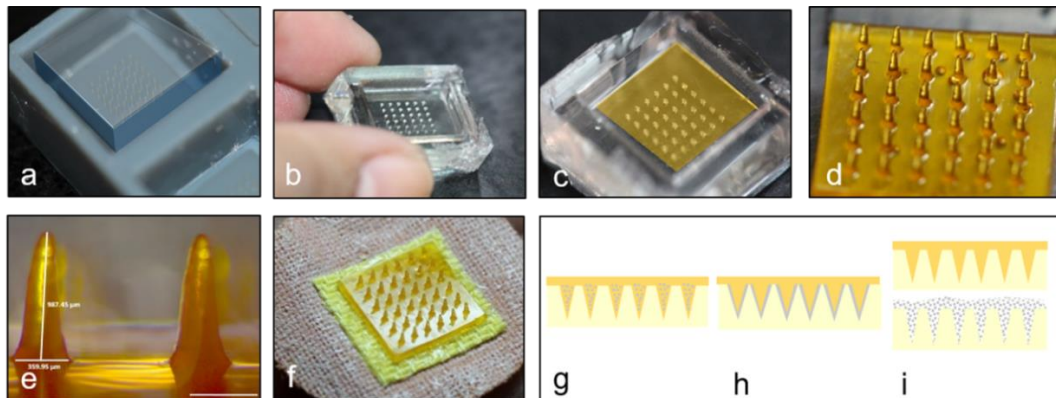
Figure 4.1 Fabrication of zein microneedles (ZMN). a. Casting of PDMS mold from 3D printed ABS mold; b. PDMS mold; c. Solvent casting of ZMN; d. Photograph of 6x6 zein microneedle array; e. Micrograph of zein microneedles; f. Microneedle array attached to an adhesive backing membrane for transcutaneous immunization. Schematic representation of OVA entrapped ZMN (g) OVA coated ZMN (h) and OVA application after ZMN pretreatment (i). Scale bar in "e" represents 500 μm.

Polymer microneedles need to have sufficient mechanical strength for penetration into the skin. It is expected that the needles do not bend or break during handling and skin insertion. Texture analysis showed a bending force of

16.09 ± 1.52 N and 19.20 ± 1.75 N for blank and OVA coated ZMN, respectively (n=3). The force-displacement curves showed no discontinuous point indicating no needle failure (Figure 4.3a). The forces required for OVA coated ZMN were greater compared with uncoated ZMN. In the absence of plasticizers, ZMN showed significantly ($p<0.05$) lower bending forces (Figure 4.2) and were observed to be brittle.
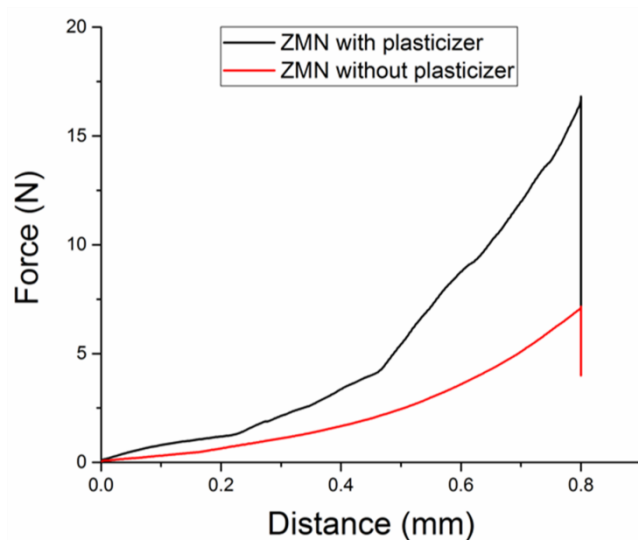
Figure 4.2 Texture analyser force displacement plots for investigating the effect of plasticizer on the strength of zein MN. A cylindrical Delrin probe (10mm Diameter) was lowered on the microneedle array placed using a two sided tape on a heavy duty metal base. A test speed of 0.5 mm/s was employed for the measurement. Each plot represents average of three experiments.

To study the required skin insertional force, the ZMN were inserted into excised mouse skin at 0.4 N/needle and 1 N/needle. Figures 4.3b and 4.3c shows pores created on the mouse skin and Parafilm® respectively with the application of 0.4 N/needle force. Figure 4.3d shows a micrograph of cryosectioned mouse skin with a single pore created after insertion of ZMN at 0.4 N/needle force. The needles did not bend or break with the application of 0.4 N/needle force (Figure

4.3f). On the other hand, Figure 4.3g shows bent ZMN upon application of 1 N/needle force.
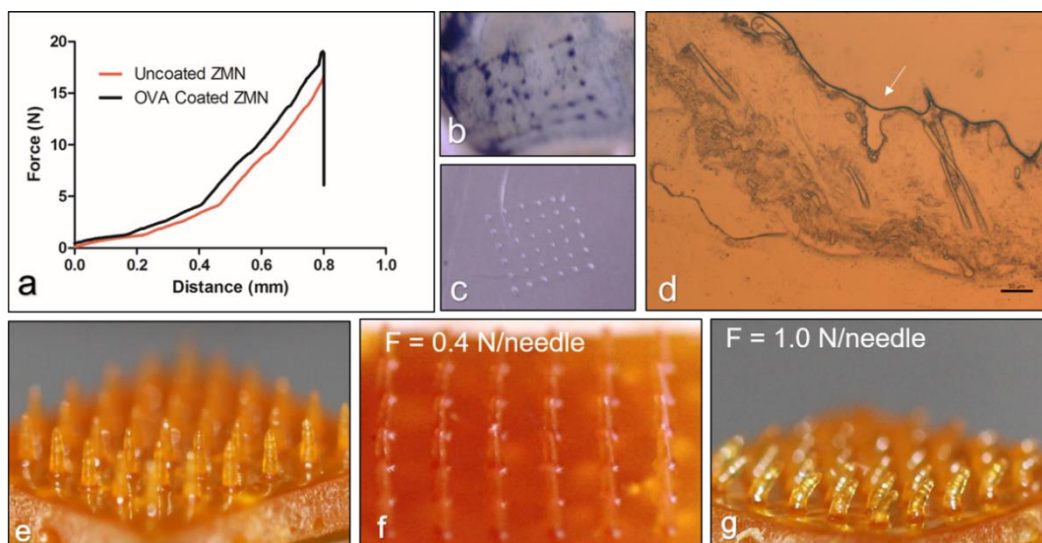
Figure 4.3 Mechanical strength of ZMN. a. Determination of bending force for blank (uncoated) and OVA coated ZMN. Each plot represents average of three experiments. b and c. Methylene blue stained skin after ZMN insertion showing pores created and reciprocal images of the etching visible on the Parafilm® placed under the skin. d. Micrograph of skin cryosection after treating with ZMN. Arrow indicates pore created after ZMN insertion. Scale bar represents 50 μm. ZMN before (e) and after insertion into the skin with a force of 0.4 N/needle (f) and 1.0 N/needle (g) using texture analyzer. A pre-test speed of 1 mm/s and test speed of 0.5 mm/s was employed.

4.3.2 Insertion of the OVA coated ZMN in mouse skin

FITC tagged OVA was used to visualize the OVA delivery inside skin. The absence of free FITC in FITC-OVA conjugate was confirmed using thin layer chromatography (Figure 4.4). FITC conjugation was confirmed by FTIR studies by the absence of a characteristic isothiocyanate stretching band at 2018 cm^{-1}, and appearance of thiourea bands at 1100-1500 cm^{-1} and 400-600 cm^{-1} (Figure 4.5). UV-visible spectroscopy was used to determine the number of moles of FITC conjugated to one mole of OVA. It was found that the λ_{max} of free FITC (490 nm)

shifted to 495 nm wavelength after conjugation with OVA (Figure 4.4). UV-visible spectroscopic analysis showed 1.23 moles of FITC conjugated to one mole of OVA.
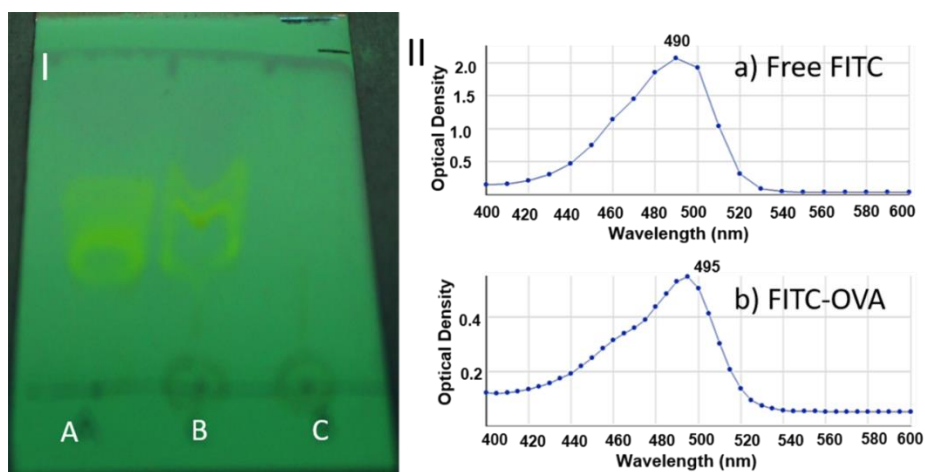
Figure 4.4 Thin layer chromatography showing spots after reaction for FITC conjugation of ovalbumin I. A) Free FITC B) Reaction mixture C) Co-spot of A and B. II. Shift in λ_{max} for FITC-OVA (b) compared to free FITC (a)
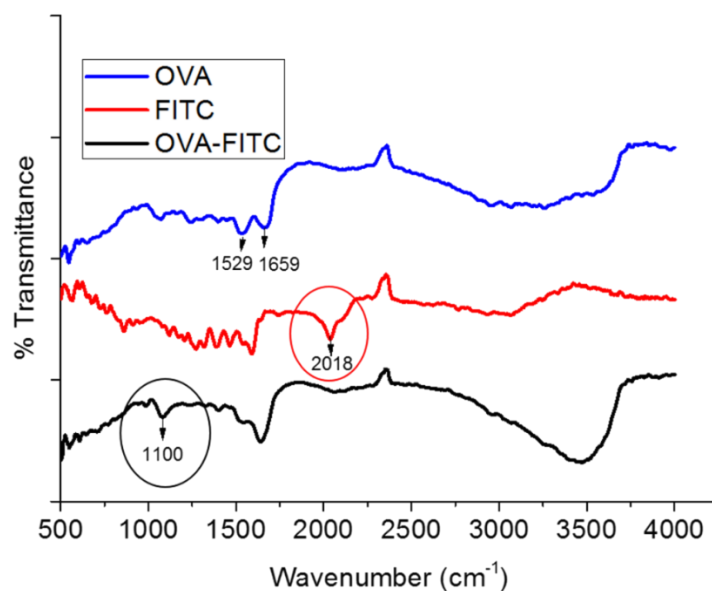
Figure 4.5 FT-IR spectra for pure ovalbumin, FITC and FITC-OVA conjugate. The ellipse represents characteristic isothiocyanate peak for FITC and appearance of thiourea stretching bands for FITC-OVA conjugate. Each spectra is representative of three different runs.
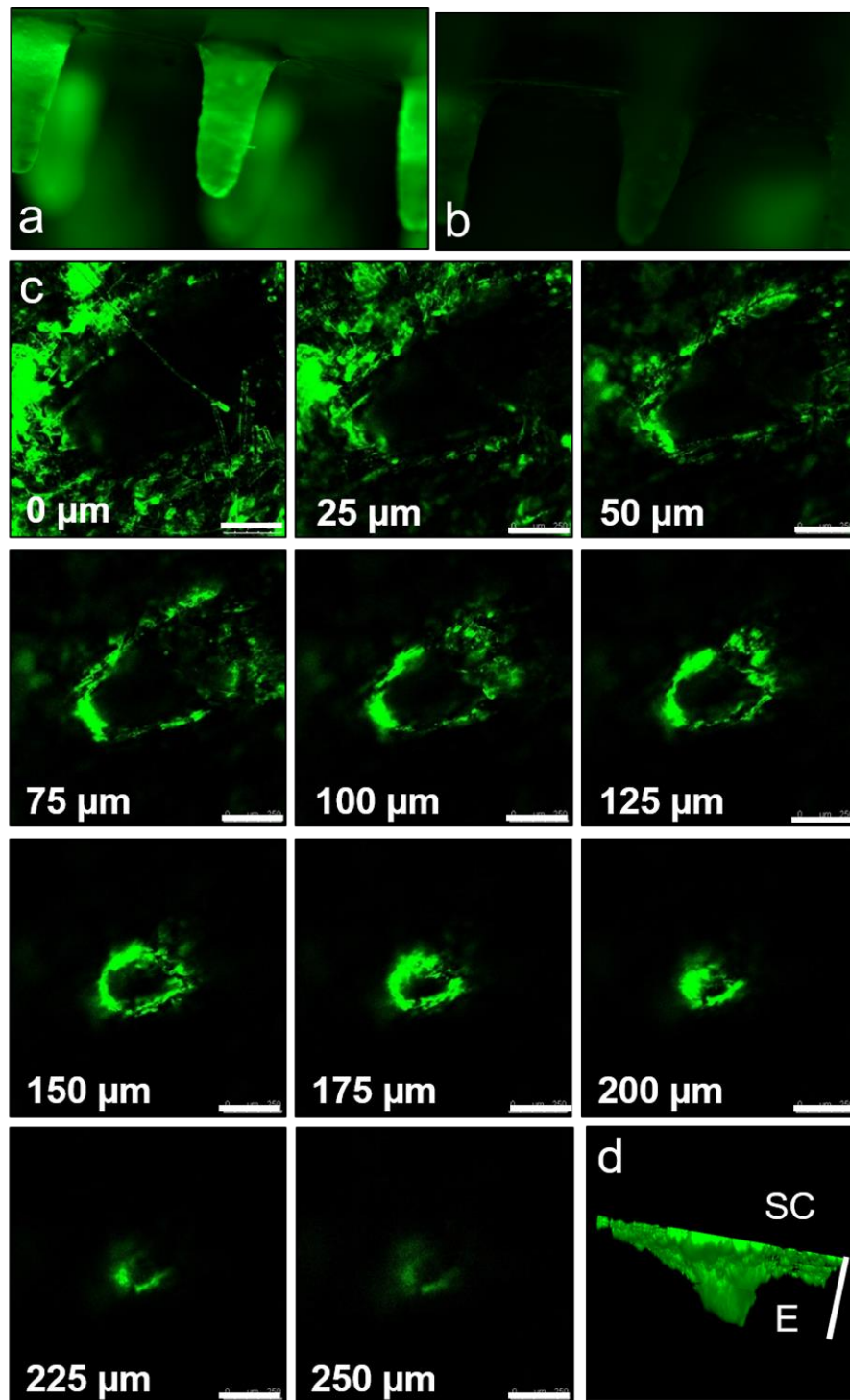
Figure 4.6 Fluorescence image of OVA-FITC coated ZMN before (a) and after (b) insertion into skin for 30 min. c. Confocal micrographs of optical sections of skin sample from surface (0µm) to 250 µm inside skin and 3D representation of the micro-channel created due to insertion of OVA-FITC coated ZMN (d). Dark areas indicate lack of fluorescence. Scale bar represents 250 µm. SC – Stratum corneum, E – Epidermis.

Figure 4.6a and 4.6b show fluorescence images of FITC-OVA coated ZMN before and after insertion into the skin for 30 minutes, respectively. Figure 4.6a shows uniform coating of ZMN with FITC-OVA. The intensity of fluorescence decreased after 30 min insertion of ZMN inside skin (Figure 4.6b). Figure 4.6c shows the confocal micrographs of skin after 30 min insertion of FITC-OVA coated ZMN at varying depths. The series of micrographs show a single pore created by microneedle insertion. Fluorescence associated with FITC-OVA was seen up to a depth of 250 μm inside skin. Figure 4.6d shows a reconstructed 3-dimensional image of the microchannel created with in skin. The pore can be seen tapering down as we move from stratum corneum to epidermis and dermis. Results from confocal microscopy confirm that the fluorescence intensity lost from the microneedle surface after insertion in skin can be attributed to adsorption of FITC-OVA within skin.

4.3.3 Skin disposition of the OVA delivered using ZMN

The amount of OVA entrapped or coated on ZMN was measured by indirect method. For all the samples, the amount of OVA released from ZMN was determined after incubation in PBS for 1 h. The amount of OVA released from ZMN entrapped with OVA was 0.088 ± 0.014 mg in 1 h. On the other hand, 0.766 ± 0.144 mg OVA released from ZMN coated with OVA. The amount of OVA released from microneedles which were previously inserted inside skin for 30 min was reduced to 0.124 ± 0.018 mg.

4.3.4 Stability of the OVA coated ZMN

SDS-PAGE was performed for OVA samples released before and after insertion of ZMN in skin. Figure 4.7a shows the bands of OVA released from

ZMN. Single band at 43 kDa represent that the OVA was intact after coating on ZMN.
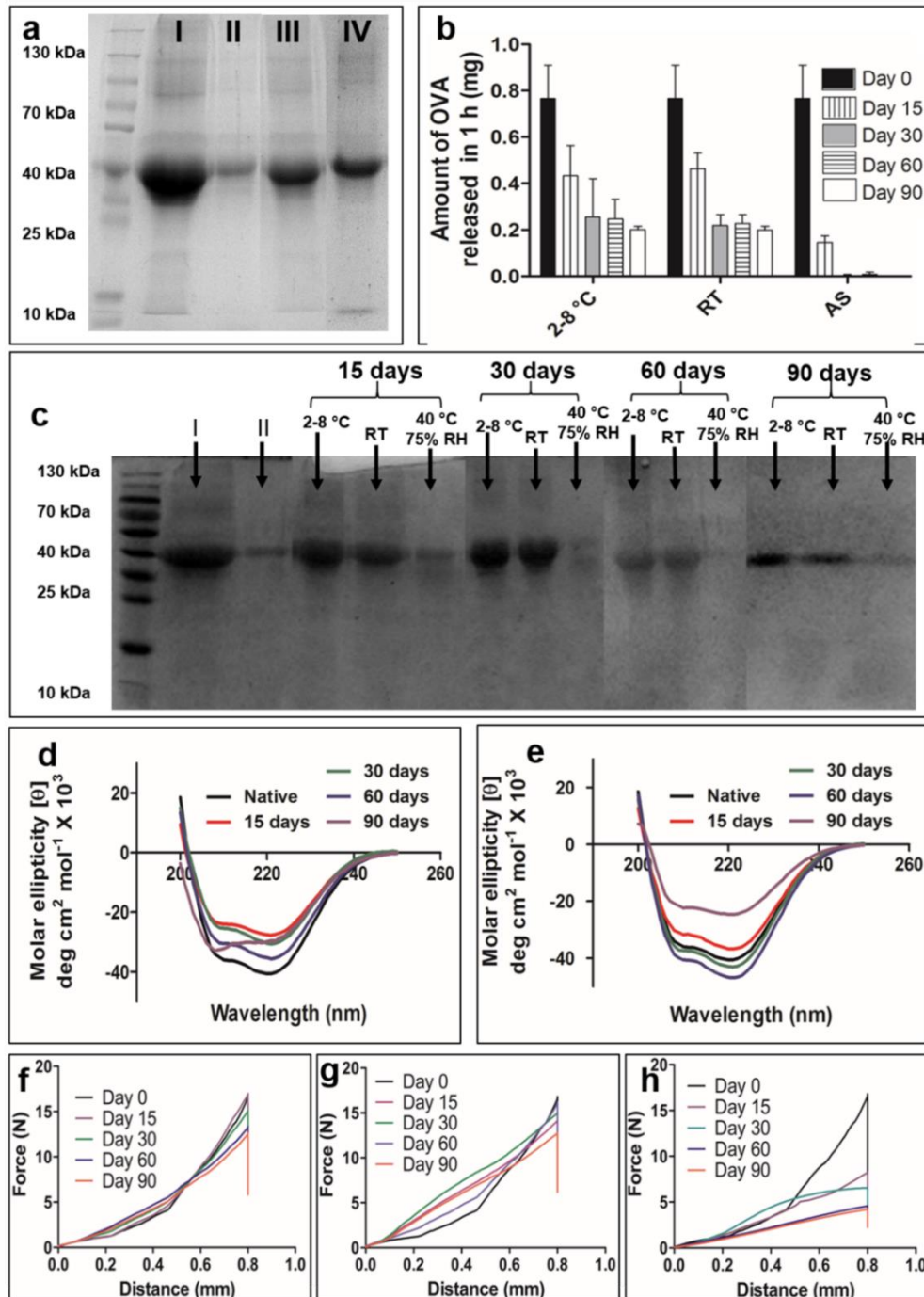
Figure 4.7 (a) SDS-PAGE analysis of OVA released from coated ZMN. Lanes: I – OVA (20 μg), II – OVA (2 μg), III – OVA released from OVA coated ZMN in 1 h, IV – OVA release post ZMN insertion in skin for 30 min. (b) Amount of ovalbumin released in 1 h from coated ZMN stored at different storage conditions. (c) SDS-PAGE analysis of stability of OVA released in 1 h from

coated ZMN. Lanes: I – OVA (20μg), II – OVA (2μg). Far-UV CD spectra of OVA released from coated ZMN stored at 2-8°C (d) and at room temperature (e). Force-displacement curves obtained using texture analyzer for ZMN stored at 2-8°C (f), room temperature (g) and 40°C/ 75% RH (h) at different days. Results represent average of three replicates. RT – room temperature. AS – accelerated storage (40°C, 75% ± 5% RH).

Figure 4.7b shows the amount of OVA released from coated microneedles in 1 h after storage at different environmental conditions for up to 90 days. The amount of OVA released had reduced with time for all storage conditions. Increase in storage temperature from 2-8°C to 40°C reduced the amount of OVA recovered from ZMN. Similarly, Figure 4.7c shows the OVA bands after SDS-PAGE, where the band densities decreased with increase in storage temperature. OVA has been shown to form aggregates in less than 2 min at temperature between 70-80°C as confirmed by gel permeation chromatography and differential scanning calorimetry (Weijers et al. 2003).

Circular dichroism spectroscopy was used to study the secondary structure of OVA after storage at different environmental conditions. Figure 4.7d and 4.7e shows the residual molar ellipticity vs. wavelength graphs of OVA released from ZMN stored at different stability conditions. The CD spectra for native OVA showed two strong negative minima at 208 and 222 nm wavelength. These bands are indicative of alpha-helical structure of OVA (Batra et al. 1989). There was no significant change in the minima at 208 and 222 nm after storage of OVA coated ZMN at cold condition and room condition for up to 60 days. The CD spectra of OVA after 90 day storage changed in comparison with the native structure. The decrease in intensity of all α-helix bands shows a change in native structure after 90 day storage (Figure 4.7d and 4.7e).

Figure 4.7f, 4.7g and 4.7h show the force vs. displacement plots obtained from texture analyzer for ZMN stored at different stability conditions for up to 90 days. There was no significant ($p>0.05$) decrease in break force for ZMN stored at room temperature or cold condition. However, storage at accelerated condition, the break force decreased significantly ($p<0.05$) compared with newly prepared ZMN. This indicates that the needles become softer during storage at accelerated conditions and the mechanical strength of ZMN depends on the temperature and humidity of storage condition.

4.3.5 Skin penetration of bacteria after ZMN and hypodermic needle pretreatment

S. epidermidis was labelled with FITC under alkaline conditions. The bacterial suspension was serially diluted, plated onto agar and incubated at 37°C for 24-48 h for validating the cfu/ml concentration. A smear of bacterial suspension on glass slide was examined under confocal microscope for bacterial morphology and fluorescence due to FITC labeling. Figure 4.8 shows the confocal images captured under bright field and dark field. *S. epidermidis* can be seen arranged in grape cluster-like structures (Wilson et al. 2011). The bacteria are reported to be 1-2 μm in size which can also be seen in Fig 4.8c. *S. epidermidis* formed raised, white colored distinct colonies when grown on nutrient agar plates (Wilson et al. 2011).

Table 4.2 shows the extent of skin penetration of *S. epidermidis*. In control group, $1.27 \pm 0.12 \times 10^6$ cfu was found to be adhered to the skin surface out of 10^7 cfu bacteria placed in the donor compartment. This number was taken as denominator for calculating percentage of bacteria permeated across the skin or

adhered to treatment devices. Approximately 4-fold greater cfu of bacteria adhered to the ZMN compared with hypodermic needle. This can be attributed to the greater exposed surface area of ZMN (117 mm^2) compared with 24G hypodermic syringe (70 mm^2). The bacteria adhered to the biopsy punch was of the order of 10^5 cfu. After application of ZMN on skin, the permeation of bacteria increased up to 6 h and then plateaued off over the next 18 h (Figure 4.8d). Of the total bacterial load, 3.29% bacteria permeated across the skin punctured with hypodermic needle in 24 h. Meanwhile, after ZMN treatment, it was only 0.44% of the total bacterial count. This could be related to the bigger size of the pores created by hypodermic needle compared to microneedles (Pikaar et al. 1995).
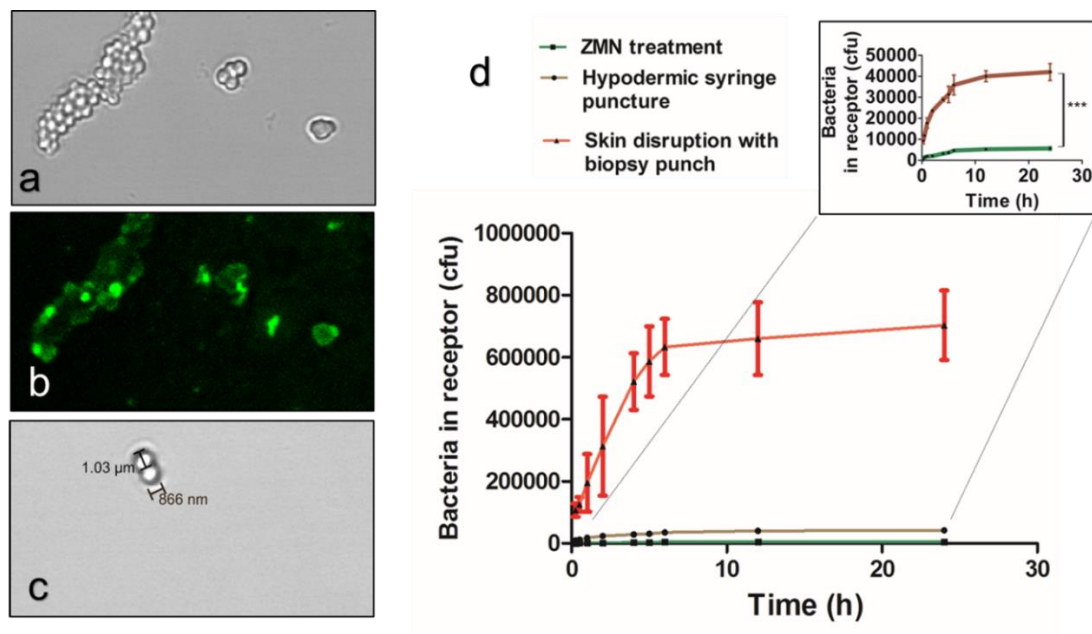
Figure 4.8 FITC labeled Staphylococcus epidermidis in brightfield (a) and dark field (b) photographed using 10x objective lens. (c) Bacteria size measurement photographed using 20x objective lens. Colony forming units of *Staphylococcus epidermidis* in the receptor compartment of Franz diffusion cell at various time points after treatment with ZMN, hypodermic syringe and biopsy punch (d). Data represents mean ± SD (n=3). *** represents that the values are significantly different (p<0.0001, t-test).

Table 4.2 Skin penetration of *S. epidermidis* after treatment with ZMN, hypodermic needle or biopsy punch.

Treatment	Bacteria cfu in the receptor after 24 h of treatment (% of cfu adhered to skin surface)	Bacteria adhered to hypodermic needle, ZMN or biopsy punch (% of cfu adhered to skin surface)
Hypodermic needle	$4.2 \pm 0.40 \times 10^5$ (3.29%)	$0.0186 \pm 0.0017 \times 10^5$ (0.14%)
ZMN treatment for 30 min	$0.0563 \pm 0.0079 \times 10^5$ (0.44%)	$0.0641 \pm 0.0091 \times 10^5$ (0.50%)
Skin disruption with biopsy punch	$7.03 \pm 1.11 \times 10^5$ (47.5%)	$0.641 \pm 0.004 \times 10^5$ (5.03%)

The values are represented as percentage of colony forming units found attached to skin surface after equilibrating skin surface with bacteria for 24 h. Data represents mean $\pm$ SD, n=3.

Confocal microscope was used to compare the depth of skin penetration of *S. epidermidis* after application of hypodermic needle or ZMN. Figure 4.9 shows the optical sections of skin at varying depths from surface up to 230 μm in XYZ plane. The fluorescence associated with the bacteria can be found up to a depth of 230 μm and 120 μm inside skin after treatment with hypodermic needle and ZMN, respectively. Figure 4.9b and Figure 4.9e shows the 3D reconstructed image.
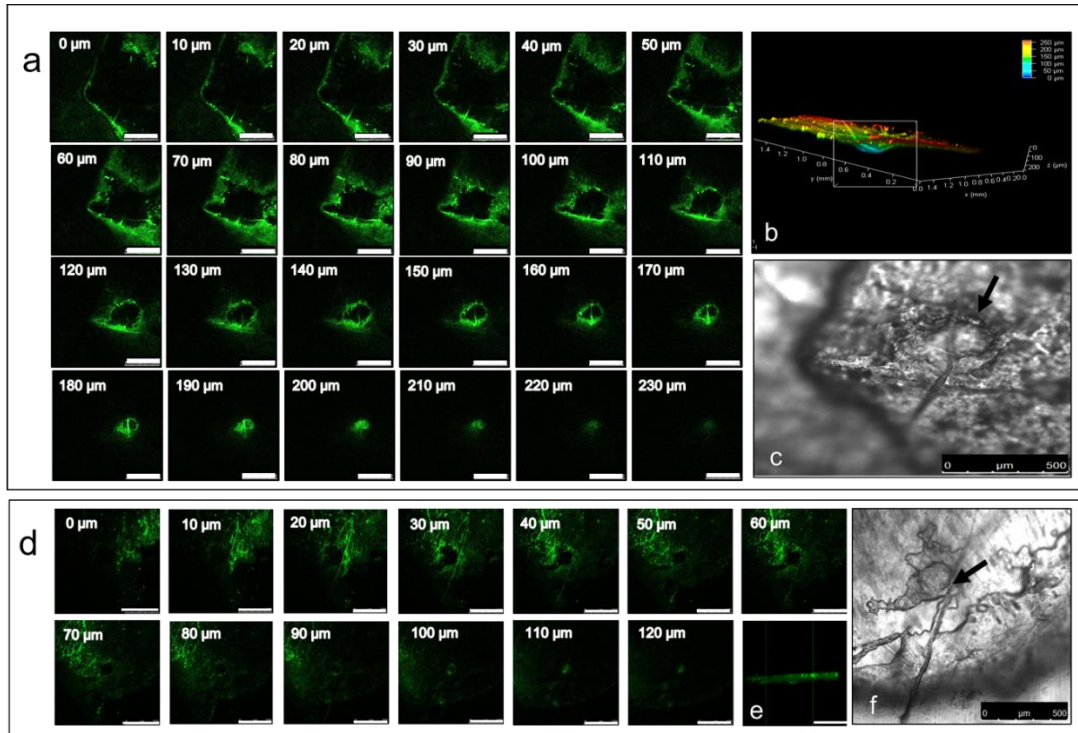
Figure 4.9 Confocal micrographs of FITC labelled Staphylococcus epidermidis obtained through optical sections from surface to inside skin after application of hypodermic needle (a) and ZMN (d). Scale bar represents 500 µm. 3D reconstruction of the micro-channel created due to bacteria permeation after puncture by hypodermic needle (b) and ZMN treatment (e). Brightfield image of pore created by hypodermic needle (c) and ZMN (f). Arrow indicates pore location.

4.3.6 Transcutaneous immunization using OVA coated ZMN

Mice were immunized with a primary and two booster doses as shown in figure 4.10a. Pattern created due to insertion of ZMN array is clearly seen in figure 4.10c. Figure 4.11 shows the total IgG (a), IgG1 (b) and IgG2a (c) anti-OVA antibody response at day 0, day 21, day 42 and day 63 for different groups. A time dependent increase in antibody titers was observed after immunization using all formulations. Blank ZMN were also studied to investigate any non-specific immune response.
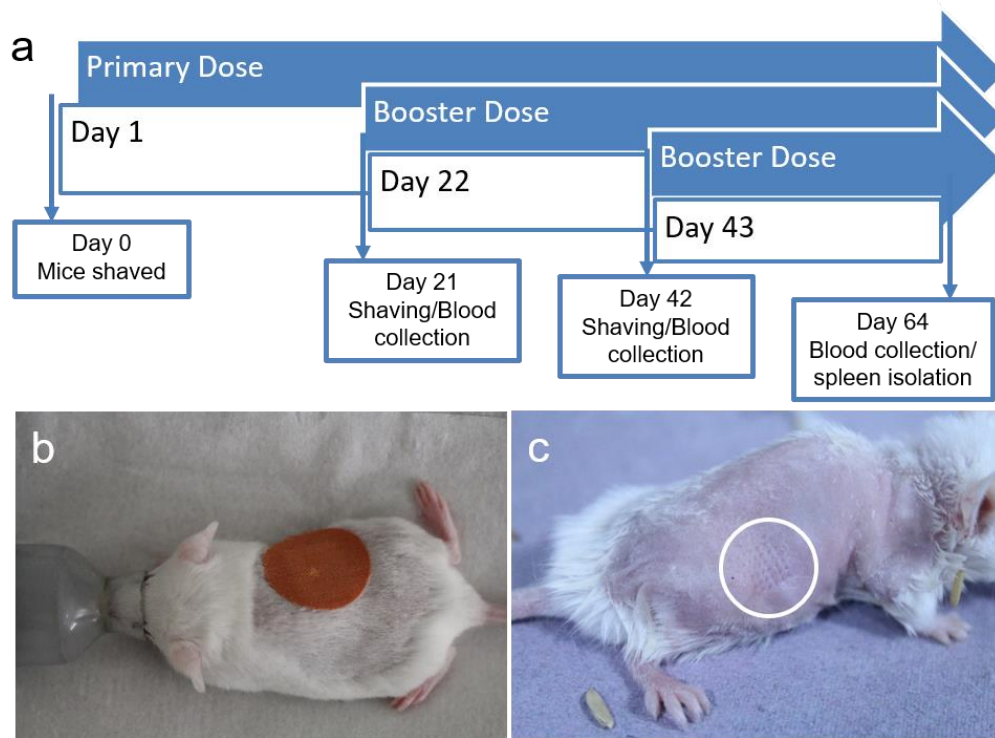
Figure 4.10 (a) Timeline for animal immunization studies. Representative image of animal with ZMN array applied to its back (a) and immediately after removal of ZMN array (c). Area of ZMN insertion is shown in white circle.

No significant antibody response was found for blank ZMN in comparison with the control animal group. Intradermal injection of OVA induced significantly ($p < 0.05$) greater antibody response for IgG2a, IgG and IgG1 compared with control group. All mice that were intradermally injected with OVA produced specific IgG antibodies after the prime immunization. In the case of OVA coated ZMN, induction of antibody response was slower compared with OVA administered through intradermal injection. After day 42 and 64, the antibody response for OVA coated ZMN and OVA intradermal injection was significantly higher ($p < 0.001$) compared with control, treatment with blank and OVA entrapped ZMN. No significant difference in the immune response with OVA

coated ZMN and OVA intradermal injection was observed. In the case of OVA entrapped ZMN or OVA topical application after ZMN pretreatment, there was no significant improvement in antibody response compared with control group. Furthermore, it was found that OVA administered through intradermal and coated ZMN provided greater humoral immune response (IgG1 response) compared with cellular response (IgG2a response, Figure 4.11).
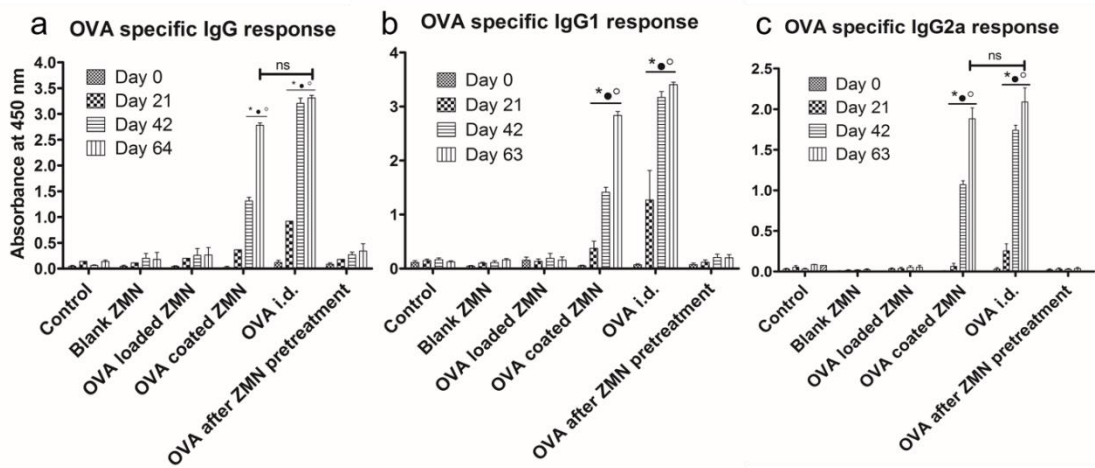
Figure 4.11. OVA-specific serum IgG (a), IgG1 (b), and IgG2a (c) responses delivered using ZMN and intradermal vaccination. Results are shown as mean ± SEM (n=4) and statistical significance was determined by a two-way ANOVA with a Bonferroni post-test. (∗), (•) and (°) represent that the values are significantly different (p<0.001) compared to control, blank ZMN and OVA entrapped ZMN, respectively for the corresponding days.

4.3.7 Splenocyte proliferation assay

The ability of memory T-cells to recognize the antigen can be determined by studying the proliferation of splenocytes of preimmunized mice upon restimulation with antigen. The use of MTT assay for this purpose has been reported earlier (Yang et al. 2007). The proliferation of splenocytes was higher in

the OVA intradermal and the OVA coated ZMN group when re-stimulated with OVA. The stimulation index of OVA coated ZMN was significantly higher (p<0.05) compared with control group (Figure 4.12).
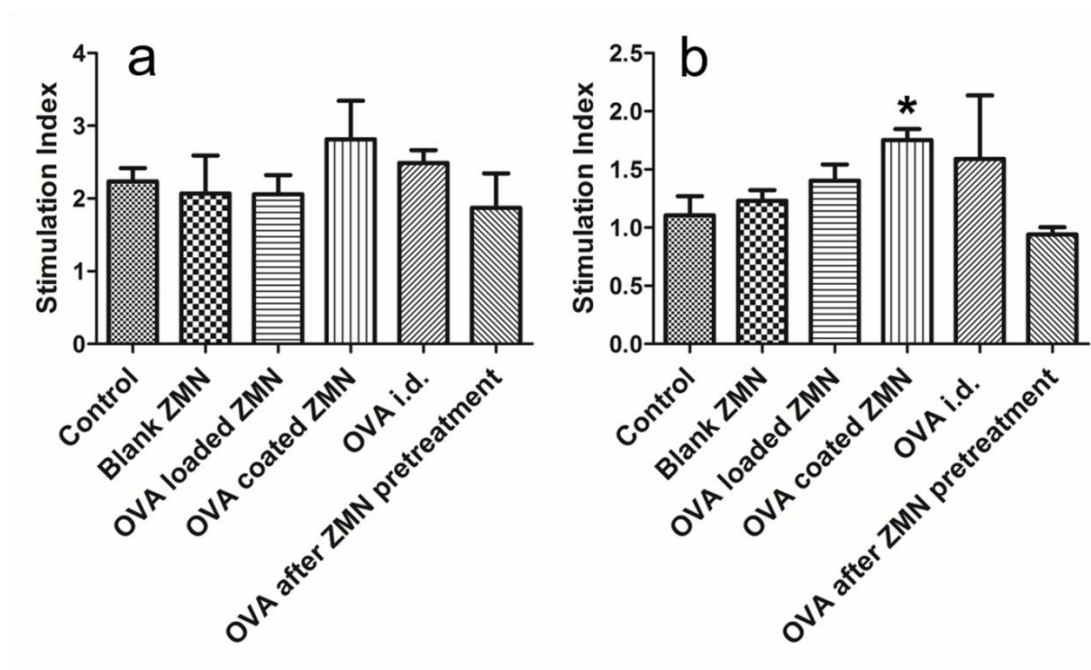
Figure 4.12. The splenocytes of preimmunized mice were stimulated with RPMI 1640 alone, OVA and concanavalin A mitogen for 72 h. Stimulation index (SI) was calculated by dividing the absorbance value of concanavalin A (a) or ovalbumin (b) treatment group with that of RPMI 1640 treated group. The values are presented as mean ± SEM (n=4). (∗) represents that the values are significantly different (p<0.05) compared with control. An unpaired t-test was used in the statistical analysis of experimental data.

4.4 Discussion

Recently, 3D printing has been used to print microstructures including microneedles (Lu et al. 2015). Only few polymeric materials can be fabricated into micro-structures using 3D printing technique. Therefore, 3D printing technique was used to produce master molds from ABS. These master molds were then used to prepare PDMS production molds that were used in casting of ZMN.

This micro-molding technique is considered to be efficient as the master mold and production mold can be reused to cast several microneedle arrays. Such a system can help in high volume manufacturing at low production costs (Lee et al. 2015; Wang et al. 2009).

Zein has been widely studied for its film forming properties. Zein films were found to be brittle in the absence of plasticizers (Lu et al. 2015). The flexibility of zein films improved with the addition of plasticizers. The effect of plasticizers including glycerol, triethylene glycol, dibutyl tartrate, levulinic acid, polyethylene glycol 300 and oleic acid was studied on the mechanical properties and moisture content of the films. Similarly, ZMN without plasticizer showed brittle behavior. The needle tips were broken with the application of <0.4 N/needle force. Furthermore, the microneedle base plate cracked during handling and pressing onto the skin. To improve the strength of microneedle array, glycerol and PEG 400 were incorporated as plasticizers in the polymer matrix. Both glycerol and PEG have previously been reported as compatible plasticizers with zein. Previous study showed that a force of 5 N was optimal for efficient insertion of polyvinyl alcohol microneedles inside porcine skin (Yang et al. 2012). In the case of ZMN, only 0.4 N/needle was sufficient. The skin insertion force will depend on the shape, aspect ratio, needle-tip diameter, distance of separation between microneedles. Since polymer microneedles are weaker (smaller Young's modulus compared to metal microneedles), they need to have a wider base for additional mechanical strength. ZMN were prepared with an aspect ratio of 2.64 with approximate tip radius and separation between microneedles of 30 μm and 1160 μm, respectively.

Three strategies can be used to deliver drugs into the skin using solid microneedles (van der Maaden, Jiskoot, and Bouwstra 2012). In this study, we have compared three approaches to study OVA-specific immunization including – OVA topical application after ZMN pretreatment, OVA entrapped ZMN, and OVA coated ZMN.

FITC tagged OVA was used to visualize the OVA delivery inside skin. Confocal microscopy results confirmed that the fluorescence intensity lost from the microneedle surface after insertion in skin could be attributed to adsorption of FITC-OVA within skin. OVA coated ZMN showed a delivery efficiency of 85% in excised mouse skin. Previously, Vitamin B coated stainless steel microneedles showed a delivery efficiency of 90% in excised pig skin (Gill and Prausnitz 2007). Similarly, influenza virus coated stainless steel microneedles showed 70% delivery efficiency (Kim et al. 2010).

Good stability of antigen entrapped polymeric microneedles have been reported over different storage periods and conditions, although long term and stress stability data for such formulations is limited (Lee et al. 2011; Lee, Park, and Prausnitz 2008). It has been proposed that coating of vaccines on microneedles can reduce the need for cold chain maintenance in contrast to injectable vaccine formulations (DeMuth et al. 2013). The CD spectroscopy results indicated that the secondary structure of OVA was not significantly altered upon storage at cold and room conditions up to 60 days. Additionally, the strength of microneedles was retained at cold condition and room temperature for 90 days. We provide a proof-of-concept, where antigen coated on ZMN were relatively stable at room conditions. However, further studies are required to investigate that

this phenomenon can be extended for longer duration and is applicable for other antigens.

Earlier reports claimed lower microbial penetration in skin after microneedle treatment; however, only a few reports presented experimental results. We found significantly lower permeation of *S. epidermidis* after treatment with MN against treatment with hypodermic syringe or biopsy punch. Donnelly and coworkers have compared the penetration of radiolabeled microorganisms *S. epidermidis, P. aeruginosa* and *C. albicans* through porcine skin after treatment with hypodermic needle or microneedle array. Following hypodermic needle treatment, 48.0% and 3.5% of load on the stratum corneum was detected in the receptor compartment for *C. albicans* and *S. epidermidis* after 24 h (Donnelly et al. 2009). Using FITC labeled bacteria, we were further able to visualize the penetration of bacteria in skin after different treatments. Surface conjugation of bacteria with FITC and other dyes have previously been reported (Pikaar et al. 1995). Bacterial penetration to significantly lower depth was seen in the MN treatment group (against hypodermic syringe application).

Application of OVA coated MN arrays to BALB/c mice significantly enhanced the antibody response. There are several reports with OVA immunization using MN arrays. Maaden et al have reported mice immunized with OVA coated pH sensitive silicon MN arrays (van der Maaden et al. 2014). Effective induction of comparable IgG responses was observed compared to intradermal or subcutaneous OVA injection. However, similar to the results from present study, the induction time was longer and required successive immunizations. Widera and co-workers reported significantly greater OVA specific IgG responses with OVA coated 400 µm long MN than that with OVA

intramuscular injection in hairless guinea pig model (Widera et al. 2006). Size and shape of needles were shown to influence delivery of OVA into skin and the subsequent immune response. Higher OVA-specific IgG response was found after application of OVA loaded nanoparticles on mouse skin previously treated with longer microneedles (1000 µm) compared with shorter microneedles (200 µm and 500 µm) (Kumar et al. 2011).

In contrast, other studies reported no effect of microneedle length on OVA delivery (Widera et al. 2006). Topical application of OVA after ZMN pre-treatment did not result in greater immune response. This could be attributed to the lower penetration of OVA in skin through the pores created by ZMN. While more studies would be required to understand the transport of OVA through skin pores created by ZMN, the negatively charged OVA at neutral pH may penetrate less through the negatively charged skin. It could be noted that a significantly greater amount of OVA was required when OVA was delivered using coated ZMN to show antibody response similar to intradermal administration. This could be attributed to the physical and chemical changes in the OVA during the preparation of OVA coated ZMN. Further studies using OVA and other model antigens would be required to provide greater understanding on the influence of coating and release mechanism on transcutaneous antigen presentation.

A long term memory response is one of the key features of an effective vaccine delivery system. The increased proliferation of splenocytes in mice treated with OVA coated ZMN suggested their ability to enhance the antigen presentation to the T cells and inducing a long lasting immune response. These results would encourage further investigation in utilization of ZMN to deliver antigen for immunization against infectious agents such as influenza virus.

4.5 Conclusion

The ability of zein for preparation of microneedles has been presented in this chapter. Zein was easily casted and shows potential for scale-up using micromolding technique. The prepared microneedle array showed sufficient mechanical strength to penetrate skin. This was the first-time zein was used to prepare microneedle array. Model antigen, OVA was entrapped or coated on to ZMN. OVA loaded ZMN were stable and provided a significantly lower microbial penetration compared with application of conventional hypodermic needle. The OVA coated ZMN approach was found efficient in skin delivery of OVA compared with OVA entrapped ZMN, and topical OVA application after ZMN pretreatment. OVA coated ZMN showed comparable antibody response to intradermal injection. *In vitro* splenocyte proliferation with OVA coated ZMN was also comparable to OVA intradermal injection. Overall, ZMN can be developed for potential delivery of antigen for transcutaneous immunization.

Chapter 5

Zein Microneedles for Localized Delivery of Chemotherapeutic Agents to Treat Breast Cancer: *in vitro* and *ex vivo* evaluation

5.1 Introduction

Microneedles have shown potential in their utility as devices for disease diagnosis, drug and vaccine delivery, and cosmetics application (Bhatnagar, Dave, and Venuganti 2017). Despite the research efforts on microneedles diversified into finding better production technologies, optimized needle dimensions, modes of insertion into tissues**,** material of construction has emerged as the most important parameter that affects drug delivery (Kim, Park, and Prausnitz 2012a; Widera et al. 2006; Bediz et al. 2014).

Micromachining tools have been used to fabricate microneedles made of stainless steel, silicon and ceramic materials (Mikszta et al. 2002; Indermun et al. 2014). However, their application in drug delivery is limited by poor drug loading efficiency. The metal-based microneedles would generally be applicable in poke-and-patch approach, where blank microneedles are inserted into the skin, and then the drug formulations are applied to allow drug permeation (Ita 2015). The amount of drug that can be coated on to the metal-based needle materials is severely limited (Tuan-Mahmood et al. 2013). An alternative to use metal-based materials is to prepare hollow microneedles. Liquid drug formulation can be transported into the skin through the hollow needles (Kim, Park, and Prausnitz 2012a). However, this is limited by the fluid volume that can be administered and the skin resistance against permeation of fluids.

In the second generation of microneedle development, micromolding technique allowed utilization of varied polymeric materials to construct microneedles (Bhatnagar et al. 2017; Bediz et al. 2014; Donnelly et al. 2011). This has significantly expanded the scope of application of microneedles to diversified

areas. Some of the most widely used polymeric materials to construct microneedles have been polyvinyl alcohol, polyvinyl pyrrolidone, sodium carboxy methyl cellulose, chitosan, alginate, poly(β-ester), acrylate polymers, polylactide among others (Lee, Han, and Park 2013). These polymeric microneedles could be tailored to be stable or dissolvable; and optimize the drug loading and release behaviour.

In general, the polymer and casting medium characteristics including molecular weight, water solubility, concentration, viscosity, entrapped air would influence the mechanical strength, skin insertional force and stability of microneedles (Milewski, Brogden, and Stinchcomb 2010; Larrañeta et al. 2016). Furthermore, these material attributes would also influence the amount of drug that can be loaded within microneedles or coated on the microneedle surface (Gill and Prausnitz 2007; Donnelly, Raj Singh, and Woolfson 2010).

To that end, the objective of this particular study was to understand the influence of water solubility of compounds in their entrapment, release behavior and skin permeation in microneedles constructed of zein. Zein microneedles were prepared for delivery of ovalbumin protein as discussed in the previous chapter. Zein is a prolamine protein derived from corn. It a cheap, GRAS ('generally regarded as safe' by FDA) protein used in the manufacture of biodegradable plastics, fibers, coatings, adhesives and inks (Shukla and Cheryan 2001). Zein microneedles have not been studied for delivery of small molecules before. This work involved loading of two widely used anti-breast cancer agents, tamoxifen and gemcitabine in zein microneedles. These two drugs possess different water solubility. The physicochemical properties of tamoxifen included molecular weight - 371.5 Da, melting point - 95°C , water solubility - 0.04 µg/ml, log P -

4.44, pKa ~ 8.8, clinical dose requirement - 20–40 mg/day (Gao and Singh 1998; Fontana et al. 2005; Heel et al. 1978; Chawla and Amiji 2002; Jena et al. 2014). On the other hand, physicochemical properties of gemcitabine included molecular weight - 299.6 Da, melting point - 277 °C, water solubility ~ 38 mg/ml, log P - (-)1.4, pKa - 3.6, and a clinical dose requirement of 800–1250 mg/m^2 (Aapro, Martin, and Hatty 1998; Trickler et al. 2010; Poulin et al. ; Joshi, Kumar, and Sawant 2014; Chitkara and Kumar 2013). The influence of these properties of drugs in the skin permeation after loading in microneedles was studied.

5.2 Materials and Methods

5.2.1 Materials

Tamoxifen was purchased from Sigma Aldrich (Bangalore, India). Gemcitabine was a kind gift sample from Fresinius Kabi India Pvt. Ltd., Gurgaon, India. Zein, polyethylene glycol 400 (PEG 400), glycerol, rhodamine B base and all other chemicals were purchased from Sigma-Aldrich Chemical Company (Bengaluru, India). PVP-K30 was obtained from Himedia Laboratories, Mumbai. Isopropyl alcohol, HPLC grade acetonitrile, methanol and ammonium acetate were procured from ThermoFisher Scientific. Milli-Q (Millipore, USA) water was used for all the experiments.

5.2.2 Preparation of drug entrapped microneedles

Zein microneedles (ZMN) were fabricated using the micromolding technique as described previously in this thesis. A master mold with 6 × 6 needle design was 3D printed with acrylobutyl nitrile styrene (ABS) polymer. This master mold was used to prepare needle-free polydimethyl siloxane (PDMS)

molds. Zein protein (60% w/w) in 90% ethanol was used to prepare ZMN. Glycerol and PEG 400 at 10% w/w concentrations were used as plasticizers. The tamoxifen and gemcitabine entrapped ZMN were prepared by mixing the drugs at 1:100 w/w of zein and 25 mg, respectively before casting the needles. Free or drug entrapped zein matrix was poured onto PDMS molds and allowed to settle in the pores under vacuum. Then the molds were allowed to air dry for 48 h after which they were gently peeled.

5.2.3 Preparation of drug coated microneedles

Blank ZMN were prepared as described in previous section. These blank ZMN were dip coated with either tamoxifen or gemcitabine. ZMN were dipped into drug solution in a controlled fashion by attaching the array to the arm of a texture analyzer setup (Stable Microsystems, UK). To optimize the coating, dipping medium was prepared using different concentrations of PVP including 10, 20, 30, 40 and 50% w/v in 100% ethanol. Rhodamine (1 mg/ml) was used as a model dye to visualize the coating property. ZMN were coated with rhodamine-PVP solution using the texture analyzer setup with a 30 s dip time. Tamoxifen was coated on ZMN using tamoxifen (5 mg/ml) dissolved in 30% w/v PVP. The needles were dipped in coating solution for 30 s and air dried for 12 h. Similarly, gemcitabine was coated on ZMN by dipping in 42 mg/ml gemcitabine in phosphate buffer.

5.2.4 Characterization of drug loaded ZMN

ZMN were examined for needle dimensions and uniformity using an optical microscope (IX53, Olympus, Japan). PVP-rhodamine coated microneedles were imaged using a stereo microscope (SZX2, Olympus, Japan) and fluorescence

microscope (DMi8, Leica, Germany). Texture analyzer (TA XT, Stable Microsystems, UK) was used to measure the compression force required to fail ZMN. A cylindrical Delrin probe (10mm, part code P/10) linked to a 50 kg load cell was set in the compression mode, while ZMN were placed on a heavy metal platform. The probe compressed the microneedle array with a speed of 0.5 mm/s up to a distance of 0.8 mm. Then the probe was held in place for 5 s. Compression force vs. distance plots were recorded for three sets of ZMN.

FTIR and differential scanning calorimeter (DSC) were used to study the drug loading in ZMN. For FTIR (FT/IR-4200, Jasco Inc., USA) studies, spectra were obtained for neat tamoxifen, gemcitabine, zein, physical mixtures (zein+gemcitabine, zein+tamoxifen), blank and drug loaded ZMN. The samples were mixed with potassium bromide in a 1:1 weight ratio and spectra obtained between wavenumbers 4000 and 400 cm^{-1} at a spectral resolution of 2 cm^{-1} in a dynamic reflectance sample holder. For the same preparations, DSC (DSC 60, Shimadzu, Japan) was used to investigate the thermal transitions. Samples (2 mg) were placed in aluminium pans and hermetically sealed. Thermograms were recorded between ambient temperature and 300°C with a constant heating rate of 10°C per min.

5.2.5 HPLC method for tamoxifen and gemcitabine

Reverse phase HPLC (LC-20, Shimadzu, Japan) method was developed for quantification of tamoxifen and gemcitabine. For tamoxifen analysis, combination of 0.5 mM ammonium acetate and methanol (15: 85) was used as mobile phase. The chromatographic separation of tamoxifen (50 µl injection volume) was achieved on an end-capped C$_{18}$ analytical column (150 × 4.6 mm

i.d., 5 μm, Phenomenex, USA), maintained at 40°C at a 1 ml/min flow rate. The absorbance was recorded at 274 nm wavelength using UV-visible detector. Standard concentrations of tamoxifen were prepared at 0.5, 1, 2, 4, 6 and 8 μg/ml in methanol (n=6). The regression equation was obtained by plotting the area under the curves against concentrations (y = 89254x + 9976.9, r^2=0.9993). For gemcitabine analysis, mobile phase included a combination of phosphate buffer pH 7.4 and methanol at 90:10 ratio. The column temperature was maintained at 10°C. The injection volume was 40 μl and flow rate was maintained at 1 ml/min. Absorbance corresponding to gemcitabine was recorded at 275 nm wavelength. Standard concentrations of 5, 10, 15, 25, and 30 μg/ml (n=6) were prepared in phosphate buffer to obtain regression equation (y = 41697x + 387, r^2=0.9999).

5.2.6 Drug release studies

Franz diffusion cell setup (PermeGear Inc., USA) was used to perform the drug release studies. ZMN entrapped or coated with tamoxifen and gemcitabine were placed needles facing down at the interface of donor and receptor chamber such that the needles were freely immersed in receptor media. The receptor chamber contained phosphate buffered saline (PBS, pH 7.4, 5 ml) that was mixed using a magnetic stir bar. Tamoxifen release studies also contained 20% methanol in the receptor chamber to improve solubility. Tamoxifen is known to be soluble in chloroform, DMSO, isopropanol, methanol and propylene glycol. The use of alcohols up to 40% have been previously reported with drug release studies for tamoxifen loaded delivery systems.(Sharifi et al. 2009) At predetermined time points, 300 μl sample was withdrawn from the receptor chamber and restored with fresh medium. Samples were analyzed using HPLC method described above.

ZMN/release medium partitioning studies were performed to understand the partitioning of drugs into the zein matrix. Tamoxifen (1 µg/ml) and gemcitabine (0.3 mg/ml) drug solutions were prepared in PBS: methanol (80: 20) and PBS, respectively. Blank ZMN were incubated in drug solution for 24 h at 37 °C. Then the concentration of drug in the aqueous phase was analysed using HPLC. Ratio of drug concentration in ZMN: release medium was calculated.

5.2.7 In-vitro skin penetration studies

Excised porcine ear skin was used as a model to study ZMN insertion and drug permeation into and across skin. Porcine ears were purchased from a local abattoir. The ears were rinsed with water and hair on the dorsal surface was trimmed using a hair trimmer. The dorsal ear skin was harvested using a scalpel blade and any remaining subcutaneous fat was carefully removed. Excised skin was stored at -80ºC and used within 3 months for experimentation. During experiment, the skin was thawed at room temperature and stabilized at 37 ºC for 3 h. Skin sample thickness was gauged using digital micrometer (Baker gauges India Pvt. Ltd., Mumbai, India). Skin sample was mounted in Franz diffusion cell by sandwiching it between the donor and receptor chamber with epidermis facing the donor chamber. Transepidermal electrical resistance (TEER) of skin was measured by applying 1 mA of direct current (I) across the skin with a DC power source (V-care Meditech Pvt. Ltd., Bangalore, India). The dip in voltage (V) was gauged using a digital multimeter (17B, Fluke Corporation, WA, USA). Using Ohm's law (V=IR), the resistance (R) was calculated. Only skin samples with TEER > 3 kΩ were used in the study. Transepidermal water loss (TEWL) of skin samples was measured using a vapometer® (Delfin Technologies Ltd., Kuopio,

Finland). TEWL was measured by placing the probe over the donor chamber of diffusion cell. To understand the changes in TEER and TEWL after insertion of microneedles, skin was treated with blank ZMN for 5 minutes, after which TEER and TEWL values were collected at predetermined time points for 24h.

Three different experimental approaches were performed to study the drug permeation through skin using ZMN. All the studies were performed in triplicate. For the "poke and patch" approach, ZMN were inserted into skin and held for 5 min. ZMN were pressed onto the skin sample with slight thumb pressure. The pressure and duration was fixed based on the work described in previous chapter. This MN treated skin was charged with 200 μl of drug solution (0.5 mg/ml) in the donor chamber and treated for 48 h. In the other two approaches, ZMN entrapped or coated with drugs were inserted into skin and treated for 48 h. Samples (0.3 ml) were withdrawn from the receptor chamber at predetermined time points and analysed using HPLC method described above. After 48 h, the ZMN were withdrawn and skin samples were dabbed with wipes (Kimtech) to remove surface adsorbed compound. Tape stripping technique was performed to remove the stratum corneum layer using scotch book tape (845, 3M Corporation, USA). Fifteen strips were collected to remove the stratum corneum. TEER and TEWL were measured before and after tape stripping. Tamoxifen and gemcitabine from tape strips were extracted by incubation in methanol or phosphate buffer, respectively for 12 h while shaking. Viable skin remained after stripping was cut into small pieces using a sharp blade and homogenized using tissue homogenizer. Tamoxifen and gemcitabine were extracted by incubation in methanol or phosphate buffer, respectively for 12 h. All the samples were subjected to HPLC analysis. It should be noted that the drug amounts in the donor compartment for

all approaches were different and the release percentages were calculated based on loading achieved for entrapped or coated ZMN.

In a different experiment, tamoxifen-PVP coated ZMN or gemcitabine coated ZMN were inserted into the skin for 5 min. The skin samples were processed to determine amount of tamoxifen retained within stratum corneum and viable epidermis as described above.

Skin permeation parameters were calculated by plotting cumulative amount of drug permeated per unit area of skin against time. Flux (J) was obtained from the slope of linear part of the curve. The lag time (t_{lag}) was calculated from the reverse extrapolation of the steady-state portion of the curve to the time axis. Permeability coefficient (K_p) and diffusion coefficient (D) were computed using Equations (1) and (2):

$$Kp = \frac{J}{C_d} \qquad\qquad (1)$$

$$D = \frac{h^2}{6 \times t_{lag}} \qquad\qquad (2)$$

Where, 'C_d' is concentration of the drug in donor compartment and 'h' is thickness of the skin.

Statistical analysis

All the results were reported as average ± standard deviation (n≥3). The results were correlated by performing Student's t-test or analysis of variance (Graph Pad Prism, USA), where $p < 0.05$ was considered to be significant, unless specified.

5.3 Results

5.3.1 Characterization of ZMN

Figure 5.1 shows the scheme for fabricating ZMN. Figure 5.1a and 5.1b show a 3D printed ABS mold and PDMS mold, respectively. Figure 5.1c shows a stereomicroscope image of microneedle array. Microscopic image of individual needles is shown in Figure 5.1d. The ZMN were smooth conical structures with the average length and width at base of 965 ± 23 µm and 363 ± 15 µm, respectively. No observable stress marks could be seen on the needle surface. Drugs were loaded in ZMN by either entrapping into the matrix or coating onto the needles. Figure 5.1e depicts the procedure for preparing drug entrapped and drug coated microneedles. Dipping technique was used to prepare the drug coated microneedles (Figure 5.1e).
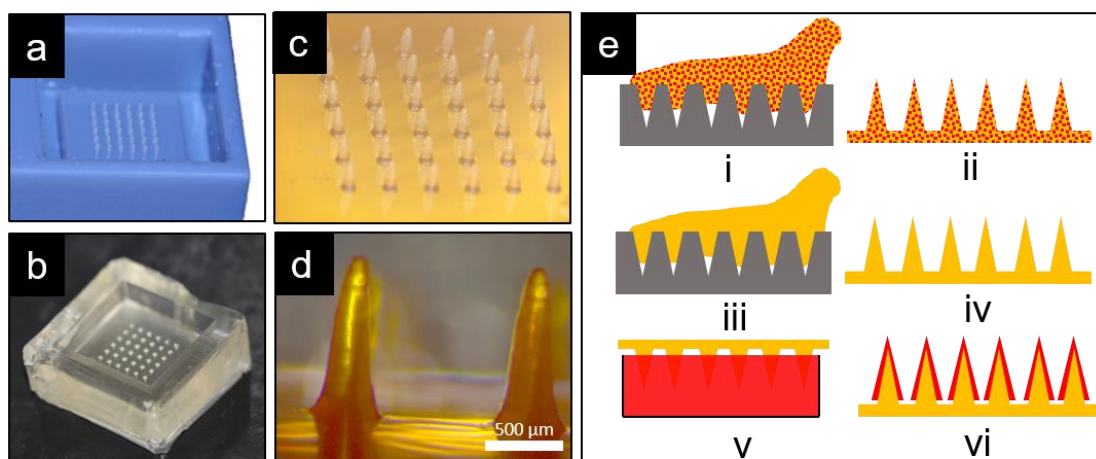
Figure 5.1 Representative photographs of 3D printed ABS mold (a) and PDMS mold (b) and microneedle array (c). Optical micrograph of a single microneedle (scale bar - 0.5 mm) (d). (e) Scheme of fabrication of drug entrapped (i-ii) and drug coated (iii-vi) microneedles. Drug incorporated matrix is poured onto PDMS molds (i) to form drug entrapped microneedles (ii) or blank microneedles (iv) are dipped into coating solution (v) to give drug coated microneedles (vi).
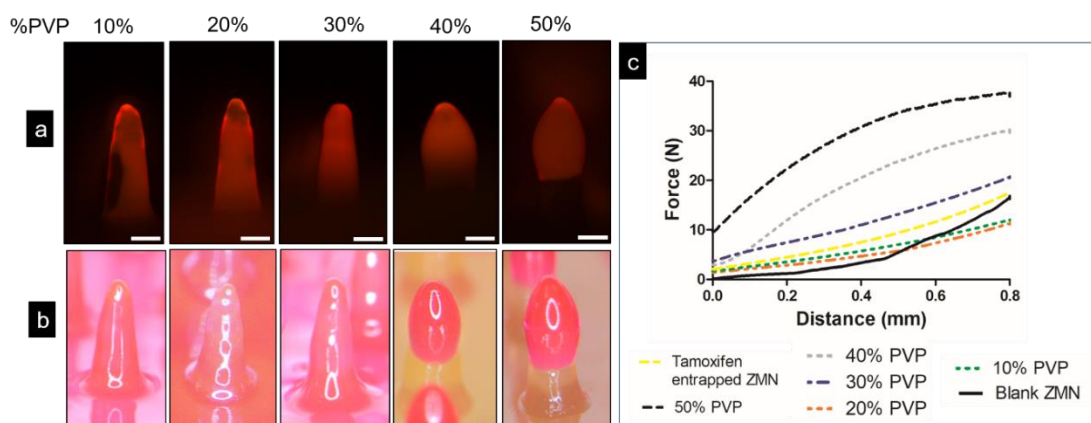
Figure 5.2 Fluorescence (a) and brightfield (b) images of zein microneedles coated with different concentrations of rhodamine-PVP (scale bar =200µm). (c) Compression force versus displacement plots for tamoxifen loaded and blank zein microneedles.

The coating solution was optimized for PVP (10–50% w/v in ethanol) concentration to prepare tamoxifen coated microneedles. Figure 5.2a and 5.2b show representative fluorescence and brightfield microscopic images of PVP-rhodamine coated ZMN, respectively. The shape of the microneedles was retained after coating with 10, 20 and 30% w/v PVP with uniform coating. Coating with higher PVP concentrations (40 and 50% w/v) led to excess deposition on the needle tips that resulted in blunt bulb structures (Figure 5.2b). Figure 5.2c shows the compression force versus displacement plots for the drug coated ZMN. Compression force increased with the increase in PVP concentration in coating solution.
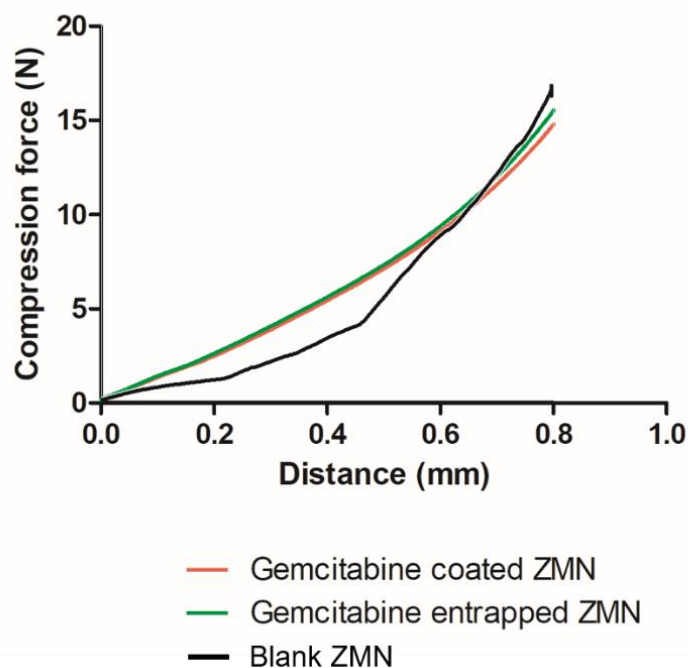
Figure 5.3. Compression force versus displacement curves for blank ZMN, gemcitabine entrapped ZMN and gemcitabine coated ZMN. Plots were obtained using the texture analyzer. Plots are representative of three individual measurements.

A compression force of 16.1 ± 1.5 N was recorded for blank ZMN. PVP concentration of 30% w/v has shown integrity of needle shape, spread deposition with suitable mechanical strength. Therefore, 30% w/v PVP was used as an optimized dipping medium for tamoxifen coating on ZMN. On the other hand, gemcitabine being water soluble compound was dip coated without using a hydrophilic polymer coating solution. Gemcitabine coated or entrapped ZMN showed similar compression force as blank ZMN (Figure 5.3). All the force-displacement curves were smooth indicating no abrupt buckling or breaking of microneedle tips (Figure 5.3). Figure 5.4 shows representative DSC thermograms of neat zein, gemcitabine, tamoxifen, and their physical mixtures and after entrapment in ZMN. Tamoxifen and gemcitabine showed an endothermic peak at

95°C and 277.5ºC temperature, respectively indicating their crystalline nature. No characteristic peak was observed for neat zein up to a temperature of 300°C. Physical mixtures of zein – tamoxifen and zein – gemcitabine showed the characteristic peaks of the respective drug molecules. This indicated presence of no physical incompatibility between the zein and drug molecules. However, the drug entrapped ZMN did not show the endothermic transitions correlating to tamoxifen and gemcitabine, indicating molecular entrapment of drugs. Figure 5.5 shows the representative FTIR spectra of the neat compounds and their physical mixtures. Zein showed its characteristic amide peaks between 1500 and 1700 cm^{-1} (1664 and 1550 cm^{-1} for amide I and amide II, respectively). FTIR spectrum of gemcitabine showed characteristic peaks at 1680, 1721 and 3393 cm^{-1} corresponding to amine bands, ureido group and NH_2 stretching vibration. The spectrum for neat tamoxifen exhibits characteristic peaks at 1610 cm^{-1} (C=C stretching) and 1512 cm^{-1} (C=C aromatic ring stretching). C–O aryl ethers stretching bands could be seen at 1246 cm^{-1}, and 1033 cm^{-1}. The spectra of physical mixtures retained characteristic peaks of both drug molecules and zein indicating their compatibility. The intensity of characteristic drug peaks for both gemcitabine and tamoxifen were weaker in the drug entrapped ZMN.
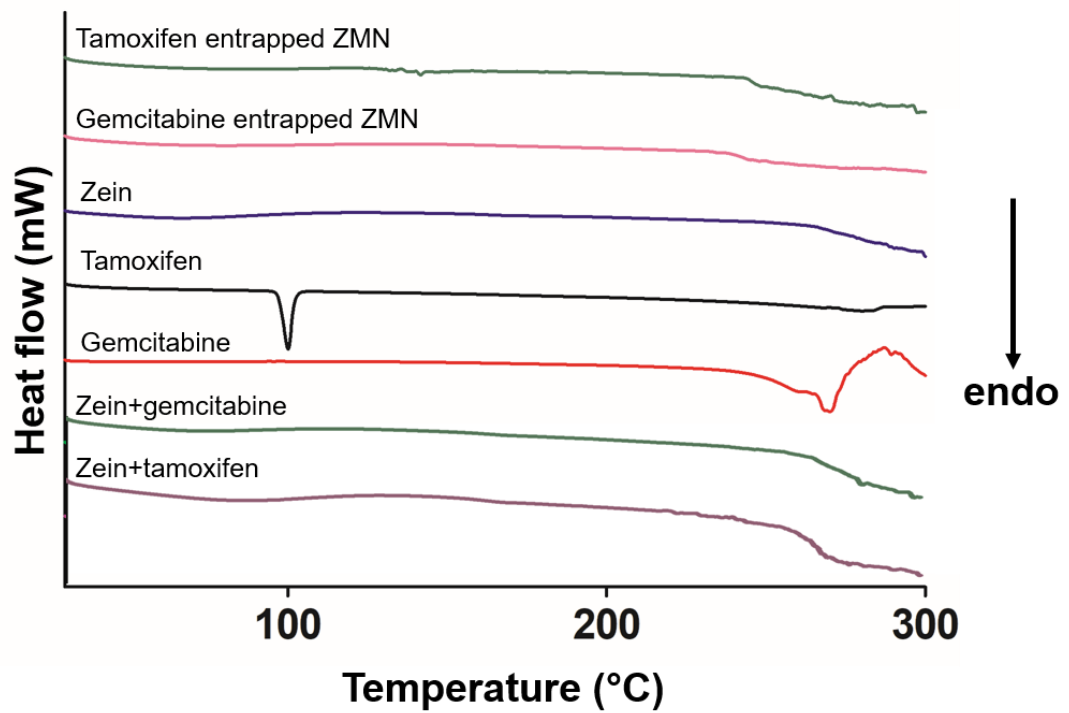
Figure 5.4 DSC thermograms for neat zein, gemcitabine, tamoxifen, drug entrapped ZMN and physical mixtures (zein+tamoxifen and zein+gemcitabine). The physical mixtures were used with drug ratios same as that in drug entrapped ZMN.
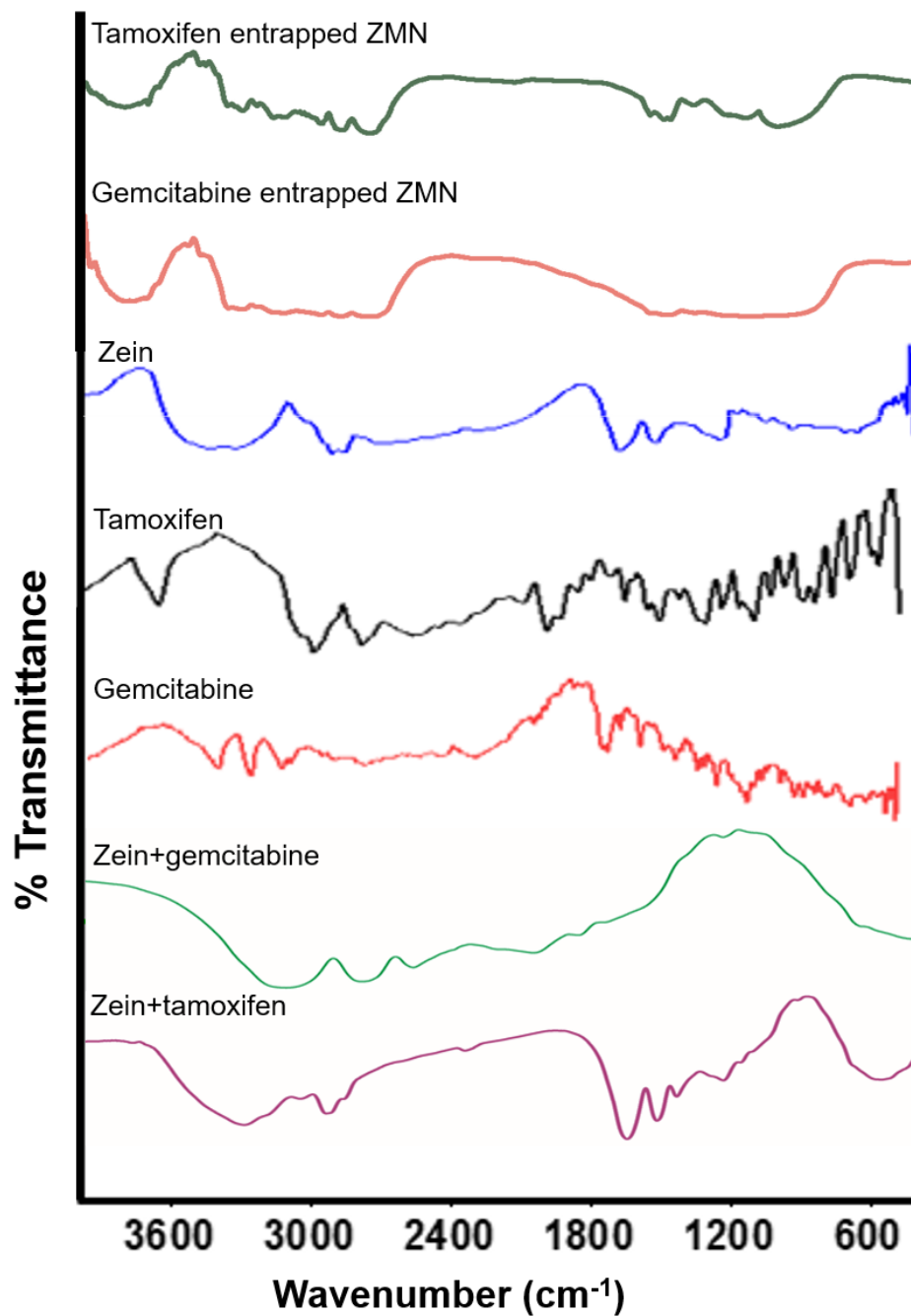
Figure 5.5 Representative FTIR spectra of neat zein, gemcitabine, tamoxifen, drug entrapped ZMN and physical mixtures (zein+tamoxifen and zein+gemcitabine). The physical mixtures were used with drug ratios same as that in drug entrapped ZMN.

5.3.2 Drug loading and release profile

HPLC chromatograms for standard samples for tamoxifen and gemcitabine used for preparation of calibration curve are shown in figure 5.6. The average amount of tamoxifen entrapped in each microneedle array was 607±21 µg. Tamoxifen drug release studies were performed in phosphate buffer and phosphate buffer containing ethanol/ methanol mixture. Tamoxifen release from ZMN was negligible at 1.2% after 12 h time (Figure 5.7).
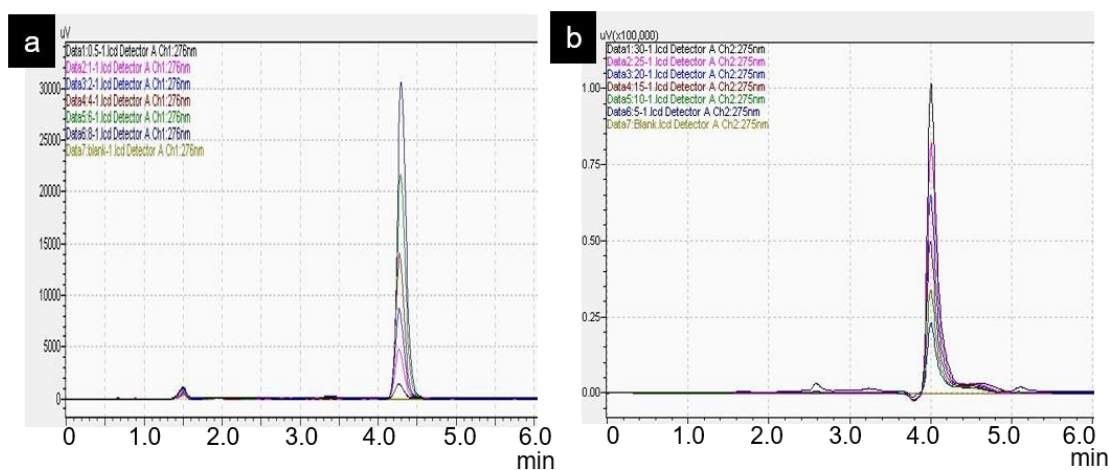
Figure 5.6 Representative chromatograms for standard samples of tamoxifen (a) and gemcitabine (b).

Tamoxifen was coated on the ZMN to improve the percentage drug release. Different coating media were used to optimize the loading of tamoxifen. Initially, dip coating was performed using tamoxifen dissolved in 1% ethyl cellulose in isopropyl alcohol. The average amount of 208 µg tamoxifen was coated in each microneedle array. However, only 1% tamoxifen released over a period of 12 h. Then, different concentrations of PVP in ethanol were used to coat tamoxifen over ZMN. PVP (30% w/v in ethanol) solution containing 35 mg/ml tamoxifen was used as optimized coating solution. Needles were cut from the MN

bases and the drug coated onto needles and bases was estimated separately. The amount of tamoxifen coated onto the base and needles was 320.7 ± 52.7 µg and 158.1 ± 44.9 µg, respectively. The loading efficiency and entrapment efficiency (EE) was calculated based on the formulas given below.

$$\% \, Loading \, efficiency = \frac{Amount \, of \, drug \, in \, ZMN \, array}{Average \, weight \, of \, ZMN \, array} \times 100 \qquad (3)$$

$$\% \, EE = \frac{Amount \, of \, drug \, coated \, on \, 36 \, needles}{Amount \, of \, drug \, in \, coating \, solution \, used \atop for \, individial \, ZMN \, array} \times 100 \qquad (4)$$

For tamoxifen entrapped ZMN, $0.17 \pm .005\%$ drug loading was seen. The entrapment efficiency would be 100% as all the added drug would be incorporated in the ZMN array. For tamoxifen coated ZMN, the drug loading was $4.59 \pm 1.30\%$. This corresponds to $4.55 \pm 0.50\%$ entrapment efficiency. Drug release studies showed that after 15 min time point, 80% of the microneedle loaded tamoxifen released into the receptor medium. Surprisingly, this cumulative amount released decreased with progression of time and showed $8.67 \pm 1.14\%$ in receptor medium after 48 h. It was found that $89.46 \pm 7.63\%$ of loaded tamoxifen remained in the microneedle array after 48 h. Several repetitions of this release study showed similar profile (Figure 5.7). It can be concluded that tamoxifen partitioned back into the zein microneedle matrix after the initial burst release. This initial burst release is attributed to the water soluble PVP used in the coating solution. The tamoxifen partitioning studies in ZMN-aqueous release medium showed that tamoxifen was completely partitioned into ZMN, while no drug was detectable in release medium after 24 h incubation.
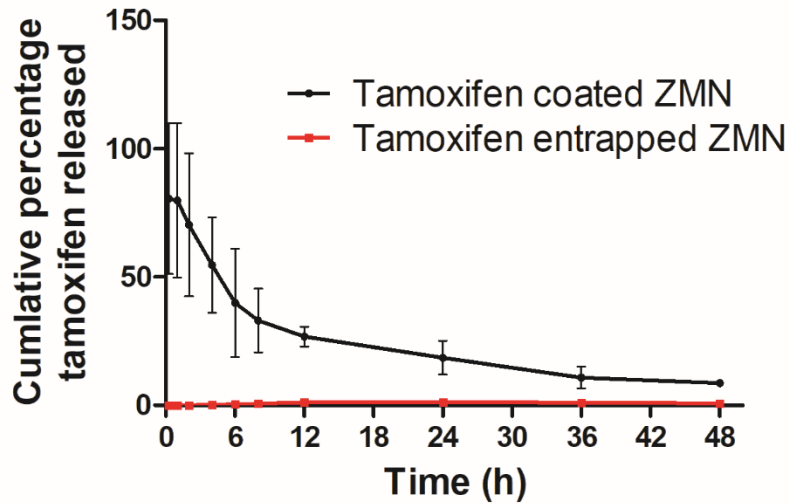
Figure 5.7 Drug release profile for tamoxifen entrapped and tamoxifen coated zein microneedles. Release studies were performed using a Franz diffusion cell with phosphate buffer and 20% methanol as receptor media. Data presented as mean±SD, n=3.
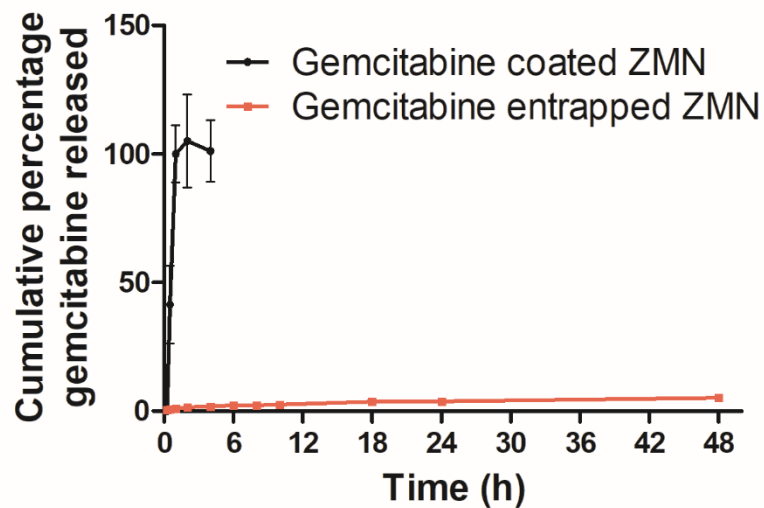
Figure 5.8 Drug release profile for gemcitabine entrapped and gemcitabine coated zein microneedles. Release studies were performed using a Franz diffusion cell with phosphate buffer as receptor media. Data presented as mean±SD, n=3.

Another anticancer agent, gemcitabine with greater water solubility compared with tamoxifen was entrapped or coated onto ZMN. The amount of gemcitabine entrapped into microneedles was 1458.55±73.57 µg. Drug loading was calculated to be 0.41±0.02% with 100% entrapment efficiency. Gemcitabine was coated onto ZMN using gemcitabine dissolved in phosphate buffer. It was found that 83.07±3.24 µg of gemcitabine was coated onto the microneedles (only 3.86±0.76 µg being on the microneedle base). The loading efficiency for coated ZMN was 2.41±0.09% with an entrapment efficiency of 0.19±0.007%. Figure 5.8 showed the release profiles of gemcitabine from entrapped and coated microneedles. Complete (100%) gemcitabine release was achieved from coated microneedles within 1 h time. On the other hand, only 5.18 ± 0.87% (75.5±12.7 µg) gemcitabine was released after 48 h time from entrapped microneedles. The gemcitabine partition studies showed that 100% of the drug was retained within the aqueous release medium and did not partition into ZMN.

5.3.3 Skin permeation studies

Skin permeation studies were performed to investigate the drug disposition within skin and permeation across the skin after application of ZMN. After skin was treated with blank ZMN for 5 minutes, the TEER was seen to decrease from 3.17±0.52 kΩ to 2.09±0.55 kΩ (34% decrease) over 48h. The TEWL, however, increased from 25.86±9.68 g/m^{2}h to 32.4±7.52 g/m^{2}h.

Tamoxifen did not permeate across the skin after 48 h application of ZMN entrapped or coated with drug. Similarly, with the poke and patch approach, where the skin was pre-treated with blank ZMN followed by charging tamoxifen solution, no permeation across skin was observed. Tape stripping method was

performed to remove stratum corneum to determine the amount of tamoxifen retained within different skin layers. Figure 5.9 shows the amount of tamoxifen retained within stratum corneum and viable epidermis. Application of tamoxifen coated ZMN showed that $33.64\pm3.58\%$ tamoxifen retained within viable epidermis, while no drug was detected in the stratum corneum. On the other hand, only $0.23\pm0.14\%$ tamoxifen was found in viable epidermis after insertion of tamoxifen entrapped microneedles. With the poke and patch approach, $16.95\pm3.30\%$ and $0.52\pm0.85\%$ tamoxifen was recovered from viable epidermis and stratum corneum, respectively.
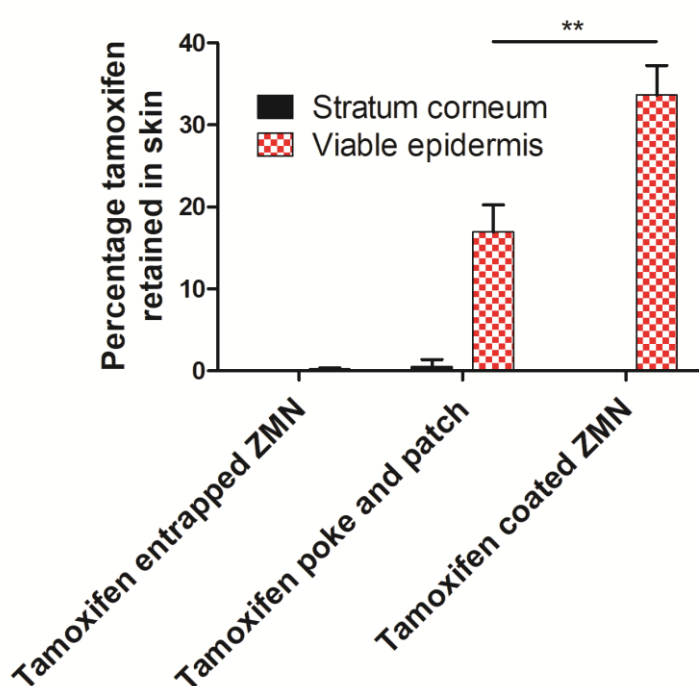
Figure 5.9 Percentage of Tamoxifen retained within the stratum corneum and viable epidermis after 48h of treatment. Tamoxifen did not permeate across the skin after application of any of the formulations over 48h. Data presented as mean$\pm$SD, n$\geq$3. ** is indicative of significant difference (p<0.05) in tamoxifen amount retained in viable epidermis for poke and patch approach against coated ZMN approach.

In the case of gemcitabine microneedles, poke and patch approach provided the greatest percentage permeation across excised skin (Figure 5.10a). The cumulative amount of gemcitabine permeated across the skin after 48 h was 41.48±2.82% (41.48±2.82 µg) and 34.55 ± 3.09% (27.64±2.47) µg for poke and patch approach and application of coated microneedles, respectively (Figure 5.10a). Gemcitabine entrapped microneedles showed 3.40±0.46% gemcitabine permeation across the skin. However, the actual amount of gemcitabine permeated after application of gemcitabine entrapped microneedles was greater (52.18±6.35 µg) compared with other strategies. This is expected as gemcitabine was also entrapped in the MN base and was available for release. Table 5.1 shows the skin permeation parameters of gemcitabine. The cumulative amount of gemcitabine permeated after 24 h application for entrapped microneedles was 81.9±9.9 µg/cm^2. However, the lag time was found to be 4.9±2.6 h. There was no significant difference in flux between the three application strategies. The change in TEER and TEWL values followed the same trend across all experiments. With poke and patch studies, TEER and TEWL values did not change significantly after 48h. With coated or entrapped MN skin permeation, a 33.8% decrease in TEER was seen after 48h of study while TEWL values were not altered significantly. Figure 5.10b shows the amount of gemcitabine retained within viable epidermis was 50% and 9.5% of the loaded amount after application of coated microneedles and poke and patch approach. Gemcitabine was not detected in the stratum corneum with gemcitabine coated ZMN, thus no bar appears for the same in figure 5.10b.

Table 5.1. Skin permeation parameters of gemcitabine.

Treatment	Lag time (h)	J ($\mu g/cm^2/h$)	Q_{24} ($\mu g/cm^2$)	D (cm^2/h)	K_p (cm^2/h)
Gemcitabine entrapped ZMN	4.97±2.57	5.36±0.83	81.92±9.97	0.21±0.32	0.0037±0.0006
Gemcitabine coated ZMN	0.26±0.10	4.62±1.35	43.39±3.88	0.26±0.10	0.06±0.01
Gemcitabine-poke and patch approach	0.26±0.08	8.14±3.48	65.13±4.42	0.48±0.19	0.08±0.03

ZMN: zein microneedle; J: Flux; Q_{24}: Cumulative amount permeated at the end of 24 h per unit area; D: Diffusion coefficient; K_p: Permeability coefficient.
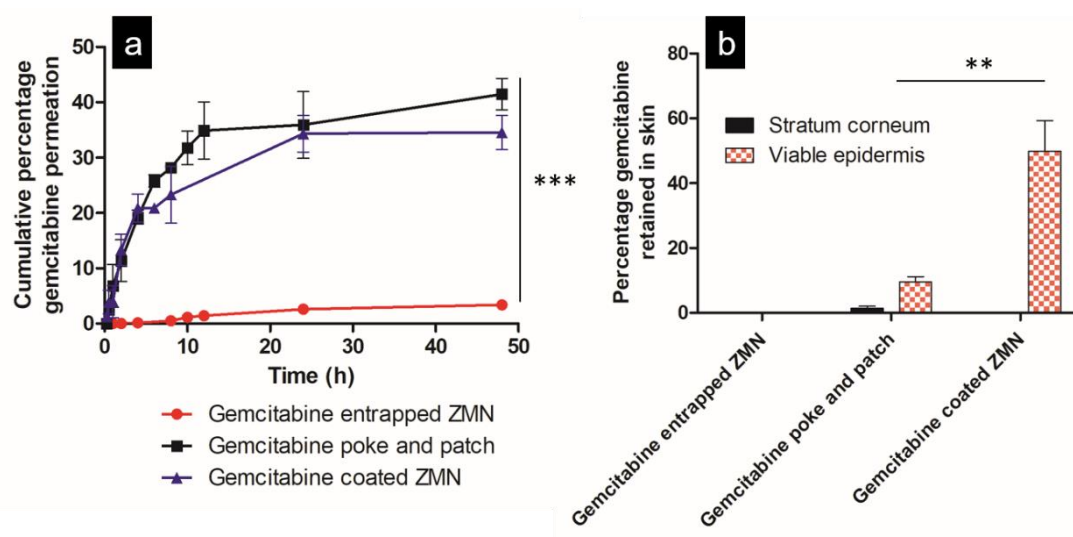
Figure 5.10 (a) Gemcitabine permeation across porcine ear skin over 48h from various ZMN formulations. Permeation studies were performed using Franz diffusion cell. (b) Gemcitabine recovered from the stratum corneum and viable epidermis after 48h of permeation studies. Stratum corneum was isolated using 15 tape strips. (mean±SD, n≥3). *** in (a) indicates that gemcitabine permeation across skin was significantly higher with gemcitabine coated ZMN and the poke and patch approach at p<0.001. ** in (b) is indicative for significant difference (p<0.05) in gemcitabine amount retained in viable epidermis between coated ZMN and poke and patch approach.

5.4 Discussion

Zein is a prolamine protein obtained from *Zea mays* (Osborne 1924). Zein protein has three major components alpha, beta and gamma (Coleman and Larkins 1999). The alpha-subunit is the major component followed by beta and gamma subunits (Thompson and Larkins 1989). Zein is not soluble in water because of the presence of hydrophobic residues leucine, proline, alanine, phenylalanine (total ~ 35%) and glutamic acid (~24%) (Wilson 1987; Paliwal and Palakurthi 2014; Jane et al. 1994). Zein is soluble in hydro-alcoholic mixtures containing 80 – 90% ethanol (Lawton 2002). The microneedles casted using 60% w/v zein showed sufficient mechanical strength for insertion into porcine skin (Bhatnagar et al. 2017). The compression force and skin insertion force of ZMN were reported earlier (Bhatnagar et al. 2017). While the ZMN are plastic, they are not dissolvable in aqueous medium or skin tissue (Bhatnagar et al. 2017). However, it was observed that the zein microneedles would imbibe water and swell upon prolonged incubation in aqueous medium.

Therapeutic agents can be entrapped within the matrix or coated on the microneedle surface for transdermal administration (Kim, Park, and Prausnitz 2012b). Tamoxifen is an estrogen receptor modulator that competitively competes with endogenous estradiol, thereby reducing cell growth and multiplication (Clemons, Danson, and Howell 2002). Tamoxifen shows poor water solubility of 0.04 µg/ml (Gao and Singh 1998). It has fewer hydrogen bond donors and acceptors (0 and 2, respectively). This hydrophobic tamoxifen appeared to be a suitable molecule to load in ZMN, where 4 mg of tamoxifen could be solubilized in 1 ml of 90% ethanol to cast microneedles. However, tamoxifen did not diffuse

out of the needles into aqueous release medium. This is attributed to the poor solubility of tamoxifen in aqueous release medium. To overcome this limitation different proportions of methanol or ethanol were mixed with release medium. This did not enhance the tamoxifen release from ZMN. To improve the rate of release, tamoxifen was surface coated on ZMN. Then again, the rate of tamoxifen release was poor when a hydrophobic polymer, ethyl cellulose was used in coating medium for dip coating. The addition of hydrophilic PVP in the coating solution resulted in burst release of tamoxifen (80% tamoxifen released within 15 min). The reverse partitioning of tamoxifen into ZMN can be confirmed by the partitioning studies of tamoxifen in ZMN and release medium. The tamoxifen present in the aqueous release medium of partition studies was below the detection limit of HPLC method. On the other hand, the highly water soluble gemcitabine possess 7 hydrogen bond acceptors and 4 hydrogen bond donors. This greater water solubility allowed more gemcitabine release from ZMN compared with tamoxifen. Furthermore, the reverse partitioning phenomenon observed after release of tamoxifen was not found with gemcitabine when released from coated ZMN.

It has been documented that highly hydrophobic drugs would not significantly permeate across the skin membrane when studied using in-vitro diffusion cell setup (Bhatia, Kumar, and Katare 2004; Manosroi, Kongkaneramit, and Manosroi 2004). This is a drawback of experimental setup of in-vitro skin diffusion studies (Ng et al. 2010). The hydrophobic molecules released into the epidermal layers could be partitioned into lipidic hypodermal layer. This would hinder its further diffusion into the aqueous release medium. Therefore, tamoxifen permeation studies showed negligible amount of skin permeation while,

gemcitabine showed 34.55±3.09 % of the loaded dose permeated across the skin. Dermatomed skin samples with ≤0.5 mm thickness or epidermal membrane would be more suitable to perform skin permeation studies of hydrophobic molecules (Williams 2006). In the cases where drug loading is poor in MN, poke and patch approach could be used to improve the skin permeability. It was found that this approach is more suitable for gemcitabine than tamoxifen. Among the three different strategies used to enhance skin permeation, poke and patch approach showed greater tamoxifen permeation. In the case of gemcitabine, coated MN administration showed greatest permeation in correlation to loading concentration. Water solubility of chemotherapeutics would influence their loading, release behaviour and skin permeation for application using polymeric MN.

5.5 Conclusion

Micromolding through solvent casting can be used to prepare ZMN loaded with different small molecule drugs. Anti-cancer agents can be either entrapped within the matrix or coated on to the surface of ZMN. While the loading of tamoxifen is more within ZMN, the release was negligible. Reverse partitioning of tamoxifen was observed after release from ZMN. A contrasting loading and release profile was shown by highly water soluble drug, gemcitabine. Skin permeation studies showed negligible permeation of tamoxifen while, gemcitabine showed greater permeation. In conclusion, optimal water solubility of drugs would provide greater skin permeation when delivered using ZMN. A dissolvable microneedle system could allow for more drug loading, and faster and greater drug permeation of chemotherapeutics across skin, however, further studies are warranted.

Chapter 6

Dissolvable microneedles for delivery of anticancer agents: proof-of concept in *in vivo* breast cancer animal model

6.1 Introduction

Surgical resection is the first interventional choice to clear localized tumors. Chemotherapy and/ or radio-therapy are performed as adjunct treatment strategies to limit the tumor recurrence (Brown & Giaccia, 1998; Labala et al., 2017). In general, chemotherapeutics are administered by infusion assisted by a catheter. This systemic administration of chemotherapeutics is associated with severe adverse drug reactions including bone marrow suppression, cardiotoxicity and neurotoxicity (Jia-You, Pei-Feng, & Chun-Ming, 2008). Doxorubicin (DOX) and docetaxel (DTX) are the two important chemotherapeutic agents commonly used for treatment of breast cancer. Doxorubicin (DOX) is a non-selective class I anthracycline antibiotic compound clinically approved to treat various types of cancers including breast cancer, neuroblastoma, and ovarian cancer (Hortobagyi, 1997). DOX intercalates with DNA and inhibits macromolecular biosynthesis. Intravenous DOX administration causes non-selective cardiotoxicity, myelosuppression, and mucositis (Licata, Saponiero, Mordente, & Minotti, 2000; Pugazhendhi, Edison, Velmurugan, Jacob, & Karuppusamy, 2018). Similarly, docetaxel (DTX) is approved for the treatment of breast, ovarian and non-small-cell lung cancers. It is a semi-synthetic analog of paclitaxel with a molecular weight of 807.9 g/mol (Qiu, Gao, Hu, & Li, 2008). Commercial DTX injections contain polysorbate 80 and cause adverse events such as severe hypersensitivity reactions, neutropenia, neurotoxicity and musculoskeletal toxicity (Zhang, Dou, Zhai, Liu, & Zhai, 2014).

The patients are required to be hospitalized for the duration of the chemotherapy to continuously monitor vital parameters affected by

chemotherapeutics. Over the decades, multiple new approaches to deliver chemotherapeutics to improve their safety profile have been investigated. Largely, the objective of these studies has been to target the tumor cells to minimize adverse effects. Some of the prominent among these new approaches are nanoparticle-based targeting systems and antibody-drug conjugates (Sliwkowski & Mellman, 2013; Wicki, Witzigmann, Balasubramanian, & Huwyler, 2015). While these methods have passed through generational changes, reducing the overall toxicity for some of the drug candidates, there need be further alternatives to improve the effectiveness of the delivery system.

Microneedle patch provides a painless alternative to deliver anticancer agents to localized areas (Ma, Boese, Luo, Nitin, & Gill, 2015). The micron-scale needles would breach the stratum corneum barrier to release the payload within epidermis and dermal layers. The first-generation silicon and metal-based microneedles had disadvantage of poor drug loading. The microneedles fabricated with polymeric matrix improved the amount of drug loaded(Bhatnagar, Dave, & Venuganti, 2017). However, there need to be a careful consideration of the physico-chemical properties of the drug and polymer materials to optimize the drug loading and release characteristics. The challenges of drug release from stable microneedles is addressed by development of dissolvable microneedles. These devices penetrate the skin and dissolve after getting hydrated by water present in the skin membrane (Zhu et al., 2014). The polymeric matrix would act as a depot for absorption of drugs into deeper skin layers. Dissolvable microneedles can be easily prepared using micromolding technique. This technique also allows for low-cost scalable manufacture of polymer microneedles (Bhatnagar et al., 2018).

The precondition to prepare dissolvable polymeric microneedles is the ability of polymer or polymer composite to interact with aqueous medium. On the other hand, the interpenetrative matrix formation would be required to obtain sufficient strength for skin insertion (Hong et al., 2014). The rate of dissolution of microneedles in skin would be inversely related to their compression strength. Furthermore, the dissolvable microneedles would have be biodegradable and should not show accumulative property (Park, Allen, & Prausnitz, 2005). This biodegradability would allow for repeatable application of microneedles (S. G. Lee et al., 2014). Hence, polyvinyl alcohol (PVA), a water-soluble biodegradable polymer and polyvinyl pyrrolidone (PVP), a super disintegrant has been used to fabricate dissolving microneedles. High molecular weight grades of PVP and blends of PVA and PVP have previously been shown to form microneedles with sufficient strength for skin insertion (Cole et al., 2017; I. C. Lee, Wu, Tsai, Chen, & Wu, 2017). Microneedles prepared out of PVA and PVP have also been used for preparing microneedles for ocular delivery (Bhatnagar et al., 2018).

To this end, the aim of this work was to fabricate dissolving microneedles (DMN) encapsulating two potent anti-breast cancer agents, DOX and DTX, and investigate their effectiveness in controlling the tumor progression in 4T1 cell xenografted tumor bearing mice.

6.2 Materials and Methods

6.2.1 Materials

Polyvinyl alcohol (PVA; molecular weight 160 kDa) was purchased from Himedia Labs, Mumbai, India. Polyvinyl pyrrolidone (molecular weight 40 kDa, PVPK30; and 360 kDa, PVPK360) was purchased from Sigma Aldrich chemical

company (Bengaluru, India). Doxorubicin hydrochloride (DOX) was provided as a gift sample by Natco Pharma Ltd., India. Docetaxel was a gift sample from Fresinius Kabi Pvt. Ltd., Gurgaon, India. Dulbecco's modified Eagle's medium (DMEM), heat inactivated fetal bovine serum (FBS), Dulbecco's phosphate-buffered saline (PBS), 0.25% trypsin-EDTA and 100x pencillin antibiotic solution were procured from Himedia Labs, Mumbai, India. Basement membrane matrix (Cultrex PathClear BME, Type 3) was purchased from Trevigen Inc., MD, USA. All chemicals were analytical grade and used without further purification. Milli-Q (Millipore Corporation, CA, USA) water was used for all the experiments.

6.2.2 Cell culture

Murine mammary carcinoma cell line, 4T1 (ATCC$^®$ CRL-2539™), was grown in tissue culture treated flasks in DMEM supplemented with 10% FBS and 1% antibiotic (penicillin and streptomycin) at 37°C with 5% CO_2 in a humidified cell culture incubator.

6.2.3 Animals

Female athymic nude mice (NCr-Foxn1^{nu}; Taconic Biosciences Inc.) were purchased from Vivo Bio Tech Ltd. (Hyderabad, India). Animal experiments were performed in accordance with the guidelines of council for the purpose of care and safe and effective use of animals (CPCSEA, India). The experimental protocols were approved by the institutional animal ethics committee (IAEC) of BITS Pilani Hyderabad Campus (IAEC/BITS/Hyd/2017/9). Mice were housed in sterilized individually ventilated cages (80 air changes per hour) with sterilized bedding and provided sterilized chow and water *ad libitum*. Animals were housed in 12h/ 12h light/ dark cycle.

6.2.4 Preparation of blank dissolvable microneedles

DMN were prepared using micromolding technique. A commercially available microneedle system (3M™ Microchannel Skin System) was used to prepare needle-free PDMS molds. The needles were prepared using 21% w/v PVPK360 and base plate of DMN array was prepared using a mixture of 6% w/v PVA and 11% w/v PVPK360. The 21% PVPK360 solution was prepared in ethanol: water (50:50) mixture. PVA-PVP mix was prepared by dissolving 0.6 g PVA in 10 ml ethanol: water (50:50) at 40 °C. After dissolution of PVA, 1.1 g of PVPK360 was added. Initially, needle-free PDMS molds were filled with 21% w/v PVPK360 and centrifuged at 500×g for 60 min at 25 °C to fill the needle cavities. Then, excess polymer was removed and PVA-PVP mixture was smeared to form the base plate. The mold was dried at room temperature for 24-48 h before collecting the DMN. The DMN were stored in a desiccator until further use. Also, DMN were prepared with a PVPK360 base plate using a similar procedure. Microneedle base plates without needles were also prepared using PVA-PVP or only PVP in a similar fashion but without vacuum application or centrifugation.

6.2.5 Preparation of drug loaded dissolvable microneedles

Single or dual drug loaded DMN were prepared by encapsulating DOX, DTX or a combination of both. For preparing DOX loaded DMN (DOX-DMN), 50 mg DOX was mixed with 1 g of PVPK360 solution (21% w/v) to cast the needles. Similarly, to prepare DTX loaded DMN (DTX-DMN), 30 mg DTX was dissolved in 150 μl ethanol and mixed with 1 g of PVPK360 solution (21% w/v). To prepare both DOX and DTX loaded DMN, DOX and DTX were added to PVPK360 solution at the same concentration as individual preparations. The

combination drug DMN were casted similar to the individual drug containing DMN.

The amount of drug loaded in DMN was determined by carefully separating the needles from the base plate using a scalpel blade under a stereomicroscope. The detached needles were dissolved in water: acetonitrile (50: 50) by vortexing and ultrasonication for 15 min. The samples were passed through a 0.22 μm PVDF syringe filter (Merck Millipore) before determining the drug concentration using HPLC method. Blank needles processed similarly were used as control.

6.2.6 Characterization of DMN

6.2.6.1 Microscopy

DMN were imaged using a stereomicroscope (SZX2, Olympus, Japan) and inverted fluorescence microscope (IX53, Olympus, Japan) to evaluate the needle shape and dimensions. Blank and drug loaded DMN were also imaged using scanning electron microscope (SEM). Microneedles were mounted on a metal stub using double-sided carbon tape and sputter coated (10nm thick) with Au/Pd using Leica EM ACE200 Sputtering System (Leica, Germany). Microneedles were examined using field emission SEM (Apreo S, Fei Company, USA) integrated with a critical dimension measurement system. Primary beam accelerating voltage was 15 kV and secondary ion images were collected.

6.2.6.2 Mechanical strength

The mechanical strength of blank and drug loaded DMN was determined using a texture analyzer (Stable Microsystems, UK). For this, the force required

for compression of DMN to a specified distance was measured. DMN were placed on a heavy-duty metal platform with the needles facing up. A 10 mm cylindrical Delrin probe (part code P/10) connected to a 50-kg load cell was set at the same distance from the platform for all the test measurements. The texture analyzer was set in compression mode with the probe compressing the DMN array at a speed of 0.5 mm/s up to a distance of 0.5 mm. Compression force versus displacement curves were plotted to calculate the compression strength. DMN images were collected before and after compression test using an optical microscope.

In a separate experiment, the strength of DMN base plates was assessed. Bases plates (without needles) prepared using PVA-PVP or only PVP were compressed to a distance of 0.5 mm as described before and the compression forces were recorded. Digital images of the base plates before and after compression were collected using a digital camera (Canon EOS 1200D).

6.2.6.3 Fourier transform infrared microscopy (FTIR)

FTIR (FT/IR-4200, Jasco Inc., USA) was used to characterize the drug loading in DMN. Spectra were recorded for PVP, DOX, DTX, physical mixtures (PVP + DOX, PVP + DTX, PVP+DOX+DTX) with drug concentrations in the same ratio as final drug loading in DMN, blank, and drug loaded DMN. The samples were mixed with potassium bromide at 1: 100 ratio and a pellet were prepared using high pressure hydraulic press (Riken Seiki, Japan). Spectra were recorded within the range of $4000–400$ cm^{-1} at a spectral resolution of 2 cm^{-1}. For drug loaded DMN, three needles from the array were carefully cut using a scalpel and mixed with potassium bromide before preparing pellet.

6.2.6.4 Powder X-ray diffraction

Neat DOX, DTX, PVP, PVA, blank and drug loaded microneedles were characterized using powder X-ray diffraction (Rigaku Ultima IV multipurpose XRD, Texas, USA). The samples were exposed to CuK radiation (40 kV×30 mA). Analysis was performed at ambient temperature using a linear position-sensitive detector, over a scan range of 5–90° 2θ at a scan speed of 5 degrees per min and a step width of 0.02 degrees.

6.2.7 Skin insertion studies

Previously shaved and excised mouse skin was used to understand the force required for insertion of DMN into the skin. Mouse skin was maintained at 37°C for 2 h before start of the experiment. The skin was flattened, placed on a styrofoam block and held in place using push pins. Blank DMN was attached to a texture analyzer probe using two-way sticky tape. The probe was lowered onto the skin and allowed to penetrate the skin up to a distance of 0.5 mm and held in place for 30 s. Methylene blue solution was added onto the treated skin for 30 s and the excess removed before imaging the skin.

In a similar manner, DOX-DMN were inserted into the mouse skin, but held in place for 2 h using an occlusive tape. After 2 h, the treated skin was placed onto a glass slide and covered with cellophane tape. The skin was immediately subjected to analysis using confocal laser scanning microscope (DMi8, Leica Microsystems, Germany). Argon laser (495 nm wavelength) was used to excite doxorubicin, and the emission intensity was detected at 590 nm wavelength.

Optical sections were captured in the XYZ plane (plane parallel to the mouse skin) using a 10× objective lens and a step size of 1 μm. The 3D reconstructed images were obtained to visualize the penetration of DOX in the mouse skin.

6.2.8 Analytical method for doxorubicin and docetaxel

The concentration of DOX was analyzed by fluorescence spectroscopy (Spectramax M4, Molecular Devices Inc., USA). Calibration curve was developed in phosphate buffer saline (pH 7.4) using opaque 96 well plates (0.2–6.0 μg/ml; r^2=0.9997). Fluorescence units were recorded at an excitation wavelength of 475 nm and emission wavelength of 595 nm. Drug loading and release samples were similarly analyzed after appropriate dilution and background subtraction. A RP-HPLC (Shimadzu LC20, Japan) method was developed for estimation of DTX. Chromatographic separation was achieved using an octadecylsilane column (150 × 4.6 mm i.d., 5 μm, Shimadzu, Japan) maintained at 25°C temperature using mobile phase comprised of water: acetonitrile (50: 50) at 1 ml/min flow rate. DTX concentration in the samples was determined after recording the absorbance at 230 nm wavelength and comparing with the standard curve (10–60 μg/ml in mobile phase, $r^2 = 0.9999$).

6.2.9 Drug release studies

Blank DMN were placed in 5 ml phosphate buffer saline (pH 7.4) stirred at 150 rpm and maintained at 37°C with needles facing downwards. The time taken for the needles and the complete array to dissolve was recorded.

Drug release studies were performed in 6 well plates. Each well was filled with 5 ml of either PBS or PBS with 5% ethanol (for DTX-DMN and DOX-DTX-

DMN). The media was maintained at 37°C and constantly stirred at 150 rpm using a magnetic stir bar. The DMN were placed needles facing down. Samples (0.2 ml) were collected from the release media at predetermined time points and analyzed following the respective analytical methods for DOX and DTX described above.

6.2.10 *Ex-vivo* skin permeation studies

Previously shaved and excised mouse skin was used for skin permeation studies. Transepidermal electrical resistance (TEER) of the skin was recorded by applying direct current across the skin using a power supply unit. Voltage drop (V) was measured using a digital multimeter (Fluke Corporation, USA). The resistance (R) was calculated using Ohm's law (V =IR). The transepidermal water loss (TEWL) was measured using VapoMeter$^{®}$ (Delfin Technologies Ltd., Kuopio, Finland).

A jacketed Franz diffusion cell apparatus (PermeGear Inc., USA; area available for diffusion is 0.637 cm^2) was used for skin permeation studies. Franz diffusion cell receptor chamber was filled with 5 ml of PBS (or PBS + 5% ethanol for DTX) and stirred continuously while being maintained at 37°C using circulating heated water. Mouse skin was placed dermis side down over the receptor chamber and maintained at 37°C for 2 h before the start of experiment. Drug loaded DMN were inserted into the skin manually. Samples (300 µl) were collected from the sampling port using Hamilton syringes up to 48 h and analyzed using respective analytical method for DOX and DTX. TEER and TEWL were measured before insertion of DMN and after completion of the study. After 48 h, the skin sample was wiped gently with delicate task wipes (Kimtech) and the skin area available for diffusion was carefully cut using a scalpel blade. Tape stripping

technique was performed to remove the stratum corneum layer using Scotch book tape (845, 3M Corporation, USA). Ten strips were collected to remove the stratum corneum. Drugs were extracted from the tape strips and analyzed. The viable skin remaining after stripping was minced into smaller pieces followed by tissue homogenization. Drug was extracted from homogenized skin and analyzed for drug concentration. The drug amounts loaded within 0.64 cm2 of microneedle array was considered as the amount in donor compartment for calculation of permeation parameters.

6.2.11 Efficacy of drug loaded microneedles in tumor bearing immunodeficient mice

Female athymic nude mice (5–6 weeks, 15–17 g) were acclimatized at the animal facility for 3 weeks. 4T1 cells were harvested from 70–80% confluent tissue culture flasks by trypsinization. The cells were centrifuged at 1200 rpm (37°C, 5 min). The pellet was washed with sterile PBS and counted using an automated cell counter (Countess™ II Automated Cell Counter, Life Technologies, USA). Cells were resuspended in thawed basement membrane matrix: ice cold PBS (50:50). Using precooled 1 ml syringes, 1×10^6 cells/animal were injected in right flanks of the mice. Animal weight was recorded daily after cell injections. Tumor size was measured using digital Vernier calipers and the tumor volume was calculated using Equation 1.

$$Tumor\ volume\ (mm^3) = \frac{\left(\begin{matrix} Longitudinal \\ diameter\ (mm) \end{matrix}\right) X\ (Transverse\ diameter\ (mm))^2}{2} \ldots (1)$$

When the tumor volume reached 50–100 mm^3 (about 10–14 days after cell injection), animals were randomized into seven groups (Table 6.1). Multiple

dosing regimen was followed with treatments administered on Day 0, Day 2, Day 4, Day 7, Day 10, and Day 13 as shown in Table 6.1. For treatments, animals were anesthetized using isoflurane gas (E-Z Anesthesia, E-Z, USA). Injections were given using a 30G needle intratumorally under anesthesia. For microneedle treatment, mice were anesthetized and microneedles were inserted using thumb pressure for 2 minutes and held in place using occlusive tape for 1h under continuous anesthesia. Tumor volumes were measured until Day 16 when animals were sacrificed (CO_2 asphyxiation). Normalized average tumor volumes were calculated using equation 2 and plotted against time for all treatment groups.

$$Normalized\ tumor\ volume = \sqrt[3]{\frac{Current\ tumor\ volume}{Initial\ tumor\ volume}} \dots\dots\dots\dots\dots\dots(2)$$

Tumors were surgically removed from the animals after sacrificing and stored at -80°C until further use. Animals were euthanized if tumor size reached 1000 mm^3 at any point during the study.

Table 6.1. Randomization of mice in different treatment groups and the followed dosing regimen.

Treatment	Number of mice	Dosing regimen
Control (no treatment)	6	No dosing
DOX i.t. injection	6	Two doses (Day 1 and 4)
DTX i.t. injection	6	Two doses (Day 1 and 4)
DOX+DTX i.t injection	6	Two doses (Day 1 and 4)
DOX MN	6	Four doses (Day 1, 4, 7, and 10)
DTX MN	6	Four doses (Day 1, 4, 7, and 10)
DOX+DTX MN	6	Four doses (Day 1, 4, 7, and 10)

6.2.12 Tumor histology and TUNEL assay

Tumor tissues were embedded in optimum cutting temperature (OCT) medium and stored at -80ºC overnight. Tumor tissues were sectioned at a thickness of 10-15 μm using a cryotome (Leica CM 1520, Leica biosciences, Germany). These sections were mounted on a polylysine coated microscope slide, fixed in 95% ethanol and allowed for overnight drying at room temperature. Later the sections were stained regressively with hematoxylin (MHS16 Mayer's Hematoxylin, Sigma Aldrich Company, Bengaluru, India) and counterstained with eosin (Eosin Y, Sigma Aldrich Company, Bengaluru, India). Stained sections were observed under optical microscope.

Apoptotic and non-apoptotic cells in tumor tissues were histologically evaluated using the 4',6-diamidino-2-phenylindole (DAPI) and terminal transferase dUTP nick- end labeling (TUNEL) assays, with a commercial apoptosis detection kit (Fluorescein FragEL DNA Fragmentation Detection Kit, Calbiochem, Germany). Samples were washed with PBS for 5 min each time and incubated with equilibration buffer for 10 min at room temperature. The equilibration buffer was drained and a reaction buffer containing equilibration buffer, nucleotide mix, and TdT enzyme was added to the tissue sections, which then were incubated in a dark, humidified atmosphere at 37 °C for 1 h. The reaction was terminated by immersing the samples in 2× standard saline citrate for 15 min, and the samples then were washed three times for 5 min each to remove unincorporated FITC-TdT. The apoptotic cells in tissues were determined by TUNEL assay and the slides were counterstained with DAPI. TUNEL data were analyzed by at 40× magnification, using a computer-aided inverted fluorescence microscope.

Statistical analysis

All the results were presented as mean ± standard deviation. The results were compared by performing student's t-test or analysis of variance (Version 6, Graph Pad Prism, USA), and the results were considered to be significant at $p<0.05$.

6.3 Results

6.3.1 Preparation and characterization of microneedles

The microneedles used in this work were prepared from PVA and PVP using the micromolding technique. Figure 6.1 shows the scheme of fabrication of microneedles. Figure 6.2a is the master mold used for preparation of secondary PDMS molds (Figure 6.2b). Figure 6.2c and 6.2d are stereomicroscope images of the prepared PDMS molds. Figure 6.2e and 6.2f are stereomicroscope images of prepared docetaxel and doxorubicin loaded microneedles. Brightfield and dark field images of doxorubicin loaded microneedles taken using an inverted fluorescence microscope are further shown in figure 6.2g and figure 6.2h respectively. Microscopic analysis revealed the prepared pyramidal shaped needles to be 597.16±31.48 μm in length and 245.83±16.13 μm wide at the base. No observable cracks or fractures were observed on the needle surface. Figure 6.3 shows scanning electron microscope images of the prepared microneedle structures. The needles can be observed with sharp tips and a smooth surface finish in figure 6.3c.
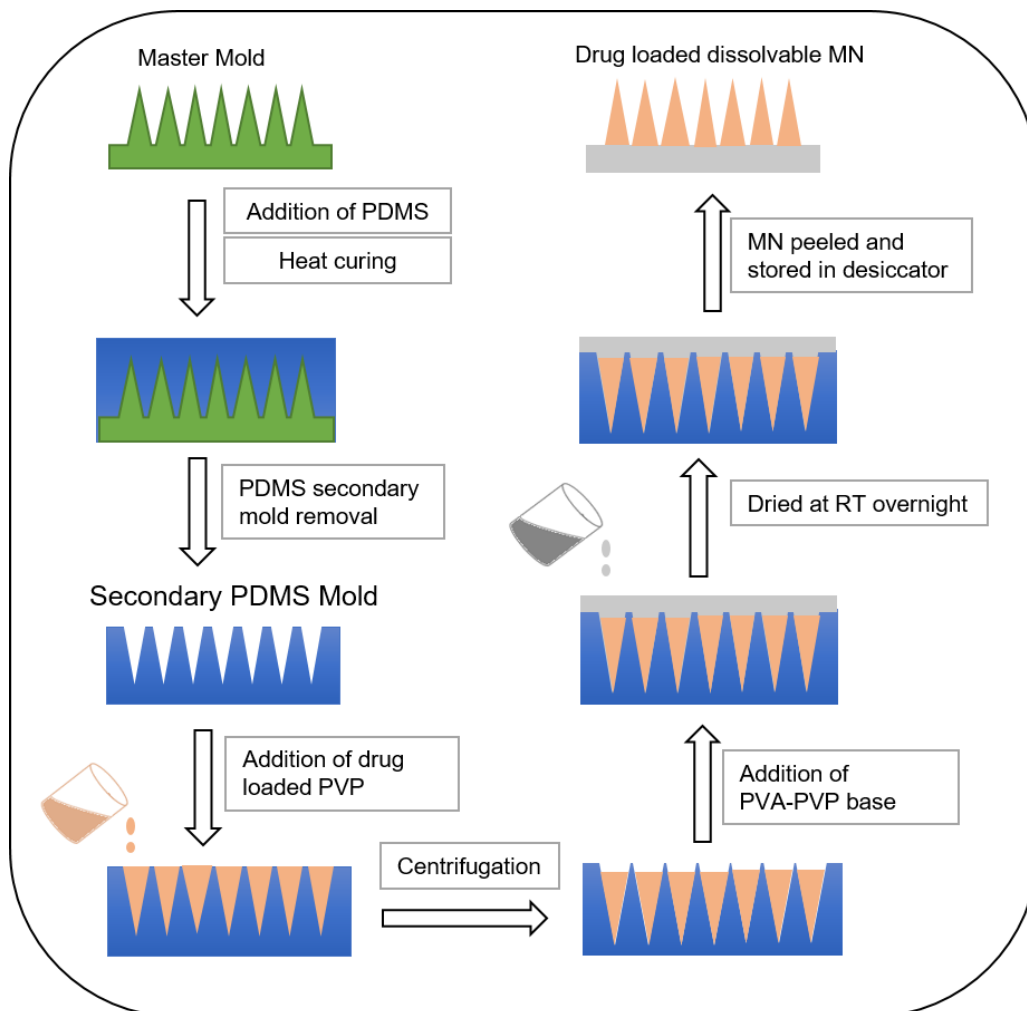
Figure 6.1 Scheme of preparation of dissolvable microneedles.
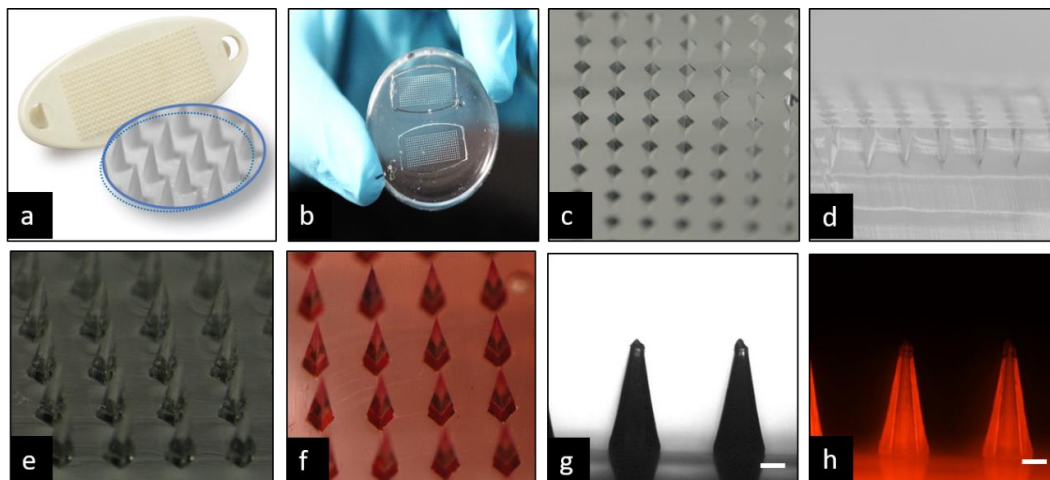
Figure 6.2 Image of master mold (a) used for preparation of secondary PDMS mold (b). Stereomicroscope images of prepared PDMS molds (c) and its cross sectional image (d). Stereomicroscope images of prepared docetaxel loaded (h) and doxorubicin loaded (i) microneedles. Brightfield (j) and darkfield images (j) of doxorubicin loaded microneedles. Scale bar = 100μm.
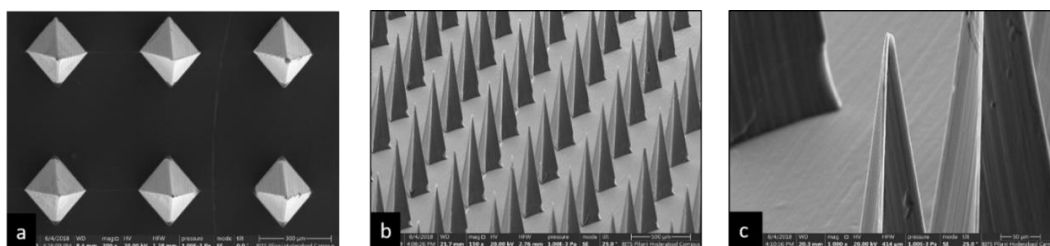
Figure 6.3 Scanning electron microscope images of prepared microneedles.

Figure 6.4 depicts FTIR spectra of neat drugs and polymers (figure 6.4a) and prepared drug loaded microneedles (figure 6.4b). Figure 6.4c includes FT-IR spectra of physical mixture of PVP and drug with concentration ratios same as that in final microneedle preparations. With PVP, major peaks could be seen at 1630.56 cm-1 for C=O) stretch and 1266 cm-1 for C–N stretch (Soltani et al., 2012). Doxorubicin spectra showed its characteristic peaks at 3222 cm^{-1} (N–H amine), 2884 cm^{-1} (C–H stretch), 1725 cm^{-1} (C=O stretch) and 1277 cm^{-1} (C–O stretch for strong alkyl aryl ether) (Fan, Li, Wu, Li, & Wu, 2011). Characteristic absorption bands for docetaxel were observed at 3420 cm^{-1} (N–H vibration), 700 cm^{-1} (out of plane vibration of N–H), and the ester stretching observed at 1685 cm^{-1}(Shaw et al., 2017). Figure 6.4b includes IR spectra for prepared microneedles and figure 6.4c shows IR spectra for physical mixtures of polymer and drugs. With physical mixtures, both DTX and DOX peaks could not be detected. Similarly, with prepared MNs, reduced intensities of PVP characteristic peaks were seen with no drug peaks.
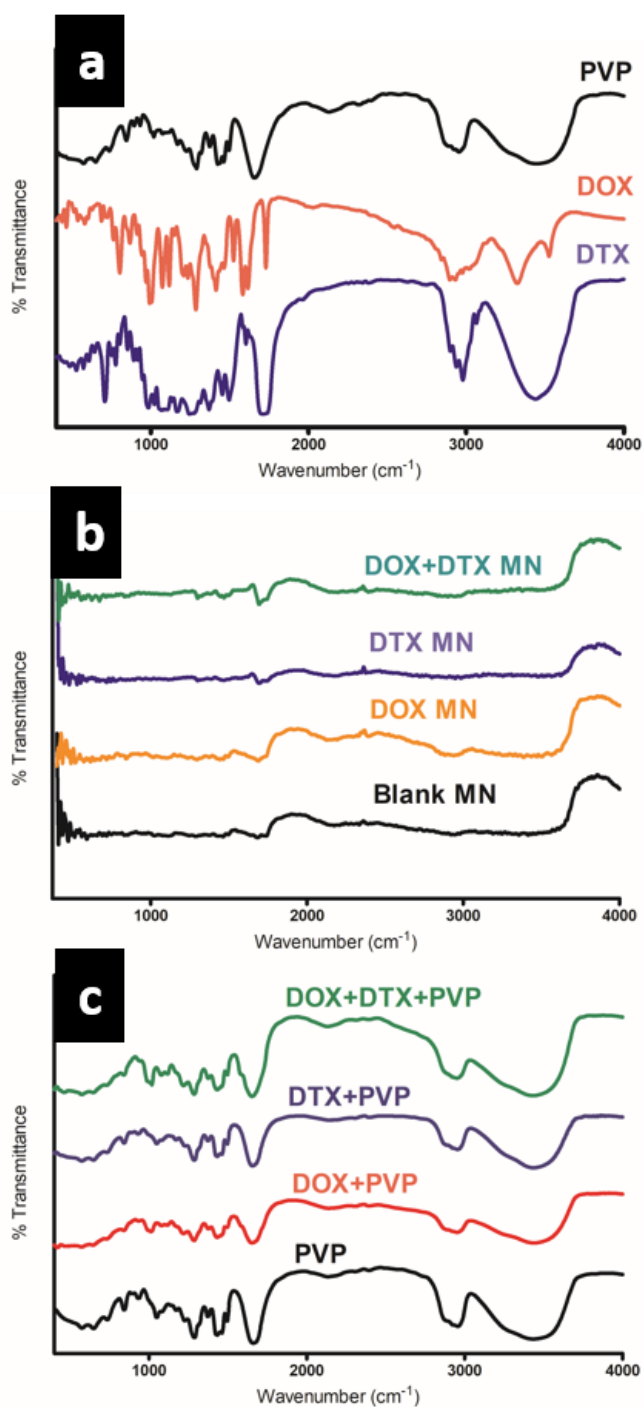
Figure 6.4 Fourier transform-infrared spectroscopy spectra for pure drugs and polymer (a), prepared microneedles (b) and physical mixtures (c). DOX: doxorubicin; DTX: docetaxel.

Figure 6.5 shows wide angle diffraction patterns for neat drugs and polymer, physical mixtures, and prepared microneedles. The physical mixtures contained the same drug:polymer ratio as in the final microneedle preparation. It can be observed from the figure that PVP showed two peaks at 2θ ~ 11.66 and 19.38° which is consistent with the literature values (Ragab, 2011). Pure PVA shows a peak at 2θ~ 21° confirming the semi crystalline nature of the polymer. The XRD data revealed the crystalline nature of doxorubicin. Docetaxel showed peaks at 9.48 and 18.68°. With physical mixtures, PVP peaks close to 11 and 19 were retained as seen in figure 6.5d. For prepared microneedles, majorly peaks close to 21° were seen which is generally observed with PVA/PVP blends with higher PVA ratios (Hodge, Edward, & Simon, 1996).
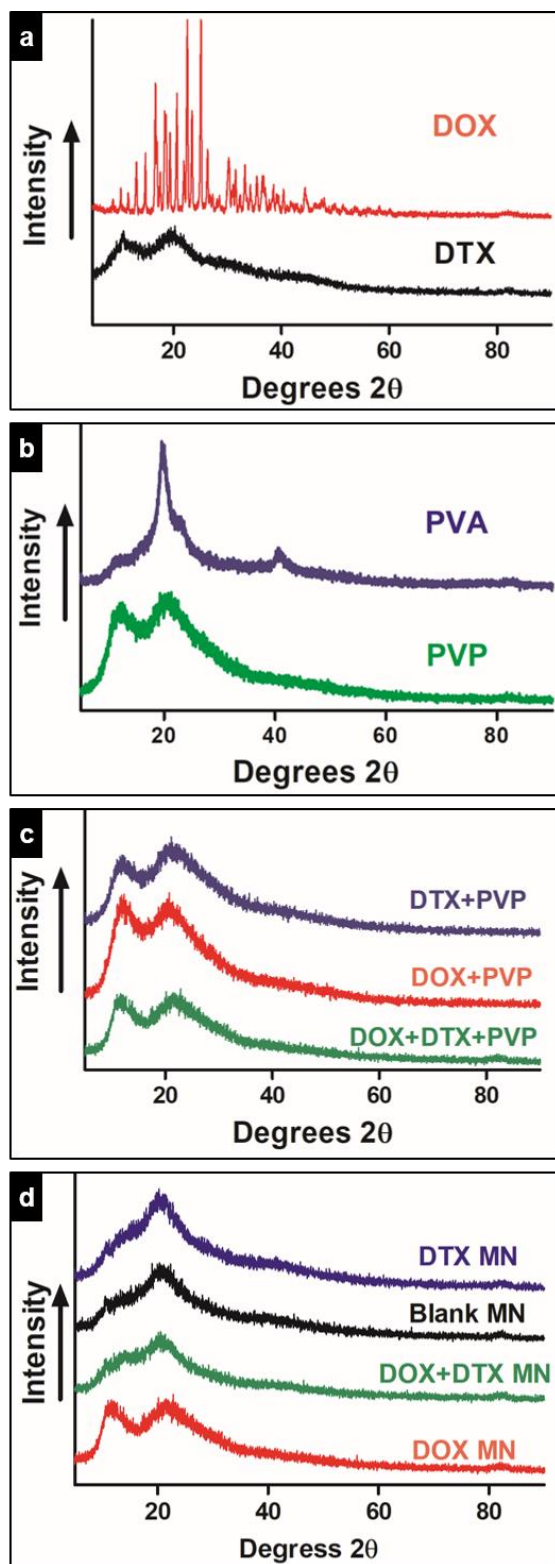
Figure 6.5. Wide angle X-ray diffraction patterns for pure drugs (a), pure polymers (b), prepared microneedles (c) and physical mixtures (d). DOX: doxorubicin; DTX: docetaxel.

Mechanical strength testing of microneedles was performed to assess the mechanical strength of prepared microstructures. The compression force required for compressing the needles by 0.5mm was calculated. Figure 6.6a shows force Vs displacement plots for different microneedle formulations. Blank microneedles were seen to experience about 15N of force. A reduction in strength was seen with loading of drugs especially docetaxel and combination of doxorubicin and docetaxel, however force as little as 0.089 N per needle is enough for insertion into the skin. Needles maintained their general shape after compression, did not fracture, becoming compressed instead. Also, no cracks were found at the bases of the needles. Figure 6.6b shows a flexible PVA/PVP MN base. A brittle and non flexible MN base was formed with use of only PVP in the base. Figure 6.6 shows murine skin treated with blank MN followed by staining with trypan blue. Dye could be seen in the microchannels created due to insertion of MN. Insertion of all the needles into the skin was observed. To further understand the insertion of microneedles into the skin, confocal microscopy was used. Figure 6.7 shows confocal micrographs of skin at various depths after insertion of doxorubicin loaded microneedles. Dark areas indicate lack of fluorescence. Fluorescence could be well observed until 140 μm with the instrument. A brighfield image showing the microchannels created due to MN insertion is shown in figure 6.6a. 3D reconstructed image of the confocal sections is shown in figure 6.6b.
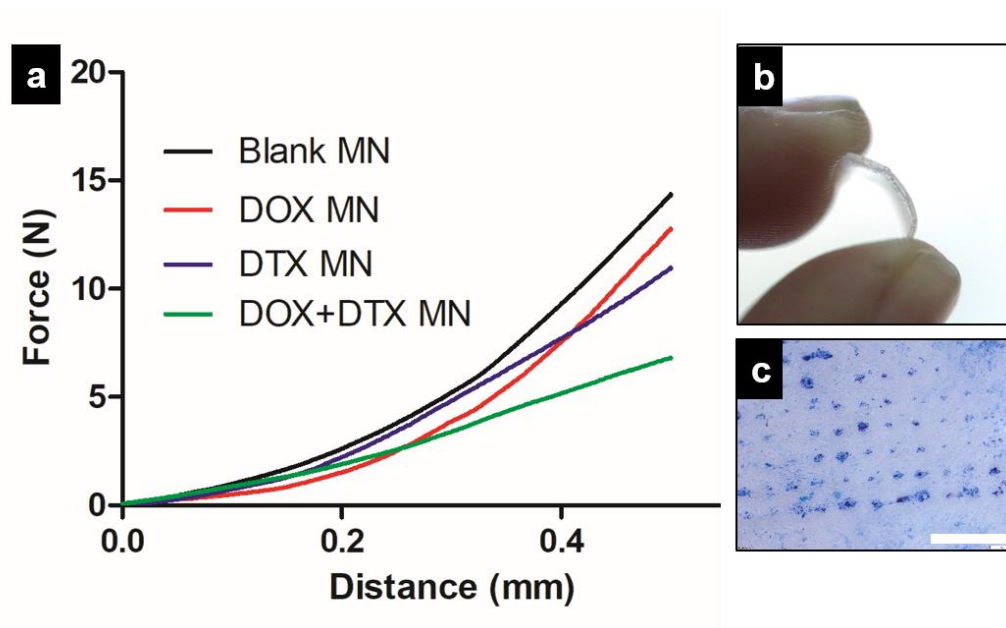
Figure 6.6. Force Vs. displacement graph for assessing the compression force for prepared microneedles (a). Image showing the flexible PVA PVP MN base between fingers (b), MN base made with only PVP was observed to be brittle. Microscopic images of mouse skin treated with blank microneedles and stained using dye (c). Scale bar = 1mm.
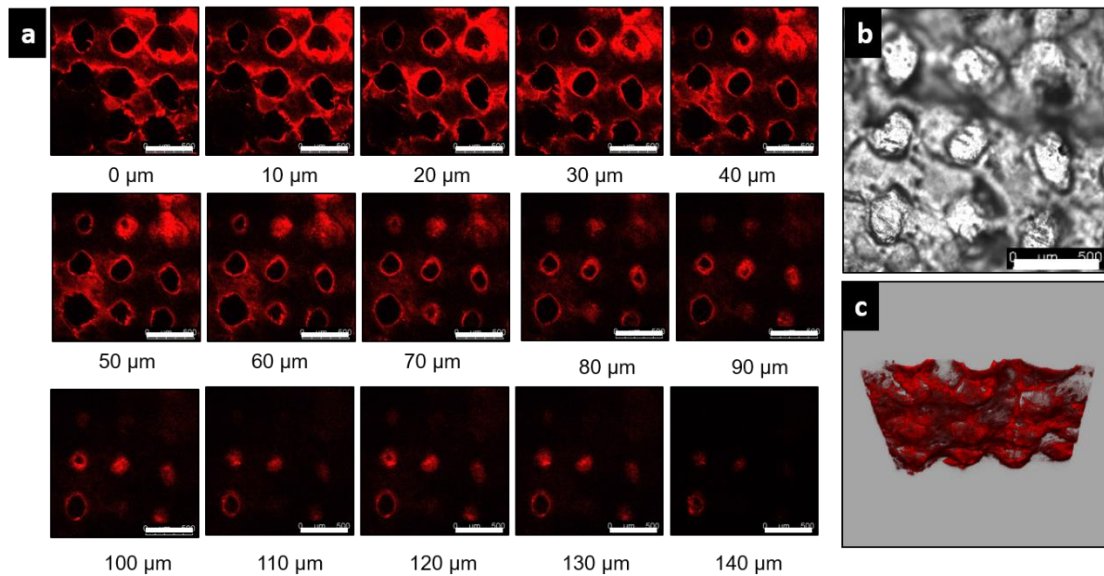
Figure 6.7 (a) Confocal micrographs of optical sections of the skin sample from the surface (0 μm) to 140 μm inside of the skin and a representative brightfield image of the pores created with doxorubicin loaded microneedle insertion (b). 3D representation of the microchannels created with the insertion of doxorubicin loaded microneedles (c). Dark areas indicate lack of fluorescence. The scale bar represents 500μm.

6.3.2 Drug release and skin permeation

DOX was estimated using spectroflourimetry. Figure 6.8 shows absorption and emission spectra of doxorubicin in phosphate buffer. Representative HPLC chromatograms of DTX standard samples are shown in figure 6.9. Drugs were extracted from the needles separated from the MN base followed by concentration estimation. For DOX, 621.78± 33.07 μg and 533.46±65.07 μg DOX/array was found to be loaded into DOX MN and DOX+DTX MN respectively. Amount of DTX loaded was 302.38±44.01 μg and 227± 23.58 μg/array in DTX MN and DOX+DTX MN respectively.
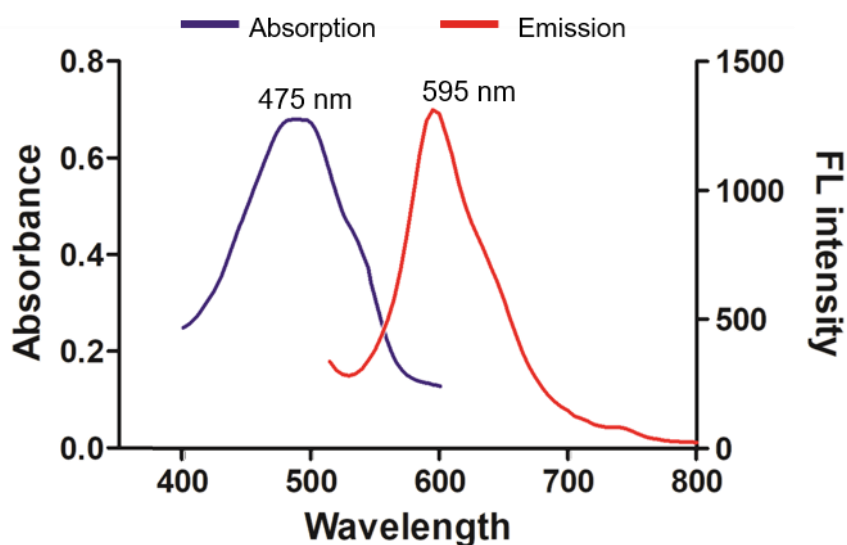
Figure 6.8 Absorption and emission spectra for doxorubicin. FL=fluorescence.
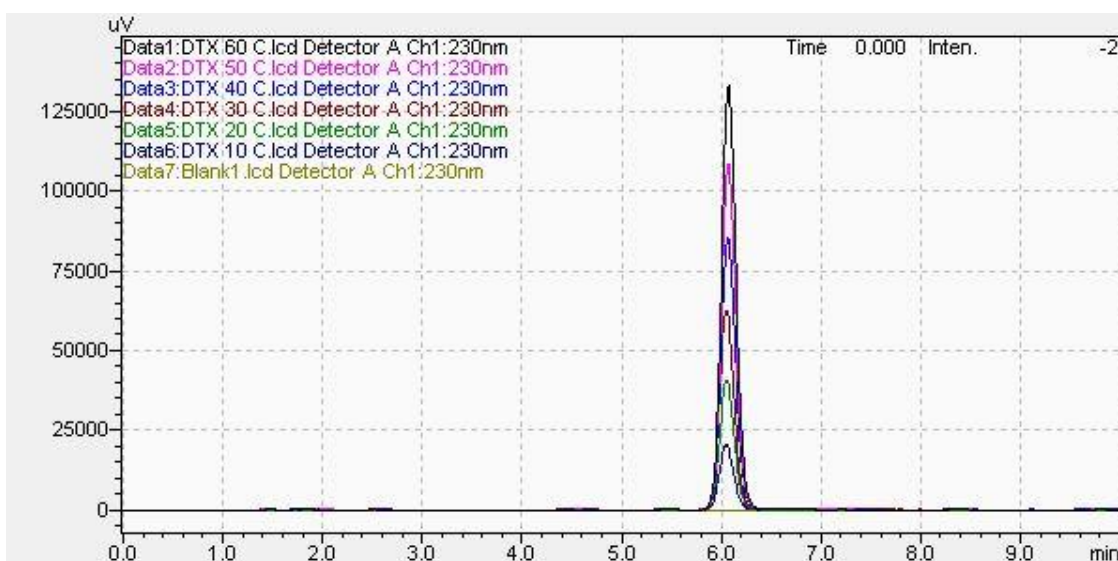
Figure 6.9 Representative HPLC chromatrograms for different concentrations of docetaxel used for preparation of standard calibration curve. Retention time is 6.1 minutes.

To study the dissolution of microneedle in physiological conditions, blank microneedles were dissolved in phosphate buffer maintained at 37 °C under mild stirring. The needles were seen to dissolve in 90±10 s, while the complete array including the base was observed to dissolve in 33±4.5 min. Figure 6.10 shows the release profiles of drugs from microneedles. Complete (100% of loaded amount) doxorubicin released within 5 min from DOX+DTX loaded MN and within 15 min from DOX loaded MN. DTX showed slower release compared with DOX. About 90% of DTX released within 15 min. The complete microneedle array dissolved in 30 min.
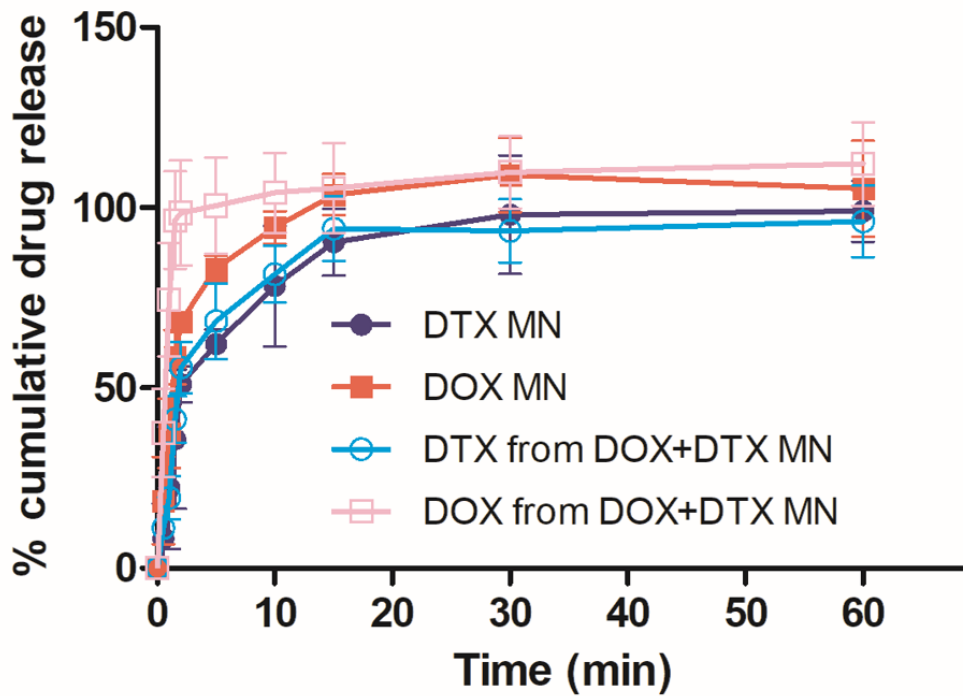
Figure 6.10 Percentage cumulative drug release from different drug loaded microneedles. Data presented as Mean±SD (n=3). DOX: doxorubicin; DTX: docetaxel.

Skin permeation studies were performed to investigate the effect of microneedle application on transport of DOX and DTX across murine skin. Figure 6.11 shows the permeation profiles of DOX and DTX delivered using microneedles. Application of DOX-MN resulted in skin permeation of 67.8 ± 5.4% of loaded DOX after 48 h. Skin permeation of DOX from DOX-DTX-MN was found to be 73.1±7.2% of loaded dose after 48 h. Drug disposition within stratum corneum and viable epidermis was 3.6±1.9% and 21.9±3.9% after 48 h application of DOX-MN. Similar drug disposition for DOX was found after application of DOX-DTX-MN.

In the case of DTX, overall skin permeation was lower compared with DOX. After 48 h of application, 33.6±1.6% and 26.7±3.4% of loaded dose has

permeated through skin for DTX-MN and DOX-DTX-MN, respectively. DTX-MN application resulted in 5.3±1.3% and 49.9±6.0% retention of DTX within stratum corneum and viable epidermis, respectively. Similarly, DOX-DTX-MN application resulted in retention of 3.0±1.0% and 67.2±15.2% of DTX within stratum corneum and viable epidermis, respectively. Table 6.2 shows the skin permeation parameters of DOX and DTX.

Table 6.2 Skin permeation parameters for different microneedle formulations.

Drug	Formulation	Q_{48}/cm^2 $(\mu g/cm^2)$	J $(\mu g/cm^2/h)$	t_{lag} (h)	D $(cm^2/h \times 10^{-5})$	P (cm^2/h)
DOX	DOX MN	397.36±31.67	18.50±4.67	0.44±0.32	78.86±42.53	0.050±0.012
DOX	DOX + DTX MN	367.44±36.10	26.26±3.62	0.32±0.02	114.6±29.84	0.082±0.011
DTX	DTX MN	95.35±4.68	6.45±0.91	2.05±0.87	8.68±5.23	0.036±0.005
DTX	DOX+DTX MN	57.01±5.58	2.72±0.47	3.48±0.76	4.49±1.7	0.020±0.003

DTX: Docetaxel; DOX: Doxorubicin; Q_{48}: Cumulative amount permeated across skin after 48h; J (flux) calculated from slope of linear portion of Q_{48}/cm^2 Vs. time; t_{lag} (lag time) calculated by extrapolating the linear portion of Q_{48}/cm^2 Vs. time to time axis; D (Diffusivity) calculated by formula $D=d^2/6t_{lag}$ where d is thickness of skin; P calculated as J/drug amount in donor compartment. Data presented as Mean±SD (n=3)

The greatest cumulative amount of DOX and DTX permeated through skin in 48 h was 397.4±31.7 µg/cm2 (with DOX-MN application) and 95.3±4.7 µg/cm2 (with DTX-MN application). The greatest flux values for DOX and DTX permeation were 20.5±4.8 µg/cm2/h (after DOX-DTX-MN application) and 6.0±1.0 µg/cm2/h (after DTX-MN application), respectively.

A decrease in lag time from 0.44±0.32 (with DOX MN) to 0.32±0.02 h (with DOX+DTX MN) was observed for DOX permeation across mouse skin. For permeation of DTX, a cumulative permeation of 95.35±4.68 (with DTX MN) and 57.01±5.58 µg/cm2 (with DOX+DTX MN) was observed. An increase in lag time

was seen with permeation of DTX from DOX+DTX loaded MN (2.05±0.87 against 3.48±0.76 h from DTX MN).
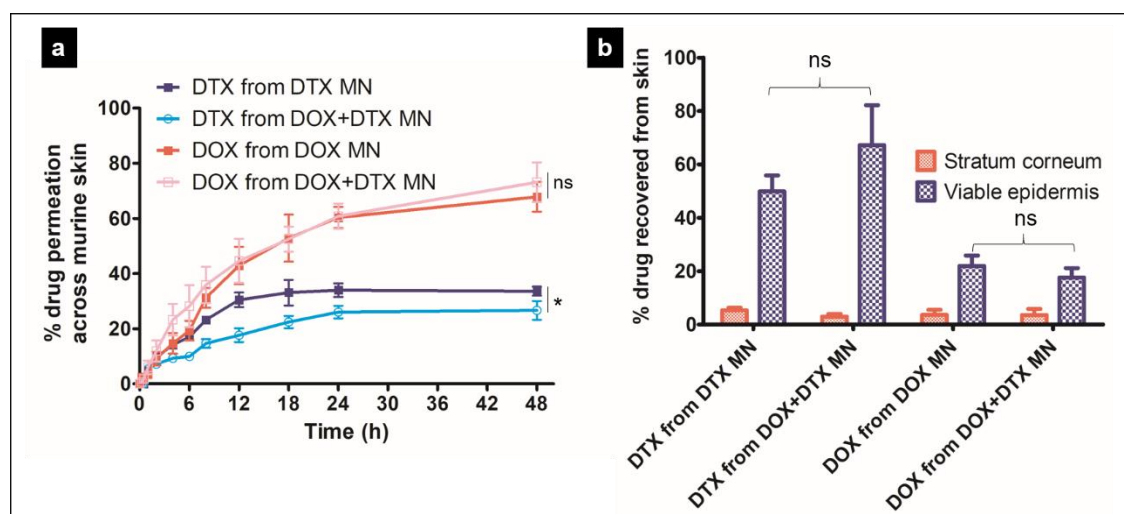
Figure 6.11 Permeation of drugs across murine skin after treatment with various microneedle formulations (a) and the percentage drug amount recovered from the stratum corneum and viable epidermis after 48h of treatment (b). Data presented as Mean ± SD (n=3). Statistical analysis performed using t-test. * indicates significance between groups (time=48h) at p<0.05; ns= not significantly different.

6.3.3 Effect of drug loaded microneedle application in tumor bearing mice

Xenografted subcutaneous tumors were developed in athymic mice after 4T1 breast cancer cells injection. Cancer treatment was initiated when the tumor volume was approximately 100 mm3. Figure 6.12a shows the timeline of therapeutic dosing. Figure 6.12b shows the photograph of mouse with microneedle applied on the tumor surface. It is observed that majority of the microneedles penetrated the skin over the tumor surface; however, the microneedles on the periphery in few cases did not penetrate because of the contoured nature of the surface (figure 6.13). The microneedles inserted within the skin dissolved within 1 h. Representative images of MN array after insertion can be seen in figure 6.14. The amount of the drug retained within the microneedle

array after 1 h insertion in the animal was quantified. It was found that 71.75±8.67 % of DOX and 62.83±19.48 % of DTX of the total loaded dose in DOX+DTX MN was administered to the animal.
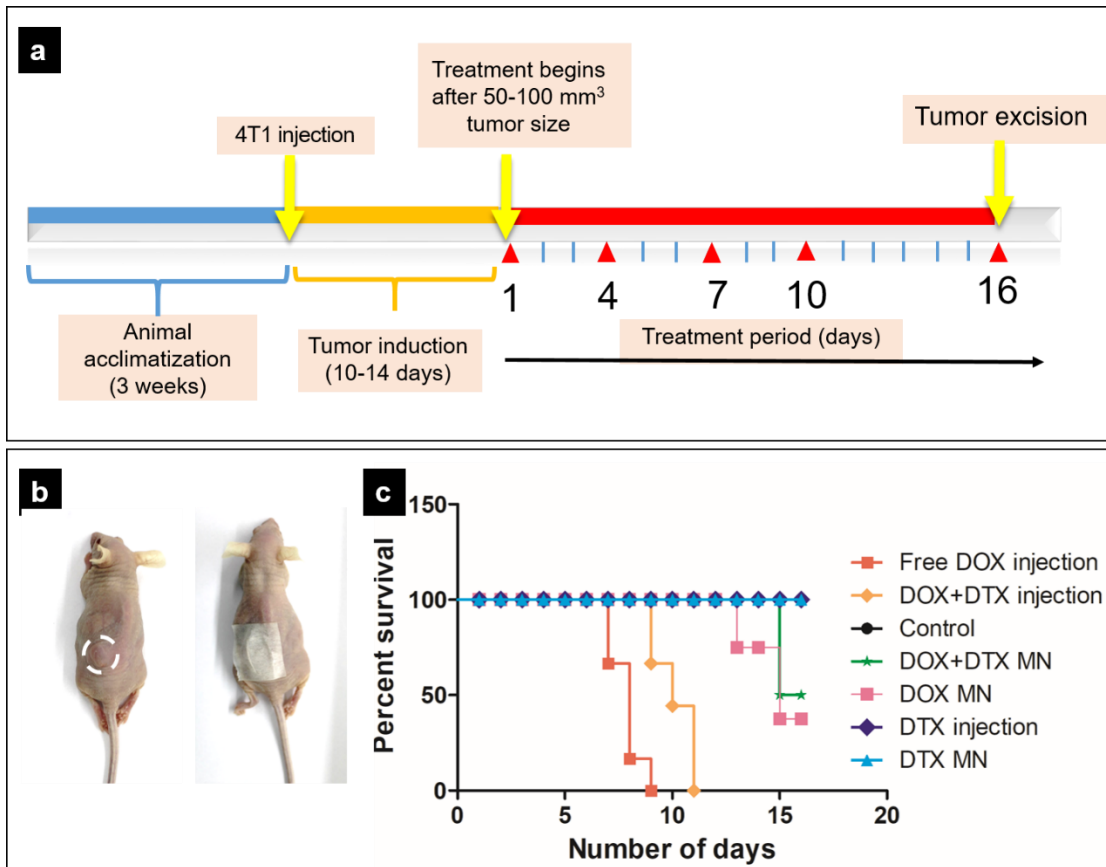
Figure 6.12 (a) Timeline for tumor inhibition study in athymic nude mice. (b) Representative image of tumor bearing mouse before and with microneedle array applied to it. (c) Kaplan-meier survival plot for different animal groups.

Figure 6.13 Representative image of 4T1 tumor in athymic nude mice immediately after treatment with microneedle array for 1 hour. Scale bar = 1mm.

Figure 6.14 Representative images of residual microneedle arrays after insertion into tumor for 1h. Scale bar = 1mm.
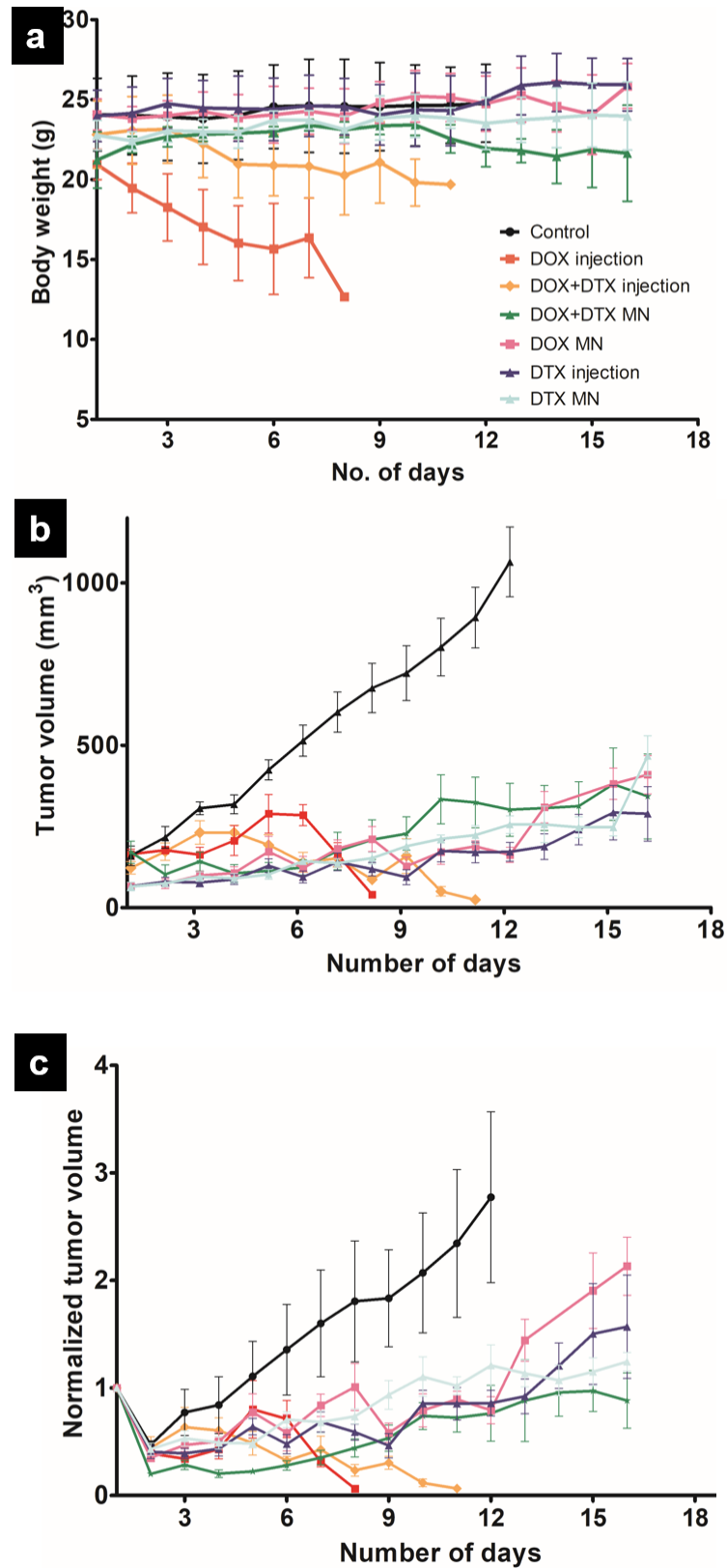
Figure 6.15. Absolute body weights (a), absolute tumor volumes (b) and normalized tumor volumes (c) of mice in different treatment groups during the study. Data presented as Mean ± error (n=3–6).

Overall, body weight of the control group animals (without any treatment) remained same throughout the study time (figure 6.15a). A similar stable body weight was also observed for the animals treated with DTX-injection, DTX-MN, DOX-MN, DOX-DTX-MN. However, there has been a significant weight loss recorded after treatment with DOX-injection and DOX-DTX-injection. Especially, with DOX-injection, the weight loss was observed immediately after first dose administration that continued to drop until all the animals within group dead by 9th day after treatment initiation. A similar profile was observed with DOX-DTX injection group, wherein 5 of the 6 animals dead by 11th day after treatment initiation.

Figure 6.15b and 6.15c show the absolute and normalized tumor volumes, respectively. Tumor volumes rapidly increased with time (1000 mm^3 by 10th day) for the animals within control group. Animals were euthanized when the tumor volume was 1000 mm^3. Tumor volume increased after DOX-injection until day 6. Then after, a decrease in both tumor volume and body weight was observed until the animals died by day 9. In the DOX-DTX-injection group, tumor volume decreased gradually until all the animals died by day 11.
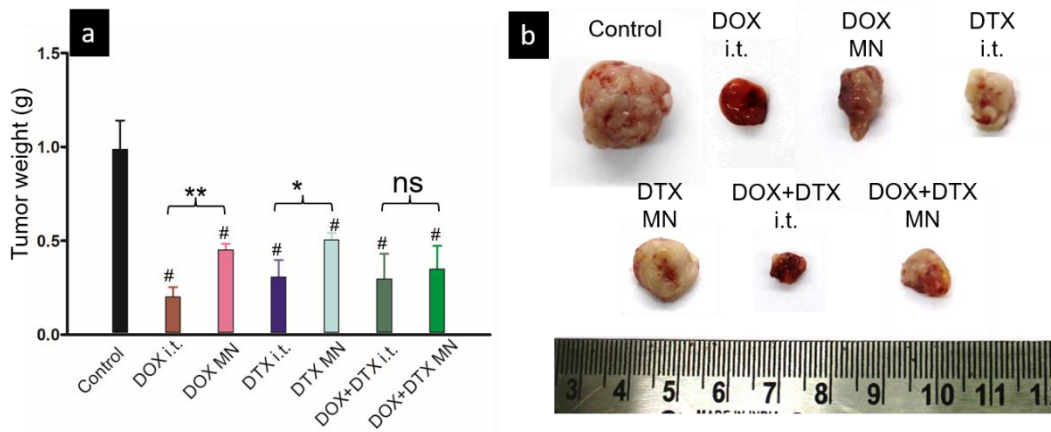
Figure 6.16 Tumor weight in grams (a) and representative images of tumors excised from different treatment groups (b) at the end of study. Data presented as Mean±SD (n=3). Data represents mean (n=3) ± standard deviation. * and ** represents that the values are significantly different at $p<0.05$ and $p<0.01$, respectively. # indicates significantly different values compared to control group at $p<0.01$.

All other treatment groups showed stable or non-significant increase in tumor volume over the period of 16 days. Since the starting tumor volumes were not same for all animals, tumor volumes were normalized with respect to tumor volumes at the start of treatment (Figure 6.15c). After treatment with DOX-injection, DOX-DTX-injection, DOX-DTX-MN, DTX-MN, DTX-injection, the tumor volume decreased compared with the initial tumor volume. For the groups treated with DOX-MN and DTX-injection there was an increase in tumor volume on 16th day of treatment.

Figure 6.12c shows the Kaplan-Meier survival plots for different treatment groups. 100% survival of the animals was observed after treatment with DOX-DTX-MN, DTX-MN. Animal groups treated with DOX-injection and DOX-DTX-injection showed the least survival time of 9 and 11 days, respectively. Mice were

euthanized on day 16 and tumors were harvested. Figure 6.16 shows the photograph of tumors and their average weights.

Detection of apoptotic nuclei in tumors from different treatment groups was performed using TUNEL immunohistological staining. Figure 6.17 shows brighfield, TUNEL (apoptosis), and DAPI (nuclei) stained tumor sections. The apoptotic nuclei are hardly seen in the control animal group. Apoptotic nuclei are present in the intratumoral injections and the MN groups. Notably, more apoptotic cells are seen in the DOX i.t. injection, DOX+DTX i.t. injection and DOX+DTX MN group. This trend in apoptosis is consistent with the in-vivo tumor inhibition results.
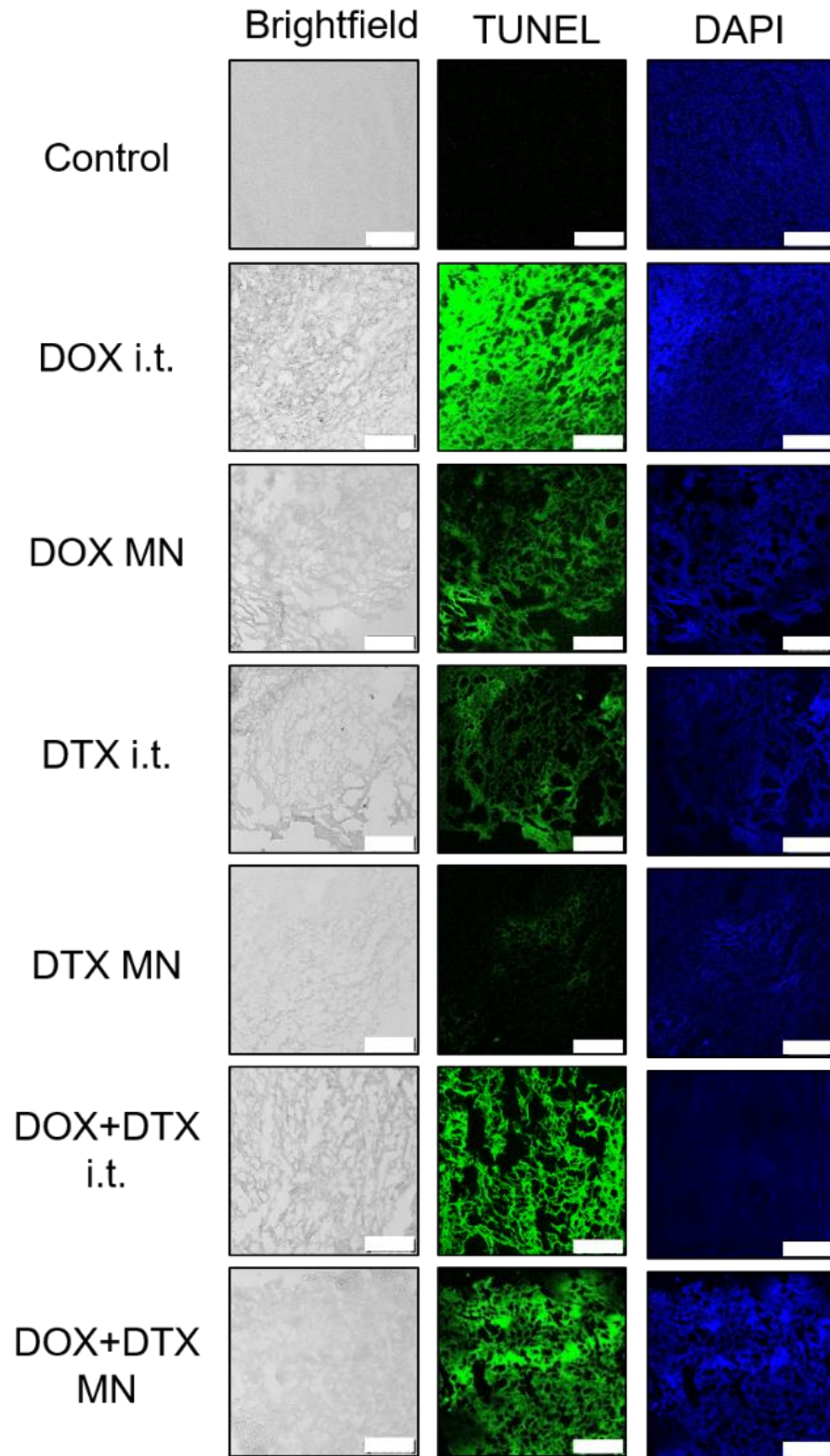
Figure 6.17 TUNEL immunostain in tumor sections of 4T1 tumor xenografts grown in athymic nude mice. Scale bar represents 250 μm.

Further, tumor inhibition efficacy of the developed formulation was ascertained using hematoxylin and eosin staining of tumor sections (figure 6.18). Normal cell pattern with larger vividly stained nuclei were seen in the control group. A decreased cell density, decreased nuclear stain intensity, cell shrinkage, appearance of spindle shaped nuclei, a condensed nucleoplasm, even a disappearance of cells and appearance of necrotic areas within the sections was observed in the intratumoral injections and MN treatment notably the DOX+DTX intratumoral injection and DOX+DTX MN group.
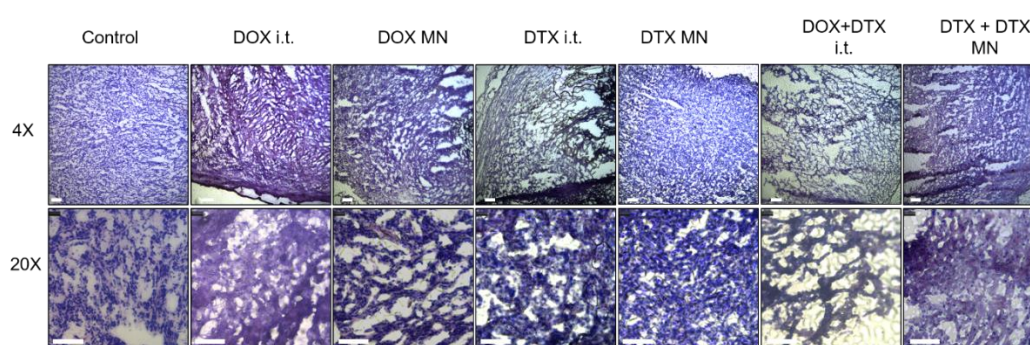
Figure 6.18 Hematoxylin and eosin stained tumor sections from 4T1 tumor bearing nude mice in various treatment groups.

6.4 Discussion

Cancer is a complex disease affecting millions every year. Breast cancer is the second leading cause of cancer deaths among women. (Breast cancer Facts and Figures 2017-18. American Chemical Society.) Surgical resection in combination with chemotherapy is the frontline treatment for breast cancer.(Pockaj & Gray, 2009) Even with extensive resection, complete removal of cancer tissue is not possible. Rates of recurrence are high with recurring tumors not responding well to systemic treatments.(Niibe & Hayakawa, 2010) Direct

administration of drugs into tumors as intratumoral injections has been studied in various cancer models. The most common method for intratumoral delivery is using a hypodermic needle to inject the drug. However, numerous problems limit the use of this approach including painful multiple injections, irregularly spaced drug concentrations within tumor, higher intratumoral pressures and the limitation with injection volumes. Moreover, if not carefully administered, drug leakage from the tumor could cause systemic toxicities.(Ma et al., 2015) Given these current limitations of intratumoral drug delivery, there is a crucial need for better delivery techniques for intratumoral administration of anticancer agents.

We hypothesized that dissolvable microneedles could be used to deliver anti-cancer drugs to tumors in a minimally invasive and painless way overcoming the aforesaid inadequacies. Dissolvable microneedles have been explored for delivery of a variety of therapeutics into and across the skin. In this work, we have prepared microneedles using PVA and PVP for transdermal delivery of DOX and DTX to solid breast tumors. MN arrays were prepared with PVP in the needles and PVA+PVP combination in the microneedle base. PVA has a weakly elastic nature and does not result in needles with sufficient mechanical strength when used alone. When combined with materials like PVP, sucrose or trehalose, the strength of microneedles can be improved. Higher molecular weights of PVP can be used to prepare microneedles of higher mechanical strength. Preparation of microneedles with PVP ensured dissolution of needles in skin tissue while addition of PVA in the MN pedestal provided flexibility to the MN array while being robust enough for handling and application. This is important since local solid tumors are not flat surfaces and MN patches need to be flexible allowing

insertion of all needles into the tumor. A brittle and non flexible MN array was obtained with use of only PVP to prepare the MN base.

Microneedles were prepared using the micromolding technique. Micromolding technique provides a low-cost scalable way of manufacturing polymer microneedles. The prepared microneedles were pyramidal in shape with no observable fractures on its surface. DOX and DTX, dissolved in water and ethanol respectively were added to PVP matrix before MN casting. Contrary to our expectation, DTX was not seen to precipitate after mixing with PVP. It was found that PVP has been shown to increase solubility of drugs that exhibit poor water solubility like acetaminophen and gidazepam (Kadajji & Betageri, 2011). With the use of highly viscous matrices for preparation of needles and base, limited diffusion of drugs was seen into base of MN. Drug loaded microneedles did not show any difference in respect to surface texture of MN or dimensions as observed by scanning electron microscopy. Fluorescence with DOX loaded microneedles could be easily observed using a fluorescence microscope. Although the prepared microneedles were observed to become soft upon storage, this issues was easily resolved with storage of MN in a desiccator.

Delivery of DOX using microneedles has been reported recently. Chen et al. reported a NIR activable MN system for treating local 4T1 tumors. MN were prepared with polycaprolactone and contained a photosensitive nanomaterial and DOX. The MN base was prepared using PVA+PVP combination. MN were shown to be completely embedded into the skin with the MN base plate dissolving over time. Upon exposure to NIR, the embedded array heats and melts to release DOX for local action.(Chen, Lin, & Ling, 2015) More recently, Nguyen et al.

reported DOX loaded PVA MN. MN were fabricated using the micromolding technique with DOX loaded in different locations within the MN array.(Nguyen et al., 2018)

While FT-IR and XRD were useful for characterization of polymers and drugs, little information for drug loaded MN could be gathered with these analyses. This could be due to the low concentrations of drugs in the needles, below the sensitivity of these techniques for detection. With FT-IR, characteristic peaks for PVP were observed reduced intensities were observed for drug loaded microneedles and physical mixtures. It needs to be noted that the physical mixtures contained the same ratio of drug:polymer as in final prepared microneedles. Similar results were obtained with XRD where characteristic peaks of DOX and DTX were absent from the prepared microneedles and physical mixtures.

A complete release of both drugs was seen in-vitro. DOX release was observed to be faster than DTX. The complete drug loaded MN arrays had dissolved in 30 minutes will all the drug released in the media before 15 minutes. Mouse skin was used for skin permeation experiments since further in-vivo studies were to be performed in mice. DOX permeation across mouse skin was higher than DTX which was expected considering high water solubility of DOX. DTX permeation was slower and lower with a significantly high amount retained in the viable epidermis. This could be attributed to the higher log P, low water solubility and high molecular weight of DTX.

The in-vitro studies were followed by subsequent in-vivo testing to determine the anti-tumor efficacy following intratumoral and MN assisted

delivery of individual drugs and the combination. Subcutaneous injections of 1×10^6 4T1 cells/mouse resulted in 100% tumor induction with tumors reaching a size of 50–100 mm^3 within 10–14 days. Treatments were given over a 16 day period. Intratumoral injections were administered using a 30G needle with the same amount of drugs administered intratumorally or using MN. Toxicity with DOX was most clearly seen with DOX intratumoral injection group. Although intratumoral injections were given into and in the tumor vicinity, chances of systemic toxicity are high considering leakage from tumor tissues. DOX treatments also resulted in visible necrosis of the tumor tissue in the animal. The rate of increase of tumor volume with DTX injection was seen to be slower than DTX MN. This could be attributed to the lower skin permeation of DTX observed with in-vitro permeation studies. Comparable tumor inhibition was seen between DOX+DTX MN and DOX+DTX intratumoral injection groups. Compared with nanocarriers, MNs are easily retained in local tissues, allowing long-term and multiple chemotherapy without the pain and adverse effects associated with multiple syringe injections.

Efficacy and toxicity of chemotherapeutics are two sides of the same coin. Most chemotherapeutics show dose dependent efficacy and toxicity. Attaining a balance between tumor reduction and survival (or quality of life) is a major challenge with most chemotherapeutic therapies. A higher survival rate was seen in animal groups with MN treatments especially with delivery of DOX alone or in combination with DTX. With respect to general side effects, body weight of mice treated with DOX or DOX+DTX intratumoral injections drastically reduced during the study while that with DOX or DOX+DTX MN gradually decreased comparably to untreated control mice.

H&E histology showed normal cell morphology and density in the control group against intratumoral injection or MN treatments, where appearance of necrotic tissue and abnormal cell morphology was observed. Moreover, TUNEL assay revealed large areas of apoptotic cells in tumors injected with free DOX and DOX+DTX or DOX+DTX MN. Contrarily, no apoptotic cells were observed in tumors from the untreated animal group.

6.5 Conclusions

This study demonstrated co-delivery of doxorubicin and docetaxel using dissolvable microneedles prepared with PVA and PVP. In vitro studies showed that microneedles were efficiently inserted into skin, dissolved within the skin and could permeate across mouse skin. Transdermal application of doxorubicin and docetaxel loaded MN in 4T1 tumor bearing athymic nude mice showed greater reduction in tumor volume and tumor weight compared with control group. MN groups fared well in terms of survival against intratumoral injection groups. Effectiveness of drug loaded microneedle treatment is comparable to intratumoral administration.

Chapter 7

Conclusions

Syringe injections are notoriously painful. Administration of an injection, especially an intravenous one, requires trained medical personnel. Accidental needles sticks and multiple uses of a single syringe are a common threat with use of syringe based injections. On the other hand, single use syringes pose a problem of huge amount medical waste and its disposal. Moreover, sterility and stability of injectable formulations is imperative, making their manufacture, transport and storage conditions critical.

This thesis work involved design and fabrication of polymeric microneedles arrays for transcutaneous delivery of therapeutics. These studies were performed with different polymeric microneedle systems, different microneedles designs and geometries, and different drug molecules

The drawbacks associated with glass or metal based microneedles have previously been discussed. Zein, a novel polymer to prepare microneedles was identified. Zein is protein derived from corn and used in the pharamaceutical and cosmetic industry. Zein microneedles were shown to be effective for transcutaneous immunization. Ovalbumin, a model antigen was either coated or entrapped into the zein microneedles. Ovalbumin was administered to Balb/c mice as a poke and patch approach or treatment with entrapped or coated zein microneedles. Zein microneedles were shown to have sufficient mechanical strength for skin inserted and could deliver ovalbumin to the skin effectively as confirmed by histological and confocal microscopy studies. The stability of ovalbumin after coating onto zein microneedles was assessed. Ovalbumin was seen to be stable in ovalbumin loaded microneedles for up to 2 months at both cold and room temperature conditions. Ovalbumin coated zein microneedles fared better than entrapped or topically applied ovalbumin in terms of recorded anti-ovalbumin IgG levels in

sera. However, a higher dose of ovalbumin coated zein microneedles was required to generate antibody responses similar to intradermal injection.

Following the same polymer of choice, zein microneedles were studied for delivery of anticancer agents. The aim of this study was to explore the influence of physico- chemical properties of two chemotherapeutic agents in their loading, release behavior, and skin permeation using zein microneedles. While tamoxifen has extremely low water solubility and a high log P, gemcitabine has a high water solubility and lower log P value. Tamoxifen was seen to release from zein microneedles only when coated using a hydrophilic polymer coating solution but was soon to partition back into the zein matrix once released. Moreover, it was not seen to permeate across porcine skin after treatment with tamoxifen entrapped microneedles or the poke and patch approach. Gemcitabine on the other hand, permeated across skin after treatment with coated microneedles or the poke and patch approach. Water solubility of chemotherapeutics played an important role in the loading, release behavior, and skin permeation of these molecules using polymeric microneedles.

Lesser loading of chemotherapeutics and unfavourable release profiles from zein microneedles called for modification of the delivery system. Dissolvable microneedles prepared with PVA and PVP provided a better drug co-loading of two different chemotherapeutics – doxorubicin and docetaxel. The needles were shown to have sufficient mechanical strength for insertion into murine skin. Confocal studies confirmed efficient insertion of microneedles into the skin. The needles were seen to dissolve in 60 minutes when inserted into the skin. Doxorubicin was release efficiently from the matrix upon insertion with about 60% of it permeated across the skin at the end of 48h. Docetaxel was seen to

permeate lesser with more than 60% of the loaded amount recovered from the viable epidermis. In-vivo efficacy studies performed in 4T1 tumor bearing mice showed comparable therapeutic efficacy between codelivery of doxorubicin and docetaxel using microneedles against intratumoral injection of both drugs. Moreover, the survival rates were improved with MN assisted delivery against intratumoral administration especially for doxorubicin which is known to have a high cardiotoxicity. Tumor weights from tumor excised from animals upon end of study further showed significant reduction in tumor weights for all treatment groups against control.

Chapter 8

Future Perspectives

The use of microneedles for drug delivery evolved in the 1970's but gained rapid interest in the 1990's with advances in the micromachining industry. With the advent of biocompatible materials for different biomedical applications, use of such systems for microneedle applications haven recently been considered. Moreover, the last 3–4 saw a high number of research publications focused on design and development of polymeric microneedles for delivery of a wide variety of drugs. Polymeric microneedles for delivery of doxorubicin for treatment of cutaneous T-cell lymphoma are already in clinical trials.

In the present work, we have shown delivery of different molecules using zein and PVA/PVP based microneedles. The physicochemical properties of drugs have been shown to influence the drug permeation across skin. One major limitation with microneedles is the amount of drug that can be loaded. Coated microneedle approaches provide lesser drug loadings than dissolvable microneedle systems for obvious reasons. Drug coating of microneedles is accompanied by a number of problems. Techniques to improve the loading of drug into microneedles need to be explored. Use of layer by layer casting of needles or layer by layer coatings of drug could help in achieving higher drug loadings into the microneedles.

Significant loss of drug during coating procedures need to be brought down. Since complete insertion of microneedles in the skin is rarely achieved, any drug in or on the microneedle base is generally not easily available for delivery into skin. Contamination of microneedle base with during coating procedures is hard to avoid and adds to wastage of drug. While coating microneedles without contaminating the base and methods to reduce wastage during microneedles coating have been reported, they involve use of sophisticated instruments to

selectively coat areas of needles. Simple and effective techniques to coat microneedles need to be found.

Zein microneedles present a novel substrate for delivery of macromolecules. Delivery of ovalbumin using zein microneedles provided a proof-of-concept. The system can be further studied for delivery of other protein based drugs.

Sterility of polymeric microneedles is an issue rarely discussed. Only few studies report studies related to sterilization of microneedles. While glass, metal and silicon based microneedles can be easy to sterilize, it can be very challenging for polymeric microneedles especially those containing Thermosensitive drugs and proteins. Addressing the sterility aspects of these microneedle systems while maintaining drug stability is a need of the hour.

Dissolvable microneedles, especially preparations with PVA and PVP have potential for ocular drug delivery. While reports for the same have been published, further studies in terms of formulation sterility and elimination of drugs from these systems after application need to be understood.

Microneedles have shown promising clinical outcomes and are expected to significantly impact the field of drug delivery in the near future.

Bibliography

Aapro, Matti S, Christophe Martin, and Sarah Hatty. (1998). 'Gemcitabine—a safety review', Anti-Cancer Drugs, 9: 191-202.

Ali, A. A., McCrudden, C. M., McCaffrey, J., McBride, J. W., Cole, G., Dunne, N. J.,. McCarthy, H. O. (2017). DNA vaccination for cervical cancer; a novel technology platform of RALA mediated gene delivery via polymeric microneedles. Nanomedicine: Nanotechnology, Biology and Medicine, 13(3), 921-932. doi: https://doi.org/10.1016/j.nano.2016.11.019

Alkilani, A. Z., McCrudden, M. T., & Donnelly, R. F. (2015). Transdermal drug delivery: innovative pharmaceutical developments based on disruption of the barrier properties of the stratum corneum. Pharmaceutics, 7(4), 438-470.

Ameri, M., Wang, X., & Maa, Y. F. (2010). Effect of irradiation on parathyroid hormone PTH(1–34) coated on a novel transdermal microprojection delivery system to produce a sterile product—adhesive compatibility. J Pharm Sci, 99(4), 2123-2134. doi: https://doi.org/10.1002/jps.21985

Amodwala, S., Kumar, P., & Thakkar, H. P. (2017). Statistically optimized fast dissolving microneedle transdermal patch of meloxicam: A patient friendly approach to manage arthritis. European Journal of Pharmaceutical Sciences, 104, 114-123. doi: https://doi.org/10.1016/j.ejps.2017.04.001

Arnou, R., Icardi, G., De Decker, M., Ambrozaitis, A., Kazek, M. P., Weber, F., & Van Damme, P. (2009). Intradermal influenza vaccine for older adults: a randomized controlled multicenter phase III study. Vaccine, 27(52), 7304-7312. doi: 10.1016/j.vaccine.2009.10.033

Babiuk, Shawn, Maria Baca-Estrada, Lorne A Babiuk, Catherine Ewen, and Marianna Foldvari. (2000). 'Cutaneous vaccination: the skin as an immunologically active tissue and the challenge of antigen delivery', Journal of Controlled Release, 66: 199-214.

Bal, S. M., Caussin, J., Pavel, S., & Bouwstra, J. A. (2008). In vivo assessment of safety of microneedle arrays in human skin. European Journal of Pharmaceutical Sciences, 35(3), 193-202. doi: http://dx.doi.org/10.1016/j.ejps.2008.06.016

Banga, Ajay K. 2011. Transdermal and intradermal delivery of therapeutic agents: application of physical technologies (CRC Press).

Baron, N., Passave, J., Guichardaz, B., & Cabodevila, G. (2008). Investigations of development process of high hollow beveled microneedles using a combination of ICP RIE and dicing saw. Microsystem Technologies, 14(9), 1475-1480. doi: 10.1007/s00542-008-0596-1

Barry, B. W. (1987). Mode of action of penetration enhancers in human skin. Journal of Controlled Release, 6(1), 85-97.

Batra, Prem P, Katsushi Sasa, Takuya Ueki, and Kunio Takeda. (1989). 'Circular dichroic study of conformational changes in ovalbumin induced by modification of sulfhydryl groups and disulfide reduction', Journal of protein chemistry, 8: 609-17.

Bediz, B., E. Korkmaz, R. Khilwani, C. Donahue, G. Erdos, L. D. Falo, Jr., and O. B. Ozdoganlar. (2014). 'Dissolvable microneedle arrays for intradermal delivery of biologics: fabrication and application', Pharm Res, 31: 117-35.

Bevers, T. B. (2001). Breast cancer chemoprevention: current clinical practice and future direction. Biomed Pharmacother, 55(9-10), 559-564.

Bhatia, Amit, Rajiv Kumar, and Om Prakash Katare. (2004). 'Tamoxifen in topical liposomes: development, characterization and in-vitro evaluation', J Pharm Pharm Sci, 7: 252-59.

Bhatnagar, S., Chawla, S. R., Kulkarni, O. P., & Venuganti, V. V. K. (2017). Zein Microneedles for Transcutaneous Vaccine Delivery: Fabrication, Characterization, and in Vivo Evaluation Using Ovalbumin as the Model Antigen. ACS Omega, 2(4), 1321-1332. doi: 10.1021/acsomega.7b00343

Bhatnagar, S., Dave, K., & Venuganti, V. V. K. (2017). Microneedles in the clinic. Journal of Controlled Release, 260, 164-182. doi: https://doi.org/10.1016/j.jconrel.2017.05.029

Bhatnagar, S., Saju, A., Cheerla, K. D., Gade, S. K., Garg, P., & Venuganti, V. V. K. (2018). Corneal delivery of besifloxacin using rapidly dissolving polymeric microneedles. Drug Delivery and Translational Research, 8(3), 473-483.

Boehm, R. D., Miller, P. R., Schell, W. A., Perfect, J. R., & Narayan, R. J. (2013). Inkjet Printing of Amphotericin B onto Biodegradable Microneedles Using Piezoelectric Inkjet Printing. Jom, 65(4), 525-533. doi: 10.1007/s11837-013-0574-7

Boks, M. A., Unger, W. W. J., Engels, S., Ambrosini, M., Kooyk, Y. v., & Luttge, R. (2015). Controlled release of a model vaccine by nanoporous ceramic

microneedle arrays. International Journal of Pharmaceutics, 491(1-2), 375-383. doi: 10.1016/j.ijpharm.2015.06.025

Brown, J. M., & Giaccia, A. J. (1998). The Unique Physiology of Solid Tumors: Opportunities (and Problems) for Cancer Therapy. Cancer Research, 58(7), 1408-1416.

Caffarel-Salvador, E., Kearney, M. C., Mairs, R., Gallo, L., Stewart, S. A., Brady, A. J., & Donnelly, R. F. (2015). Methylene Blue-Loaded Dissolving Microneedles: Potential Use in Photodynamic Antimicrobial Chemotherapy of Infected Wounds. Pharmaceutics, 7(4), 397-412. doi: 10.3390/pharmaceutics7040397

Chambers, R. (1914). Some physical properties of the cell nucleus. Science, 824-827.

Chambers, R. (1921). Microdissection studies, III. Some problems in the maturation and fertilization of the echinoderm egg. Biological Bulletin, 41(6), 318-350.

Chawla, Jugminder S., and Mansoor M. Amiji. (2002). 'Biodegradable poly(ε-caprolactone) nanoparticles for tumor-targeted delivery of tamoxifen', International Journal of Pharmaceutics, 249: 127-38.

Chen, J., Huang, W., Huang, Z., Liu, S., Ye, Y., Li, Q., & Huang, M. (2018). Fabrication of Tip-Dissolving Microneedles for Transdermal Drug Delivery of Meloxicam. AAPS PharmSciTech, 19(3), 1141-1151. doi: 10.1208/s12249-017-0926-7

Chen, M.-C., Chan, H.-A., Ling, M.-H., & Su, L.-C. (2017). Implantable polymeric microneedles with phototriggerable properties as a patient-controlled transdermal analgesia system. Journal of Materials Chemistry B, 5(3), 496-503. doi: 10.1039/C6TB02718K

Chen, M.-C., Lai, K.-Y., Ling, M.-H., & Lin, C.-W. (2018). Enhancing immunogenicity of antigens through sustained intradermal delivery using chitosan microneedles with a patch-dissolvable design. Acta Biomater, 65, 66-75. doi: https://doi.org/10.1016/j.actbio.2017.11.004

Chen, M.-C., Lin, Z.-W., & Ling, M.-H. (2015). Near-infrared light-activatable microneedle system for treating superficial tumors by combination of chemotherapy and photothermal therapy. ACS Nano, 10(1), 93-101.

Chen, M.-Y., Chen, Y.-Y., Tsai, H.-T., Tzai, T.-S., Chen, M.-C., & Tsai, Y.-S. (2017). Transdermal Delivery of Luteinizing Hormone-releasing Hormone with Chitosan Microneedles: A Promising Tool for Androgen Deprivation Therapy. Anticancer Research, 37(12), 6791-6797.

Chen, W., Tian, R., Xu, C., Yung, B. C., Wang, G., Liu, Y., Chen, X. (2017). Microneedle-array patches loaded with dual mineralized protein/peptide particles for type 2 diabetes therapy. Nat Commun, 8(1), 1777. doi: 10.1038/s41467-017-01764-1

Chen, Y., Shen, Y., Guo, X., Zhang, C., Yang, W., Ma, M., Wen, L.-P. (2006). Transdermal protein delivery by a coadministered peptide identified via phage display. Nat Biotechnol, 24, 455. doi: 10.1038/nbt1193

Chitkara, Deepak, and Neeraj Kumar. 2013. 'BSA-PLGA-Based Core-Shell Nanoparticles as Carrier System for Water-Soluble Drugs', Pharm Res, 30: 2396-409.

Clemons, Mark, Sarah Danson, and Anthony Howell. 2002. 'Tamoxifen ('Nolvadex'): a review: Antitumour treatment', Cancer treatment reviews, 28: 165-80.

Cole, G., McCaffrey, J., Ali, A. A., McBride, J. W., McCrudden, C. M., Vincente-Perez, E. M., . . . McCarthy, H. O. (2017). Dissolving microneedles for DNA vaccination: Improving functionality via polymer characterization and RALA complexation. Hum Vaccin Immunother, 13(1), 50-62. doi: 10.1080/21645515.2016.1248008

Coleman, C E; , and B A Larkins. 1999. 'The Prolamins of Maize.' in P R; Shewry and R Casey (eds.), Seed Proteins (Kluwer Academic Publishers: The Netherlands).

Daddona, P. E., Matriano, J. A., Mandema, J., & Maa, Y.-F. (2011). Parathyroid Hormone (1-34)-Coated Microneedle Patch System: Clinical Pharmacokinetics and Pharmacodynamics for Treatment of Osteoporosis. Pharm Res, 28(1), 159-165. doi: 10.1007/s11095-010-0192-9

Demir, Yusuf K, Zafer Akan, and Oya Kerimoglu. (2013). 'Sodium alginate microneedle arrays mediate the transdermal delivery of bovine serum albumin', PloS one, 8: e63819.

DeMuth, Peter C, Wilfredo F Garcia-Beltran, Michelle Lim Ai-Ling, Paula T Hammond, and Darrell J Irvine. (2013). 'Composite dissolving microneedles for

coordinated control of antigen and adjuvant delivery kinetics in transcutaneous vaccination', Advanced functional materials, 23: 161-72.

Diehl, M. S., & Jensen, B. D. (2007). Wet Etched Pyramidal Microneedles With Fluid-Delivery Microchannels. (42967), 181-182. doi: 10.1115/IMECE2007-43524

Donnelly, R. F., R. Majithiya, T. R. Singh, D. I. Morrow, M. J. Garland, Y. K. Demir, K. Migalska, E. Ryan, D. Gillen, C. J. Scott, and A. D. Woolfson. (2011). 'Design, optimization and characterisation of polymeric microneedle arrays prepared by a novel laser-based micromoulding technique', Pharm Res, 28: 41-57.

Donnelly, R. F., Raj Singh, T. R., & Woolfson, A. D. (2010). Microneedle-based drug delivery systems: Microfabrication, drug delivery, and safety. Drug Deliv, 17(4), 187-207. doi: 10.3109/10717541003667798

Donnelly, Ryan F, Thakur Raghu Raj Singh, Michael M Tunney, Desmond IJ Morrow, Paul A McCarron, Conor O'Mahony, and A David Woolfson. 2009. 'Microneedle arrays allow lower microbial penetration than hypodermic needles in vitro', Pharmaceutical research, 26: 2513-22.

Fan, T., Li, M., Wu, X., Li, M., & Wu, Y. (2011). Preparation of thermoresponsive and pH-sensitivity polymer magnetic hydrogel nanospheres as anticancer drug carriers. Colloids and Surfaces B: Biointerfaces, 88(2), 593-600. doi: https://doi.org/10.1016/j.colsurfb.2011.07.048

Fernandes, D. (2005). Minimally invasive percutaneous collagen induction. Oral and Maxillofacial Surgery Clinics of North America, 17(1), 51-63.

Fontana, Giacomo, Laura Maniscalco, Domenico Schillaci, Gennara Cavallaro, and Gaetano Giammona. 2005. 'Solid Lipid Nanoparticles Containing Tamoxifen Characterization and In Vitro Antitumoral Activity', Drug Deliv, 12: 385-92.

Gao, Shen, and Jagdish Singh. 1998. 'In vitro percutaneous absorption enhancement of a lipophilic drug tamoxifen by terpenes', Journal of Controlled Release, 51: 193-99.

Gardeniers, H. J. G. E., Luttge, R., Berenschot, E. J. W., Boer, M. J. d., Yeshurun, S. Y., Hefetz, M., . . . Berg, A. v. d. (2003). Silicon micromachined hollow microneedles for transdermal liquid transport. Journal of Microelectromechanical Systems, 12(6), 855-862. doi: 10.1109/JMEMS.2003.820293

Gerstel, M. S., & Place, V. A. (1976). Drug delivery device: Google Patents.

Gill, H. S., & Prausnitz, M. R. (2007). Coated microneedles for transdermal delivery. J Control Release, 117(2), 227-237. doi: 10.1016/j.jconrel.2006.10.017

Gill, H. S., Andrews, S. N., Sakthivel, S. K., Fedanov, A., Williams, I. R., Garber, D. A., Prausnitz, M. R. (2009). Selective removal of stratum corneum by microdermabrasion to increase skin permeability. European Journal of Pharmaceutical Sciences, 38(2), 95-103. doi: https://doi.org/10.1016/j.ejps.2009.06.004

Gill, Harvinder S., and Mark R. Prausnitz. (2007). 'Coating Formulations for Microneedles', Pharm Res, 24: 1369-80.

Glenn, G. M., Flyer, D. C., Ellingsworth, L. R., Frech, S. A., Frerichs, D. M., Seid, R. C., & Yu, J. (2007). Transcutaneous immunization with heat-labile enterotoxin: development of a needle-free vaccine patch. Expert Rev Vaccines, 6(5), 809-819. doi: 10.1586/14760584.6.5.809

Gorham, J. 1821. 'Analysis of Indian corn', QJ Sci. Lit. Arts, 2: 206-08.

Gupta, J., Denson, D. D., Felner, E. I., & Prausnitz, M. R. (2012). Rapid Local Anesthesia in Human Subjects using Minimally Invasive Microneedles. The Clinical Journal of Pain, 28(2), 129-135. doi: 10.1097/AJP.0b013e318225dbe9

Gupta, J., Felner, E. I., & Prausnitz, M. R. (2009). Minimally Invasive Insulin Delivery in Subjects with Type 1 Diabetes Using Hollow Microneedles. Diabetes Technol Ther, 11(6), 329-337. doi: 10.1089/dia.2008.0103

Gupta, J., Felner, E. I., & Prausnitz, M. R. (2011). Rapid pharmacokinetics of intradermal insulin administered using microneedles in type 1 diabetes subjects. Diabetes Technol Ther, 13(4), 451-456. doi: 10.1089/dia.2010.0204

Hao, Y., Dong, M., Zhang, T., Peng, J., Jia, Y., Cao, Y., & Qian, Z. (2017). Novel Approach of Using Near-Infrared Responsive PEGylated Gold Nanorod Coated Poly(l-lactide) Microneedles to Enhance the Antitumor Efficiency of Docetaxel-Loaded MPEG-PDLLA Micelles for Treating an A431 Tumor. ACS Appl Mater Interfaces, 9(18), 15317-15327. doi: 10.1021/acsami.7b03604

Hao, Y., Li, W., Zhou, X., Yang, F., & Qian, Z. (2017). Microneedles-Based Transdermal Drug Delivery Systems: A Review. Journal of Biomedical Nanotechnology, 13(12), 1581-1597. doi: 10.1166/jbn.2017.2474

Heel, R. C., R. N. Brogden, T. M. Speight, and G. S. Avery. 1978. 'Tamoxifen: A Review of its Pharmacological Properties and Therapeutic Use in the Treatment of Breast Cancer', Drugs, 16: 1-24.

Henry, S., McAllister, D. V., Allen, M. G., & Prausnitz, M. R. (1998). Microfabricated microneedles: a novel approach to transdermal drug delivery. J Pharm Sci, 87(8), 922-925. doi: 10.1021/js980042+

Herndon, T. O., Gonzalez, S., Gowrishankar, T., Anderson, R. R., & Weaver, J. C. (2004). Transdermal microconduits by microscission for drug delivery and sample acquisition. BMC Medicine, 2(1), 12. doi: 10.1186/1741-7015-2-12

Hodge, R. M., Edward, G. H., & Simon, G. P. (1996). Water absorption and states of water in semicrystalline poly(vinyl alcohol) films. Polymer, 37(8), 1371-1376. doi: https://doi.org/10.1016/0032-3861(96)81134-7

Holland, D., Booy, R., De Looze, F., Eizenberg, P., McDonald, J., Karrasch, J., . . . Saville, M. (2008). Intradermal influenza vaccine administered using a new microinjection system produces superior immunogenicity in elderly adults: a randomized controlled trial. J Infect Dis, 198(5), 650-658. doi: 10.1086/590434

Hong, X., Wu, Z., Chen, L., Wu, F., Wei, L., & Yuan, W. (2014). Hydrogel Microneedle Arrays for Transdermal Drug Delivery. Nano-Micro Letters, 6(3). doi: 10.1007/bf03353783

Hooper, J. W., Golden, J. W., Ferro, A. M., & King, A. D. (2007). Smallpox DNA vaccine delivered by novel skin electroporation device protects mice against intranasal poxvirus challenge. Vaccine, 25(10), 1814-1823. doi: https://doi.org/10.1016/j.vaccine.2006.11.017

Hortobagyi, G. (1997). Anthracyclines in the treatment of cancer. Drugs, 54(4),

1-7.

Hsu, T., & Mitragotri, S. (2011). Delivery of siRNA and other macromolecules into skin and cells using a peptide enhancer. Proceedings of the National Academy of Sciences, 108(38), 15816-15821. doi: 10.1073/pnas.1016152108

Huh, I., Kim, S., Yang, H., Jang, M., Kang, G., & Jung, H. (2018). Effects of two droplet-based dissolving microneedle manufacturing methods on the activity of encapsulated epidermal growth factor and ascorbic acid. European Journal of Pharmaceutical Sciences, 114, 285-292. doi: https://doi.org/10.1016/j.ejps.2017.12.025

Hutton, A. R. J., Quinn, H. L., McCague, P. J., Jarrahian, C., Rein-Weston, A., Coffey, P. S., Donnelly, R. F. (2018). Transdermal delivery of vitamin K using dissolving microneedles for the prevention of vitamin K deficiency bleeding.

International Journal of Pharmaceutics, 541(1), 56-63. doi: https://doi.org/10.1016/j.ijpharm.2018.02.031

Indermun, S., R. Luttge, Y. E. Choonara, P. Kumar, L. C. du Toit, G. Modi, and V. Pillay. (2014). 'Current advances in the fabrication of microneedles for transdermal delivery', J Control Release, 185: 130-8.

Ita, K. (2015). 'Transdermal Delivery of Drugs with Microneedles-Potential and Challenges', Pharmaceutics, 7: 90-105.

Ito, Y., Hagiwara, E., Saeki, A., Sugioka, N., & Takada, K. (2006). Feasibility of microneedles for percutaneous absorption of insulin. European Journal of Pharmaceutical Sciences, 29(1), 82-88. doi: https://doi.org/10.1016/j.ejps.2006.05.011

Jain, A. K., Lee, C. H., & Gill, H. S. (2016). 5-Aminolevulinic acid coated microneedles for photodynamic therapy of skin tumors. Journal of Controlled Release, 239, 72-81. doi: https://doi.org/10.1016/j.jconrel.2016.08.015

Jane, J, S Lim, I Paetau, K Spence, and S Wang. 1994. 'Biodegradable plastics made from agricultural biopolymers.' in (ACS Publications).

Jena, Sunil Kumar, Charan Singh, Chander Parkash Dora, and Sarasija Suresh. (2014). 'Development of tamoxifen-phospholipid complex: Novel approach for improving solubility and bioavailability', International Journal of Pharmaceutics, 473: 1-9.

Jeong, H.-R., Kim, J.-Y., Kim, S.-N., & Park, J.-H. (2018). Local dermal delivery of cyclosporin A, a hydrophobic and high molecular weight drug, using

dissolving microneedles. European Journal of Pharmaceutics and Biopharmaceutics, 127, 237-243. doi: https://doi.org/10.1016/j.ejpb.2018.02.014

Jia-You, F., Pei-Feng, L., & Chun-Ming, H. (2008). Decreasing Systemic Toxicity Via Transdermal Delivery of Anticancer Drugs. Current Drug Metabolism, 9(7), 592-597. doi: http://dx.doi.org/10.2174/138920008785821693

Jose, A., Ninave, K., Karnam, S., & Vamsi Krishna Venuganti, V. (2018). Temperature-sensitive liposomes for codelivery of tamoxifen and imatinib for synergistic breast cancer treatment.

Joshi, Garima, Abhinesh Kumar, and Krutika Sawant. (2014). 'Enhanced bioavailability and intestinal uptake of Gemcitabine HCl loaded PLGA nanoparticles after oral delivery', European Journal of Pharmaceutical Sciences, 60: 80-89.

Kadajji, V. G., & Betageri, G. V. (2011). Water Soluble Polymers for Pharmaceutical Applications. Polymers, 3(4), 1972.

Kaur, M., Ita, K. B., Popova, I. E., Parikh, S. J., & Bair, D. A. (2014). Microneedle-assisted delivery of verapamil hydrochloride and amlodipine besylate. Eur J Pharm Biopharm, 86(2), 284-291. doi: 10.1016/j.ejpb.2013.10.007

Kellerman, D., Lickliter, J., Mardell, J., & von Stein, T. (2016). Pharmacokinetics and Tolerability of a New Intracutaneous Microneedle System of Zolmitriptan (ZP-Zolmitriptan). HEADACHE, 56, 13-14.

Kim, Y.-C., Park, J.-H., & Prausnitz, M. R. (2012). Microneedles for drug and vaccine delivery. Adv Drug Deliv Rev, 64(14), 1547-1568.

Kim, Yeu-Chun, and Mark R Prausnitz. (2011). 'Enabling skin vaccination using new delivery technologies', Drug delivery and translational research, 1: 7-12.

Kim, Yeu-Chun, Fu-Shi Quan, Richard W Compans, Sang-Moo Kang, and Mark R Prausnitz. (2010). 'Formulation and coating of microneedles with inactivated influenza virus to improve vaccine stability and immunogenicity', Journal of Controlled Release, 142: 187-95.

Kumar, Amit, Xinran Li, Michael A Sandoval, B Leticia Rodriguez, Brian R Sloat, and Zhengrong Cui. 2011. 'Permeation of antigen protein-conjugated nanoparticles and live bacteria through microneedle-treated mouse skin', International journal of nanomedicine, 6: 1253.

Labala, S., Jose, A., Chawla, S. R., Khan, M. S., Bhatnagar, S., Kulkarni, O. P., & Venuganti, V. V. K. (2017). Effective melanoma cancer suppression by iontophoretic co-delivery of STAT3 siRNA and imatinib using gold nanoparticles. International Journal of Pharmaceutics, 525(2), 407-417. doi: https://doi.org/10.1016/j.ijpharm.2017.03.087

Lahiji, S. F., Dangol, M., & Jung, H. (2015). A patchless dissolving microneedle delivery system enabling rapid and efficient transdermal drug delivery. Sci Rep, 5, 7914. doi: 10.1038/srep07914

Larrañeta, Eneko, Rebecca E. M. Lutton, A. David Woolfson, and Ryan F. Donnelly. 2016. 'Microneedle arrays as transdermal and intradermal drug delivery systems: Materials science, manufacture and commercial development', Materials Science and Engineering: R: Reports, 104: 1-32.

Lawton, J. W. (2002). Zein: A History of Processing and Use. Cereal Chemistry Journal, 79(1), 1-18. doi: 10.1094/CCHEM.2002.79.1.1

Lee, H., Song, C., Baik, S., Kim, D., Hyeon, T., & Kim, D.-H. (2017). Device-assisted transdermal drug delivery. Adv Drug Deliv Rev. doi: https://doi.org/10.1016/j.addr.2017.08.009

Lee, I. C., Wu, Y.-C., Tsai, S.-W., Chen, C.-H., & Wu, M.-H. (2017). Fabrication of two-layer dissolving polyvinylpyrrolidone microneedles with different molecular weights for in vivo insulin transdermal delivery. RSC Advances, 7(9), 5067-5075. doi: 10.1039/C6RA27476E

Lee, I-Chi, Jheng-Siou He, Meng-Tsan Tsai, and Kai-Che Lin. (2015). 'Fabrication of a novel partially dissolving polymer microneedle patch for transdermal drug delivery', Journal of Materials Chemistry B, 3: 276-85.

Lee, J. W., Choi, S.-O., Felner, E. I., & Prausnitz, M. R. (2011). Dissolving Microneedle Patch for Transdermal Delivery of Human Growth Hormone. Small, 7(4), 531-539. doi: 10.1002/smll.201001091

Lee, J. W., Han, M.-R., & Park, J.-H. (2013). Polymer microneedles for transdermal drug delivery. J Drug Target, 21(3), 211-223. doi: 10.3109/1061186X.2012.741136

Lee, J. W., Park, J.-H., & Prausnitz, M. R. (2008). Dissolving microneedles for transdermal drug delivery. Biomaterials, 29(13), 2113-2124. doi: https://doi.org/10.1016/j.biomaterials.2007.12.048

Lee, S. G., Jeong, J. H., Lee, K. M., Jeong, K. H., Yang, H., Kim, M., . . . Choi, Y. W. (2014). Nanostructured lipid carrier-loaded hyaluronic acid microneedles for controlled dermal delivery of a lipophilic molecule. Int J Nanomedicine, 9, 289-299. doi: 10.2147/IJN.S54529

Levin, Y., Kochba, E., & Kenney, R. (2014). Clinical evaluation of a novel microneedle device for intradermal delivery of an influenza vaccine: are all delivery methods the same? Vaccine, 32(34), 4249-4252. doi: 10.1016/j.vaccine.2014.03.024

Levin, Y., Kochba, E., Hung, I., & Kenney, R. (2015). Intradermal vaccination using the novel microneedle device MicronJet600: Past, present, and future. Hum Vaccin Immunother, 11(4), 991-997. doi: 10.1080/21645515.2015.1010871

Li, X., Zhao, R., Qin, Z., Zhang, J., Zhai, S., Qiu, Y., Thomas, S. H. (2010). Microneedle pretreatment improves efficacy of cutaneous topical anesthesia. The American Journal of Emergency Medicine, 28(2), 130-134. doi: http://dx.doi.org/10.1016/j.ajem.2008.10.001

Licata, S., Saponiero, A., Mordente, A., & Minotti, G. (2000). Doxorubicin Metabolism and Toxicity in Human Myocardium: Role of Cytoplasmic Deglycosidation and Carbonyl Reduction. Chemical Research in Toxicology, 13(5), 414-420. doi: 10.1021/tx000013q

Ling, M. H., & Chen, M. C. (2013). Dissolving polymer microneedle patches for rapid and efficient transdermal delivery of insulin to diabetic rats. Acta Biomater, 9(11), 8952-8961. doi: 10.1016/j.actbio.2013.06.029

Lotze, M. T., & Thomson, A. W. (2001). Dendritic cells: biology and clinical applications: Academic Press.

Lu, Yanfeng, Satya Nymisha Mantha, Douglas C Crowder, Sofia Chinchilla, Kush N Shah, Yang H Yun, Ryan B Wicker, and Jae-Won Choi. (2015). 'Microstereolithography and characterization of poly (propylene fumarate)-based drug-loaded microneedle arrays', Biofabrication, 7: 045001.

Luttge, R. (2016). 'Drug delivery through microneedles.' in, Microsystems for Pharmatechnology (Springer).

Ma, Y., Boese, S. E., Luo, Z., Nitin, N., & Gill, H. S. (2015). Drug coated microneedles for minimally-invasive treatment of oral carcinomas: development and in vitro evaluation. Biomed Microdevices, 17(2), 44. doi: 10.1007/s10544-015-9944-y

Machekposhti, S., Soltani, M., Najafizadeh, P., Ebrahimi, S. A., & Chen, P. (2017). Biocompatible polymer microneedle for topical/dermal delivery of tranexamic acid. Journal of Controlled Release, 261, 87-92. doi: https://doi.org/10.1016/j.jconrel.2017.06.016

Manosroi, A., L. Kongkaneramit, and J. Manosroi. (2004). 'Stability and transdermal absorption of topical amphotericin B liposome formulations', International Journal of Pharmaceutics, 270: 279-86.

Manuel, O., Humar, A., Berutto, C., Ely, L., Giulieri, S., Lien, D., Kumar, D. (2011). Low-dose intradermal versus intramuscular trivalent inactivated seasonal influenza vaccine in lung transplant recipients. The Journal of heart and

lung transplantation: the official publication of the International Society for Heart Transplantation, 30(6), 679-684. doi: 10.1016/j.healun.2011.01.705

Marshall, Sarah, Laura J Sahm, and Anne C Moore. (2016). 'The success of microneedle-mediated vaccine delivery into skin', Human vaccines & immunotherapeutics, 12: 2975-83.

McAllister, D. V., Wang, P. M., Davis, S. P., Park, J. H., Canatella, P. J., Allen, M. G., & Prausnitz, M. R. (2003). Microfabricated needles for transdermal delivery of macromolecules and nanoparticles: fabrication methods and transport studies. Proc Natl Acad Sci U S A, 100(24), 13755-13760. doi: 10.1073/pnas.2331316100

McCrudden, Maelíosa TC, Emma McAlister, Aaron J Courtenay, Patricia González-Vázquez, Thakur Raghu Raj Singh, and Ryan F Donnelly. (2015). 'Microneedle applications in improving skin appearance', Experimental dermatology, 24: 561-66.

Mescher, A. L. (2013). Junqueira's basic histology: text and atlas: Mcgraw-hill.

Meyer, K. A. P., Markowicz, P. P., Rendon, S., Smithson, R. L. W., & Simmers, R. P. (2014). Article with hollow microneedles and method of making: Google Patents.

Mikszta, J. A., Alarcon, J. B., Brittingham, J. M., Sutter, D. E., Pettis, R. J., & Harvey, N. G. (2002). Improved genetic immunization via micromechanical disruption of skin-barrier function and targeted epidermal delivery. Nat Med, 8(4), 415-419.

Mikszta, J. A., Dekker, J. P., Harvey, N. G., Dean, C. H., Brittingham, J. M., Huang, J., Ulrich, R. G. (2006). Microneedle-Based Intradermal Delivery of the Anthrax Recombinant Protective Antigen Vaccine. Infection and Immunity, 74(12), 6806-6810. doi: 10.1128/IAI.01210-06

Milewski, Mikolaj, Nicole K. Brogden, and Audra L. Stinchcomb. (2010). 'Current aspects of formulation efforts and pore lifetime related to microneedle treatment of skin', Expert opinion on drug delivery, 7: 617-29.

Miyano, T., Tobinaga, Y., Kanno, T., Matsuzaki, Y., Takeda, H., Wakui, M., & Hanada, K. (2005). Sugar Micro Needles as Transdermic Drug Delivery System. Biomed Microdevices, 7(3), 185-188. doi: 10.1007/s10544-005-3024-7

Mönkäre, J., Reza Nejadnik, M., Baccouche, K., Romeijn, S., Jiskoot, W., & Bouwstra, J. A. (2015). IgG-loaded hyaluronan-based dissolving microneedles for intradermal protein delivery. Journal of Controlled Release, 218, 53-62. doi: https://doi.org/10.1016/j.jconrel.2015.10.002

Morelon, E., Noble, C. P., Daoud, S., Cahen, R., Goujon-Henry, C., Weber, F., . . . Nicolas, J.-F. (2010). Immunogenicity and safety of intradermal influenza vaccination in renal transplant patients who were non-responders to conventional influenza vaccination. Vaccine, 28(42), 6885-6890. doi: http://dx.doi.org/10.1016/j.vaccine.2010.08.015

Münch, S., Wohlrab, J., & Neubert, R. H. H. (2017). Dermal and transdermal delivery of pharmaceutically relevant macromolecules. European Journal of Pharmaceutics and Biopharmaceutics, 119, 235-242. doi: https://doi.org/10.1016/j.ejpb.2017.06.019

Naguib, Y. W., Kumar, A., & Cui, Z. (2014). The effect of microneedles on the skin permeability and antitumor activity of topical 5-fluorouracil. Acta Pharm Sin B, 4(1), 94-99. doi: 10.1016/j.apsb.2013.12.013

Naik, A., Kalia, Y. N., & Guy, R. H. (2000). Transdermal drug delivery: overcoming the skin's barrier function. Pharmaceutical Science & Technology Today, 3(9), 318-326. doi: https://doi.org/10.1016/S1461-5347(00)00295-9

Neena Washington, C. W., Clive Wils. (2001). Physiological Pharmaceutics: Barriers to Drug Absorption (Second ed., pp. 249-269): CRC Press, Taylor & Francis group.

Ng, Shiow-Fern, Jennifer J. Rouse, Francis D. Sanderson, Victor Meidan, and Gillian M. Eccleston. (2010). 'Validation of a Static Franz Diffusion Cell System for In Vitro Permeation Studies', AAPS PharmSciTech, 11: 1432-41.

Nguyen, H. X., Bozorg, B. D., Kim, Y., Wieber, A., Birk, G., Lubda, D., & Banga, A. K. (2018). Poly (vinyl alcohol) microneedles: Fabrication, characterization, and application for transdermal drug delivery of doxorubicin. European Journal of Pharmaceutics and Biopharmaceutics, 129, 88-103. doi: https://doi.org/10.1016/j.ejpb.2018.05.017

Niibe, Y., & Hayakawa, K. (2010). Oligometastases and Oligo-recurrence: The New Era of Cancer Therapy. Japanese Journal of Clinical Oncology, 40(2), 107-111. doi: 10.1093/jjco/hyp167

Nir, Yael, Alona Paz, Edmond Sabo, and Israel Potasman. (2003). 'Fear of injections in young adults: prevalence and associations', The American journal of tropical medicine and hygiene, 68: 341-44.

Norman, J. J., Brown, M. R., Raviele, N. A., Prausnitz, M. R., & Felner, E. I. (2013). Faster pharmacokinetics and increased patient acceptance of intradermal insulin delivery using a single hollow microneedle in children and adolescents with type 1 diabetes. Pediatr Diabetes, 14(6), 459-465. doi: 10.1111/pedi.12031

Ogura, M., Paliwal, S., & Mitragotri, S. (2008). Low-frequency sonophoresis: Current status and future prospects. Adv Drug Deliv Rev, 60(10), 1218-1223. doi: https://doi.org/10.1016/j.addr.2008.03.006

Olatunji, O., & Olsson, R. (2015). Microneedles from Fishscale-Nanocellulose Blends Using Low Temperature Mechanical Press Method. Pharmaceutics, 7(4), 363.

Osborne, Thomas B. (1916). The vegetable proteins (Longmans, Green and Company).

Osborne, Thomas B. (1924). 'Classification of vegetable proteins.' in Thomas B. Osborne (ed.), The Vegetable Proteins (Longmans, Green and Co.: New York).

Paliwal, Rishi, and Srinath Palakurthi. (2014). 'Zein in controlled drug delivery and tissue engineering', Journal of Controlled Release, 189: 108-22.

Pamornpathomkul, B., Ngawhirunpat, T., Tekko, I. A., Vora, L., McCarthy, H. O., & Donnelly, R. F. (2018). Dissolving polymeric microneedle arrays for enhanced site-specific acyclovir delivery. European Journal of Pharmaceutical Sciences, 121, 200-209. doi: https://doi.org/10.1016/j.ejps.2018.05.009

Park, J. H., Allen, M. G., & Prausnitz, M. R. (2006). Polymer microneedles for controlled-release drug delivery. Pharm Res, 23(5), 1008-1019. doi: 10.1007/s11095-006-0028-9

Park, J.H., Allen. M. G., and Prausnitz. M. R. (2005). 'Biodegradable polymer microneedles: fabrication, mechanics and transdermal drug delivery', Journal of Controlled Release, 104: 51-66.

Park, S. Y., Lee, H. U., Lee, Y. C., Kim, G. H., Park, E. C., Han, S. H., Lee, J. (2014). Wound healing potential of antibacterial microneedles loaded with green tea extracts. Mater Sci Eng C Mater Biol Appl, 42, 757-762. doi: 10.1016/j.msec.2014.06.021

Pasparakis, M., Haase, I., & Nestle, F. O. (2014). Mechanisms regulating skin immunity and inflammation. Nature Reviews Immunology, 14(5), 289.

Paul, P. M. L. (1975). Device for cutaneous therapeutic treatment: Google Patents.

Pawar, K. (2017). Microneedles-Based Devices: Regulatory Insights. J Pharm Drug Deliv Res 6, 1, 2.

Pettis, R. J., Ginsberg, B., Hirsch, L., Sutter, D., Keith, S., McVey, E., Kapitza, C. (2011). Intradermal microneedle delivery of insulin lispro achieves faster insulin absorption and insulin action than subcutaneous injection. Diabetes Technol Ther, 13(4), 435-442.

Pettis, Ronald J, and Alfred J Harvey. (2012). 'Microneedle delivery: clinical studies and emerging medical applications', Therapeutic delivery, 3: 357-71.

Pikaar, Jacquelien C, Wim F Voorhout, Lambert MG van Golde, Jan Verhoef, Jos AG Van Strijp, and J Freek van Iwaarden. (1995). 'Opsonic activities of surfactant proteins A and D in phagocytosis of gram-negative bacteria by alveolar macrophages', Journal of Infectious Diseases, 172: 481-89.

Pikal, M. J. (2001). The role of electroosmotic flow in transdermal iontophoresis. Adv Drug Deliv Rev, 46(1), 281-305. doi: https://doi.org/10.1016/S0169-409X(00)00138-1

Pockaj, B. A., & Gray, R. J. (2009). Current surgery for breast cancer. Future Oncology, 5(4), 465-479. doi: 10.2217/fon.09.23

Poulin, Patrick, Yung-Hsiang Chen, Xiao Ding, Stephen E. Gould, Cornelis Eca Hop, Kirsten Messick, Jason Oeh, and Bianca M. Liederer. 'Prediction of Drug Distribution in Subcutaneous Xenografts of Human Tumor Cell Lines and Healthy Tissues in Mouse: Application of the Tissue Composition-Based Model to Antineoplastic Drugs', J Pharm Sci, 104: 1508-21.

Prausnitz, M. R., & Langer, R. (2008). Transdermal drug delivery. Nat Biotechnol, 26(11), 1261-1268. doi: 10.1038/nbt.1504

Prausnitz, M. R., Mikszta, J. A., Cormier, M., & Andrianov, A. K. (2009). Microneedle-based vaccines. Curr Top Microbiol Immunol, 333, 369-393. doi: 10.1007/978-3-540-92165-3_18

Pugazhendhi, A., Edison, T. N. J. I., Velmurugan, B. K., Jacob, J. A., & Karuppusamy, I. (2018). Toxicity of Doxorubicin (Dox) to different experimental organ systems. Life Sci, 200, 26-30. doi: https://doi.org/10.1016/j.lfs.2018.03.023

Puri, A., Nguyen, H. X., & Banga, A. K. (2016). Microneedle-mediated intradermal delivery of epigallocatechin-3-gallate. Int J Cosmet Sci, 38(5), 512-523. doi: 10.1111/ics.12320

Qiu, Y., Gao, Y., Hu, K., & Li, F. (2008). Enhancement of skin permeation of docetaxel: A novel approach combining microneedle and elastic liposomes. Journal of Controlled Release, 129(2), 144-150. doi: https://doi.org/10.1016/j.jconrel.2008.04.019

Quinn, H. L., Kearney, M.-C., Courtenay, A. J., McCrudden, M. T., & Donnelly, R. F. (2014). The role of microneedles for drug and vaccine delivery. Expert opinion on drug delivery, 11(11), 1769-1780.

Ragab, H. M. (2011). Spectroscopic investigations and electrical properties of PVA/PVP blend filled with different concentrations of nickel chloride. Physica B: Condensed Matter, 406(20), 3759-3767. doi: https://doi.org/10.1016/j.physb.2010.11.030

Romanyuk, A. V., Zvezdin, V. N., Samant, P., Grenader, M. I., Zemlyanova, M., & Prausnitz, M. R. (2014). Collection of analytes from microneedle patches. Anal Chem, 86(21), 10520-10523. doi: 10.1021/ac503823p

Salmon, J. K., Armstrong, C. A., & Ansel, J. C. (1994). The skin as an immune organ. Western journal of medicine, 160(2), 146-152.

Sharifi, Shahriar, Hamid Mirzadeh, Mohammad Imani, Zimei Rong, Ahmad Jamshidi, Mohammadali Shokrgozar, Mohammad Atai, and Nima Roohpour. (2009). 'Injectable in situ forming drug delivery system based on poly(ε-caprolactone fumarate) for tamoxifen citrate delivery: Gelation characteristics, in vitro drug release and anti-cancer evaluation', Acta Biomater, 5: 1966-78.

Shaw, T. K., Mandal, D., Dey, G., Pal, M. M., Paul, P., Chakraborty, S. Mandal, M. (2017). Successful delivery of docetaxel to rat brain using experimentally developed nanoliposome: a treatment strategy for brain tumor. Drug Deliv, 24(1), 346-357. doi: 10.1080/10717544.2016.1253798

Shukla, Rishi, and Munir Cheryan. (2001). 'Zein: the industrial protein from corn', Industrial crops and products, 13: 171-92.

Sirnonsen, L, A Kane, J Lloyd, M Zaffran, and M Kane. 1999. 'Unsafe injections in the developing world and transmission of blood-bome pathogens', Bull World Health Organ, 77: 789-800.

Sliwkowski, M. X., & Mellman, I. (2013). Antibody Therapeutics in Cancer. Science, 341(6151), 1192-1198. doi: 10.1126/science.1241145

Soltani, N., Saion, E., Erfani, M., Rezaee, K., Bahmanrokh, G., Drummen, G. P. C., . . . Hussein, M. Z. (2012). Influence of the Polyvinyl Pyrrolidone Concentration on Particle Size and Dispersion of ZnS Nanoparticles Synthesized

by Microwave Irradiation. Int J Mol Sci, 13(10), 12412-12427. doi: 10.3390/ijms131012412

Stinson, J. A., Raja, W. K., Lee, S., Kim, H. B., Diwan, I., Tutunjian, S., Kaplan, D. L. (2017). Silk Fibroin Microneedles for Transdermal Vaccine Delivery. ACS Biomaterials Science & Engineering, 3(3), 360-369. doi: 10.1021/acsbiomaterials.6b00515

Strambini, L. M., Longo, A., Scarano, S., Prescimone, T., Palchetti, I., Minunni, M., Barillaro, G. (2015). Self-powered microneedle-based biosensors for pain-free high-accuracy measurement of glycaemia in interstitial fluid. Biosens Bioelectron, 66, 162-168. doi: 10.1016/j.bios.2014.11.010

Streilein, J. W. (1983). Skin-associated lymphoid tissues (SALT): origins and functions. Journal of Investigative Dermatology, 80.

Streilein, J. W., Grammer, S. R., Yoshikawa, T., Demidem, A., & Vermeer, M. (1990). Functional dichotomy between Langerhans cells that present antigen to naive and to memory/effector T lymphocytes. Immunological reviews, 117(1), 159-183.

Suh, H., Shin, J., & Kim, Y.-C. (2014). Microneedle patches for vaccine delivery. Clin Exp Vaccine Res, 3(1), 42-49. doi: 10.7774/cevr.2014.3.1.42

Sullivan, S. P., Koutsonanos, D. G., Del Pilar Martin, M., Lee, J. W., Zarnitsyn, V., Choi, S. O., Prausnitz, M. R. (2010). Dissolving polymer microneedle patches for influenza vaccination. Nat Med, 16(8), 915-920. doi: 10.1038/nm.2182

Thompson, Gary A., and Brian A. Larkins. (1989). 'Structural elements regulating zein gene expression', BioEssays, 10: 108-13.

Thompson, M. G., Shay, D. K., Zhou, H., Bridges, C. B., Cheng, P. Y., Burns, E., Cox, N. J. (2010). Estimates of deaths associated with seasonal influenza united states, 1976-2007. Morbidity and Mortality Weekly Report, 59(33), 1057-1062.

Tong, Z., Zhou, J., Zhong, J., Tang, Q., Lei, Z., Luo, H., . . . Liu, X. (2018). Glucose-and H2O2-Responsive Polymeric Vesicles Integrated with Microneedle Patches for Glucose-Sensitive Transcutaneous Delivery of Insulin in Diabetic Rats. ACS Appl Mater Interfaces.

Trickler, William J., Jatin Khurana, Ankita A. Nagvekar, and Alekha K. Dash. (2010). 'Chitosan and Glyceryl Monooleate Nanostructures Containing Gemcitabine: Potential Delivery System for Pancreatic Cancer Treatment', AAPS PharmSciTech, 11: 392-401.

Troy, S. B., Kouiavskaia, D., Siik, J., Kochba, E., Beydoun, H., Mirochnitchenko, O., Maldonado, Y. (2015). Comparison of the Immunogenicity of Various Booster Doses of Inactivated Polio Vaccine Delivered Intradermally Versus Intramuscularly to HIV-Infected Adults. J Infect Dis, 211(12), 1969-1976. doi: 10.1093/infdis/jiu841

Tsioris, K., Raja, W. K., Pritchard, E. M., Panilaitis, B., Kaplan, D. L., & Omenetto, F. G. (2012). Fabrication of Silk Microneedles for Controlled-Release Drug Delivery. Advanced Functional Materials, 22(2), 330-335. doi: 10.1002/adfm.201102012

Tuan-Mahmood, T. M., M. T. McCrudden, B. M. Torrisi, E. McAlister, M. J. Garland, T. R. Singh, and R. F. Donnelly. (2013). 'Microneedles for intradermal and transdermal drug delivery', Eur J Pharm Sci, 50: 623-37.

Van Damme, P., Oosterhuis-Kafeja, F., Van der Wielen, M., Almagor, Y., Sharon, O., & Levin, Y. (2009). Safety and efficacy of a novel microneedle device for dose sparing intradermal influenza vaccination in healthy adults. Vaccine, 27(3), 454-459. doi: 10.1016/j.vaccine.2008.10.077

van der Maaden, K., Varypataki, E. M., Romeijn, S., Ossendorp, F., Jiskoot, W., & Bouwstra, J. (2014). Ovalbumin-coated pH-sensitive microneedle arrays effectively induce ovalbumin-specific antibody and T-cell responses in mice. Eur J Pharm Biopharm, 88(2), 310-315. doi: 10.1016/j.ejpb.2014.05.003

van der Maaden, Koen, Wim Jiskoot, and Joke Bouwstra. 2012. 'Microneedle technologies for (trans) dermal drug and vaccine delivery', Journal of Controlled Release, 161: 645-55.

Wang, P. M., Cornwell, M., & Prausnitz, M. R. (2005). Minimally Invasive Extraction of Dermal Interstitial Fluid for Glucose Monitoring Using Microneedles. Diabetes Technol Ther, 7(1), 131-141. doi: 10.1089/dia.2005.7.131

Wang, P. M., Cornwell, M., Hill, J., & Prausnitz, M. R. (2006). Precise Microinjection into Skin Using Hollow Microneedles. Journal of Investigative Dermatology, 126(5), 1080-1087. doi: https://doi.org/10.1038/sj.jid.5700150

Wang, Po-Chun, Brock A Wester, Swaminathan Rajaraman, Seung-Joon Paik, Seong-Hyok Kim, and Mark G Allen. 2009. "Hollow polymer microneedle array fabricated by photolithography process combined with micromolding

technique." In Engineering in Medicine and Biology Society, 2009. EMBC 2009. Annual International Conference of the IEEE, 7026-29. IEEE.

Weijers, Mireille, Peter A Barneveld, Martien A Cohen Stuart, and Ronald W Visschers. 2003. 'Heat-induced denaturation and aggregation of ovalbumin at neutral pH described by irreversible first-order kinetics', Protein Science, 12: 2693-703.

Wicki, A., Witzigmann, D., Balasubramanian, V., & Huwyler, J. (2015). Nanomedicine in cancer therapy: Challenges, opportunities, and clinical applications. Journal of Controlled Release, 200, 138-157. doi: https://doi.org/10.1016/j.jconrel.2014.12.030

Widera, G., Johnson, J., Kim, L., Libiran, L., Nyam, K., Daddona, P. E., & Cormier, M. (2006). Effect of delivery parameters on immunization to ovalbumin following intracutaneous administration by a coated microneedle array patch system. Vaccine, 24(10), 1653-1664. doi: 10.1016/j.vaccine.2005.09.049

Wiedersberg, S., & Guy, R. H. (2014). Transdermal drug delivery: 30+ years of war and still fighting! Journal of Controlled Release, 190, 150-156. doi: https://doi.org/10.1016/j.jconrel.2014.05.022

Williams, Faith M. (2006). 'In vitro studies—how good are they at replacing in vivo studies for measurement of skin absorption?', Environmental Toxicology and Pharmacology, 21: 199-203.

Wilson, Brenda A, Abigail A Salyers, Dixie D Whitt, and Malcolm E Winkler. (2011). Bacterial pathogenesis: a molecular approach (American Society for Microbiology (ASM)).

Wilson, C. M. (1987). 'Proteins of the kernel.' in S. A. Watson and P. E. Ramstad (eds.), Corn: Chemistry and Technology (Am. Assoc. Cereal Chem.: St. Paul, MN).

Wolff, K., & Stingl, G. (1983). The langerhans cell. Journal of Investigative Dermatology, 80.

Xiaolong, L., Chuang, G., Ligang, C., Shumin, W., Jinrui, W., & Zhifei, D. (2017). Self-Assembly of an Amphiphilic Janus Camptothecin–Floxuridine Conjugate into Liposome-Like Nanocapsules for More Efficacious Combination Chemotherapy in Cancer. Adv Mater, 29(40), 1703135. doi: doi:10.1002/adma.201703135

Yang, P.-Y., Zou, H., Chao, E., Sherwood, L., Nunez, V., Keeney, M., Luo, X. (2016). Engineering a long-acting, potent GLP-1 analog for microstructure-based transdermal delivery. Proceedings of the National Academy of Sciences, 113(15), 4140-4145.

Yang, Sixing, Yan Feng, Lijun Zhang, Nixiang Chen, Weien Yuan, and Tuo Jin. (2012). 'A scalable fabrication process of polymer microneedles', International journal of nanomedicine, 7: 1415.

Yang, Zhigang, Aqin Chen, Hongxiang Sun, Yiping Ye, and Weihuan Fang. (2007). 'Ginsenoside Rd elicits Th1 and Th2 immune responses to ovalbumin in mice', Vaccine, 25: 161-69.

Yu, J., Zhang, Y., Ye, Y., DiSanto, R., Sun, W., Ranson, D., Gu, Z. (2015). Microneedle-array patches loaded with hypoxia-sensitive vesicles provide

fast glucose-responsive insulin delivery. Proceedings of the National Academy of Sciences, 112(27), 8260-8265. doi: 10.1073/pnas.1505405112

Yu, W., Jiang, G., Liu, D., Li, L., Chen, H., Liu, Y., Kong, X. (2017). Fabrication of biodegradable composite microneedles based on calcium sulfate and gelatin for transdermal delivery of insulin. Materials Science and Engineering: C, 71, 725-734. doi: https://doi.org/10.1016/j.msec.2016.10.063

Yu, W., Jiang, G., Liu, D., Li, L., Tong, Z., Yao, J., & Kong, X. (2017). Transdermal delivery of insulin with bioceramic composite microneedles fabricated by gelatin and hydroxyapatite. Materials Science and Engineering: C, 73, 425-428. doi: https://doi.org/10.1016/j.msec.2016.12.111

Yu, W., Jiang, G., Zhang, Y., Liu, D., Xu, B., & Zhou, J. (2017). Polymer microneedles fabricated from alginate and hyaluronate for transdermal delivery of insulin. Materials Science and Engineering: C, 80, 187-196. doi: https://doi.org/10.1016/j.msec.2017.05.143

Zhang, H., Dou, J., Zhai, Y., Liu, A., & Zhai, G. (2014). Advances in the formulations of non-injection administration of docetaxel. J Drug Target, 22(2), 87-94. doi: 10.3109/1061186X.2013.839686

Zhu, Z., Luo, H., Lu, W., Luan, H., Wu, Y., Luo, J., Wang, H. (2014). Rapidly dissolvable microneedle patches for transdermal delivery of exenatide. Pharm Res, 31(12), 3348-3360. doi: 10.1007/s11095-014-1424-1

Appendix

Patents filed

1. Venkata Vamsi Krishna Venuganti, **Shubhmita Bhatnagar**, Zein-based microneedle array for transcutaneous delivery of drugs, vaccines and other agents. Indian Patent Application number 201611017380, 18.05.2016.

List of publications

From thesis work:

1. **Shubhmita Bhatnagar**, Pooja Kumari, Srijanaki Paravastu Pattarabhiran, Venkata Vamsi Krishna Venuganti. Zein microneedles for localized delivery of chemotherapeutic agents to treat breast cancer: Drug loading, release behavior and skin permeation studies. *AAPS PharmSciTech* 19 (4), 1818-1826 (2018).

2. **Shubhmita Bhatnagar**, Kaushalkumar Dave, Venkata Vamsi Krishna Venuganti. Microneedles in the clinic. *Journal of Controlled Release* 260, 164-182 (2017).

3. **Shubhmita Bhatnagar**, Sumeet R. Chawla, Onkar P. Kulkarni, Venkata Vamsi Krishna Venuganti. Zein microneedles for transcutaneous vaccine delivery: fabrication, characterization and in-vivo evaluation using ovalbumin as model antigen. *ACS Omega* 2, 1321-1332 (2017).

Other publications:

1. Sudeep Kumar Gade, Nagaveni Shivshetty, Natalia Sharma, **Shubhmita Bhatnagar**, Prashant Garg, Venkata Vamsi Krishna Venuganti. Effect of mucoadhesive polymeric formulation on corneal permeation of fluoroquinolones. Journal of Ocular Pharmacology and Therapeutics (accepted, in press).

2. **Shubhmita Bhatnagar**, Amala Saju, Krishna Deepthi Cherala, Sudeep Kumar Gade, Prashant Garg, Venkata Vamsi Krishna Venuganti. Corneal delivery of besifloxacin using rapidly dissolving polymeric

microneedles. *Drug Delivery and Translational Research* 8 (3), 473-483 (2018).

3. Suman Labala, Anup Jose, Sumeet R. Chawla, Mohammed Shareef Khan, **Shubhmita Bhatnagar**, Onkar P. Kulkarni, Venkata Vamsi Krishna Venuganti. Effective melanoma cancer suppression by iontophoretic co-delivery of STAT3 siRNA and imatinib using gold nanoparticles. *International Journal of Pharmaceutics* 525 (2), 407-417 (2017).

4. Praveen K. Mandapalli, Suman Labala, Anup Jose, **Shubhmita Bhatnagar**, Renuka Janupally, Dharmarajan Sriram, Venkata Vamsi K. Venuganti. Layer-by-layer thin films for codelivery of TGF-beta siRNA and epidermal growth factor to improve excisional wound healing. *AAPS PharmSciTech* 18(3), 809-820 (2017).

5. Suman Labala, Praveen K. Mandapalli, **Shubhmita Bhatnagar**, Venkata Vamsi K. Venuganti. Encapsulation of albumin in self-assembled layer-by-layer microcapsules: comparison of co-precipitation and adsorption techniques. *Drug Development and Industrial Pharmacy* 41, 1302-1310 (2015).

6. **Shubhmita Bhatnagar**, Venkata Vamsi K. Venuganti. Cancer targeting: responsive polymers for stimuli-sensitive drug delivery. *Journal of Nanoscience and Nanotechnology* 15 (3), 1925-1945 (2015)

List of poster presentations at conferences

1. Shubhmita Bhatnagar, Pooja Kumari, Srijanaki Paravastu Pattarabhiran, Venkata Vamsi Krishna Venuganti. Zein Microneedles for Delivery of Gemcitabine. CRS India Chapter, Feb' 24-25, 2018, Mumbai, India.

2. Shubhmita Bhatnagar, Sumeet Chawla, Venkata Vamsi K. Venuganti. Fabrication of zein microneedles for transcutaneous immunization. AAPS Annual Meeting and Exposition 2016, Denver, USA. Nov' 2016

3. Shubhmita Bhatnagar, Venkata Vamsi K. Venuganti. Microneedles for drug delivery through skin and eye: Pain-free alternative to syringe injections. International Knowledge Millennium Conference 2015, Nov' 2-3, 2015, Hyderabad, India.

Shubhmita Bhatnagar

<u>Biography</u>

Ms. Shubhmita Bhatnagar completed her Bachelor of Pharmacy (Hons.) and M. Pharm. from BITS Pilani Hyderabad Campus in 2012 and 2014 respectively. Ms. Shubhmita joined Prof. Vamsi Venuganti's lab at BITS Pilani Hyderabad Campus in August 2014 for carrying out her doctoral research work. Her doctoral research work involved preparation of microneedles made from different types of biocompatible polymers, their characterization and deliverability of different small and macromolecules using these systems. Ms Shubhmita has co-authored 10 scientific peer review publications in well-renowned international journals, presented papers in various international and national conferences and has one Indian patent filed.

Prof. Venkata Vamsi Krishna Venuganti

Biography

Dr. Vamsi Venuganti is presently working as Associate Professor, in Department of Pharmacy, Birla Institute of Technology and Science, Pilani, Hyderabad Campus. He received his B. Pharm degree (2004) from University College of Pharmaceutical Sciences, Kakatiya University, India. He was awarded Ph.D. in Pharmaceutical Sciences in the year 2010 from South Dakota State University, USA. He has been involved in research for the last 15 years. Dr Venuganti has to his credit more than 25 research publications and two Indian Patent filings. He has co-authored a book chapter in Nanoparticulate delivery systems II. Formulation and Characterization. He has successfully completed many sponsored projects and currently handling projects sponsored by DST, DBT, ICMR along with few industry sponsored projects. He has supervised three Ph.D. students and currently seven students are pursuing their Ph.D. work under his guidance.